School of Electrical Engineering, Computing and Mathematical Sciences

Design and Validation of a Portable Wireless Data Acquisition System for Measuring Human Joint Angles in Medical Applications

Weiyang Xu

This thesis is presented for the Degree of
Doctor of Philosophy
of
Curtin University

October 2018

Declaration

To the best of my knowledge and belief this thesis contains no material previously published by any other person except where due acknowledgment has been made.

This thesis contains no material which has been accepted for the award of any other degree or diploma in any university.
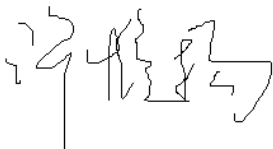
Signature:

Date: 15/10/2018

Statement of Contribution by Others

The following research paper listed below is based on data generated in this thesis. The candidate's major research contribution related to the conceptual design, experiments, algorithms and implementation and is presented in this thesis. Co-authors of these papers helped in analysis and provided advised and assistance in the interpretation of the results. A further explanation of which part of the thesis the research papers were based on is outlined below.

Paper Title: "Measuring Human Joint Movement with IMUs: Implementation in custom-made low cost wireless sensors"

The work presented in the paper was based on the algorithms which was developed in chapter 5 of the thesis. Hardware platform used in the paper was based on the work conducted in chapter 4. Co-authors contributed to 20% of the work and "Weiyang Xu" contributed to 80% of the work..

(Signature of Candidate)

:

(Signature of Supervisor)

Abstract

Many physiotherapy and kinematical studies require a precise analysis of human joint movements. Traditional methods in human joint angle measurement use mechanical measurement apparatus that often lack the accuracy necessary to support medical research. Such methods are usually not applicable in studies of active movement. Although optical systems using high-speed cameras can deliver high precision measurements, these systems are often costly and require to be applied from a fix angle. With the development of MEMs sensor technologies, wearable sensors were introduced into the human motion studies. Most MEM-based sensor systems and their compatible software work for a narrow range of targets. Limitations were found in the requirements of calibration positions, heavy computational load of complex sensor fusion algorithms and confusing sensor attachment protocol for medical applications.

The research presented in this thesis aimed at developing an efficient sensor system prototype to capture and measure human joint movements in medical applications. The two sensors based algorithm was developed to use two IMU sensors' measurements representing one human joint movement. Both custom-made hardware and software were developed during the research. The accuracy and reliability of the sensors were proved with a series of validation tests.

The latest version of the sensor is enclosed in a $22 \times 24 \times 18$ mm box providing accelerometer and gyroscope measurements at 100 samples per second within a 10 meter range. In identical movement tests with one sensor static and the other moving, the results showed less than 1° average error, and 3° maximum error. In dynamic tests when both sensors continuously move in a wide range, less than 2° average error for slow speed tests and around 2.5° average error for fast speed tests were achieved. A custom designed angle measurement mechanism verified a 0.67° maximum error in single plane static condition. A 1.56° maximum Root Mean Square Error (RMSE) was achieved throughout fixed relative joint angle tests performed on a moving wrist.

The system is currently being used in early stage research trials in Perth Children's Hospital to evaluate cerebral palsy patients. Five sets of sensor systems have also been dispatched to different research groups in Perth, Sydney and Melbourne.

Acknowledgements

brought this work into a higher level.

I would also appreciate the collaboration of the colleges of the research group, Dr. Bert Wong, Dr. Nimsiri Abhayasinghe, Shiva Sharif, Dr. Azadeh Nazemi, Jack Wiltshire which made my work easier and productive.

I thank with warm regards, Kai Sun, Xiaoyao Cong, Xixiang Chen, Angela Lai, Jun Zhang, Wei Ran, Ruoqing Zhang, Roger Lee, Lien Lee and all other friends for making my stay in Perth memorable and comfortable.

Special thanks go to my formal IEEE Curtin Student Branch committees and my dear friends: Martin Chu, Shi Pan and Tai Ding for their support and courage given throughout this work.

Last, but not the least, I would like to thank my family: my parents for bringing me to this level and supporting me with every effort. Without their financial support for my life and study in Perth, this research would never proceed. Their warm and spiritual support throughout this research brought this work to a success.

List of Publications

Some elements of the work presented in this thesis has been published in the following proceedings:

W. Xu, C. Ortega-Sanchez and I. Murray, "Measuring Human Joint Movement with IMUs: Implementation in custom-made low cost wireless sensors," in *2017 IEEE 15th Student Conference on Research and Development (SCOReD)*, Malaysia, December 2017.

This page is intentionally kept blank.

Table of Contents

List of Figures

List of Tables

Chapter 1

Introduction

1.1 Human joint measurement

The study of human joint movement describes the motion made by various joints of the human body. A human joint is an articulation where two or more bones meet [1]. Human joint movement results from the contraction and relaxation of muscles attached to the bones [2].

Kinematical studies of human joints explore the potential of the human body. In physiotherapy studies, human joint measurements provide evidence and knowledge about a person's normal and abnormal physical states.

Joint measurement by human observation using mechanical measurement apparatus is regarded as the commonly accepted method in most medical studies [3]. However, such methods usually contain high measurement errors and are hard to apply in active motion studies [4][5]. With the development of medical and biomedical research, there is a need for highly accurate measurements of joint kinematics. Optical 3D analysis has become one of the de-facto standards in medical research because of its high measurement resolution [6]. However, these systems are usually costly because they require expensive high-speed cameras and specially structured lab facilities [7]. Such optical method also limits the environment, as it requires the observed participant to be in front of the cameras. Additionally, results may be misleading if the conditions are artificial.

Wearable Micro Electro-Mechanical Systems (MEMS) sensors have been incorporated into recent human motion experiments [8]. Their portable feature is significant because then systems can be applied under different environments. Since different human joint movements are involved in different studies, specific ways of sensor placement and

unique algorithms need to be developed to serve the focus of a particular research. In most cases, an initial frame of reference is required to calibrate the system [9, 10, 11]. Thus, existing methods involving the use of sensors are not convenient for physiotherapy or kinematical research, especially when it is hard to set a standard position to be used as the calibration reference.

1.2 Problem statement

Based on the discussion in section 1.1 about human joint measurement studies, the problem statement for this research can be stated as follows:

- The traditional methods in human joint angle measurement use mechanical measurement apparatus that often lack the accuracy necessary to support medical research. Such methods are usually not applicable in studies of active movement.

- Optical methods are costly and limited by the environment. As they require participants in a special motion capture facility, it is especially inconvenient to perform tests on patients with disabilities. Considering that a large percentage of physiotherapy studies and clinical research are about people's abnormal physical behaviours [2], optical human motion methods could be a limited option for long term and regular basis studies.

- Most wearable sensors used in human motion studies focus on a specific target. Hence, sensor fusion algorithms are required to make sense of the data collected with electronic sensor systems. Furthermore, sensor based system are usually not user friendly for people who lack the necessary engineering background.

- Most MEM-based sensors for human joint angle measurement require a standard set position during the measurements. A standard set position can be the zero position for the measurements, or it can be an identical movement that happens regularly throughout trials. The standard set position serves a major role in calibrating the drift of sensors [9, 10, 11]. However, in some studies where

participants have abnormal range of motions, such calibration position can hardly be defined as the participants' are not able to deliver the standard position.

- MEMS sensors cannot be used in many paediatric studies as they need to be extremely small and flexible to be attached on children's bodies.

- Methods that use sensors in human joint measurement are quite different in terms of experiment demonstration and data processing compared to the mechanical and optical solutions. Finding a golden standard to validate the sensors before they can be trusted in medical applications could be a complex task.

1.3 Objectives of the research

The main objective of this research is to develop a flexible, low cost, human joint motion measurement system prototype for medical research. The system has to be capable of precisely capturing and measuring human joint movements.

The research aimed at developing an efficient sensor system prototype to capture and measure human joint movements in medical applications. To avoid using a standard calibration position, a sensor placement method and a compatible algorithm using multiple sensors was implemented. A small robotic arm was designed and implemented to serve as golden standard during sensor validation.

The prototype can be used to explore the feasibility of creating a product that can serve the medical community.

The goals of this research can be described more specifically as below:

- (i) Develop a solution so that multiple electronic sensors can be combined to capture and measure human joint movements.

- (ii) Design and implement a small, wireless, custom-made hardware platform.

(iii)   Design a protocol to position the sensors before human joint measurements.

(iv)   Design and develop user-friendly software to collect, organise and analyse data for medical purposes.

(v)   Use a robotic arm to determine the system's measurement accuracy.

(vi)   Conduct trials involving human participants performing specific joint movements to measure the joint's angle. Then use trials' results to determine the feasibility of the system in medical studies.

1.4 Original contributions from this research

This thesis' original contributions to the state of the art are:

(i)   The custom-made sensor system developed in this thesis contains the features of high sampling rate, wireless multi-device communication, and significantly smaller size compared to most commercially available motion capture systems.

(ii)   The two-sensor, human joint angle measurement methods and the algorithm developed in this thesis are applicable to most human joints as long as the sensor can be attached parallel to the measured joint. The novel technique of using two sensors as references of each other overcomes the need to have a zero calibration position throughout the measurement process. This is particularly convenient in studies on patients who suffer from locomotion control, making it impossible for them to produce an initial set position.

(iii)   The robotic mechanisms designed in the thesis could be adopted as golden standards in sensor validation.

(iv)   The sensor system is being used in a collaboration project studying wrist movements in cerebral palsy patients. The medical team is highly satisfied with the preliminary results.

1.5 Outline of the thesis

This thesis is organized in eight chapters as listed next.

- Chapter 2 (Existing IMU based motion capture technologies and data processing methods) presents the details of motion capture technologies and currently available human joint analysis systems.

- Chapter 3 (Methodology) discusses the methodology used in this research.

- Chapter 4 (Hardware Platform) presents the details of the hardware development.

- Chapter 5 (Joint movement measurement and algorithms) presents the software platform and algorithms developed to support the sensors.

- Chapter 6 (Results) presents the results of validation tests. Tests involving robotic arms and custom-made angle measuring mechanism were designed to validate the performance and feasibility of the sensor system.

- Chapter 7 (Collaboration projects with rehabilitation researchers) presents a discussion on a collaboration project based on the presenting system.

- Chapter 8 (Conclusions) conclude the thesis work and presents some ideas for future work.

This page is intentionally kept blank.

Chapter 2

Existing IMU based motion capture technologies and data processing methods

2.1 Introduction

Motion capture and human joint measurement techniques in medical applications are the main themes of this research. A brief history of motion capture technologies development with various methods and applications is presented in this chapter. Background investigation on motion capture and processing techniques, orientation estimation algorithms and human joint movement analysis provides a better understanding of the research topic.

More specific investigations on inertial measurement units (IMU)-based applications and research in human measurements were conducted to have a high-level view of the state of the art. This chapter briefly discusses each method, including their purpose, research usage, advantages and disadvantages. Additionally, different data fusion algorithms for IMU sensors were investigated. The purpose and specific input structure of each algorithm are discussed. Some commercial IMU systems with theirs features and limitations are also presented.

2.2 Background of Motion Capture Technologies

Motion capture, the process of recording and analysing human movement, was first introduced as a technique for recording and animating a dancer's pose in the late 1970s [12]. The technique of motion capture has spawned a variety of different methods and found use in a myriad of areas and applications, such as film animation, gesture recognition for console control systems and kinematic studies [13].

In the 1980s, researchers from Simon Fraser University used a goniometer to track knee

flexion for kinematic studies; this is regarded as the first time a biomechanics lab used a computer to analyse human motion [14]. The first 3D optical motion capture system was called "Graphical Marionette" presented by Ginsberg and Maxwell at MIT in 1983.They attached Light-Emitting Diodes (LEDs) to the body as markers, and used two cameras to obtain a 3-D world coordinate for each LED. [12]

In modern society, motion capture is also widely used in gesture recognition applications to allow computers understand human gestures [5]. Portable devices, mostly present on wearable applications, are lightweight devices which can individually run programs and complete some computing or monitoring operation [8].

In traditional motion capture techniques, film makers place reflecting stickers (frame markers) on the actors' body and record the movement with special cameras in a green room. This provides convenience for image modelling because computers can easily map the frame markers to a digital model [15]. The first attempt for using optical motion capture system in film making was in the movie "Total recall" in 1990 [16]. Optical motion capture systems such as Vicon [17] and Tracklab [18] are commercial systems used in many recent kinematical researchers. These systems offer precise human motion measurement with the requirements of costly high-speed cameras and purpose-specific facilities.

Other researchers focused on gesture control with electronic sensors such as infra-red (IR) LEDs. A gesture recognition software for advanced smart phones was presented by Ki-Ho Kong in 2013 [19]. The leap motion sensor uses IR sensors to scan finger movements within 8-cubic-feet above the device [20]. Kinect is a commercial light-weight marker-less optical system which has been introduced in many recent kinematical studies [85][86]. Although these light-weight systems are not as costly as a professional motion capture laboratory, the limitation of having a fixed position measuring reference such as a camera or other optical sensors still exists.

In clinical and kinematic research, the traditional method of using angle measuring tools, such as goniometers, is not accurate and reliable enough according to some recent studies [21]. With the development of inertial sensors technologies, inertial measurement unit (IMU)-based motion capture systems have been introduced in the study of human motion. A project about simple pose capture using IMUs and other micro sensors was developed by Z. Zhang et al in 2009 [22]. In 2012, S.Oniga and I. Orha demonstrated a basic hand gesture recognition system by combining accelerometers' measurements and radio signals [23]. N. Abhayasinghe and I. Murray developed a human gait recognition method using IMUs in 2014 [9]. In occupational health research, prototype systems using inertial sensors have been developed and validated. M. El-Gohary and J. McNames developed a novel human joint tracking method using an unscented Kalman filter (UKF) and two IMUs in 2015 [24]. The method was validated with an arm simulation robot model. D. Alvarez et al. developed a prototype system to measure the full upper limb joints movements in 2016 [25]. Their methods were validated with a pan and tilt robot mechanism under continuous dynamic conditions.

In the commercial market, wearable sensors products have been released for many purposes. The Nike fuel band is an excellent example of the use of IMUs in commercial wearable devices to count the users' steps and synchronise data with a smartphone's GPS signal [26]. The control VR demo presented on 15th June 2014, used multiple IMUs attached on gloves to capture gestures. It was calibrated with a camera using a sensor attached to the user's neck [27]. Yost Lab's 3-space sensor [28], X-IMU [29], Xsense [30] and Opal sensors [31] are other commercial sensor systems supporting kinematic data measurements. By the date this thesis was drafted, more research using IMUs has been published. Some of the most recent IMU based studies and commercially available products are discussed in the following section.

2.3 Inertial Sensors and Existing Work in Sensor Fusion Algorithms

2.3.1 Inertial Sensors

An inertial sensor is commonly referred to as an inertial measurement unit (IMU). It measures acceleration (gravitation), rotation (angular velocity), and magnetic field strength by using a combination of accelerometer, gyroscope and magnetometer. Most IMU-based, human movement analysis systems use sensor fusion algorithms for orientation estimation [9, 10, 32, 33]. The individual devices included in an IMU are discussed in the following subsections.

Accelerometer

Accelerometers measure linear acceleration in three dimensional axes. They are also regarded as gravity sensors as their readings are equivalent to gravitation measurements when the sensor is static or under low speed movements [34]. Modern micro electro-mechanical systems (MEMS) accelerometers consist of a microscopic cantilever beam with a proof mass. The proof mass deflects from its neutral position under the external acceleration influence [35].The deflection is encoded under a certain ratio of the accelerometer's maximum measurement scale.

By using Trigonometric algorithms, the gravitation readings can then be used to calculate the sensor's orientation and position. Figure 2.1 shows an example when net acceleration R is measured by the sensor.
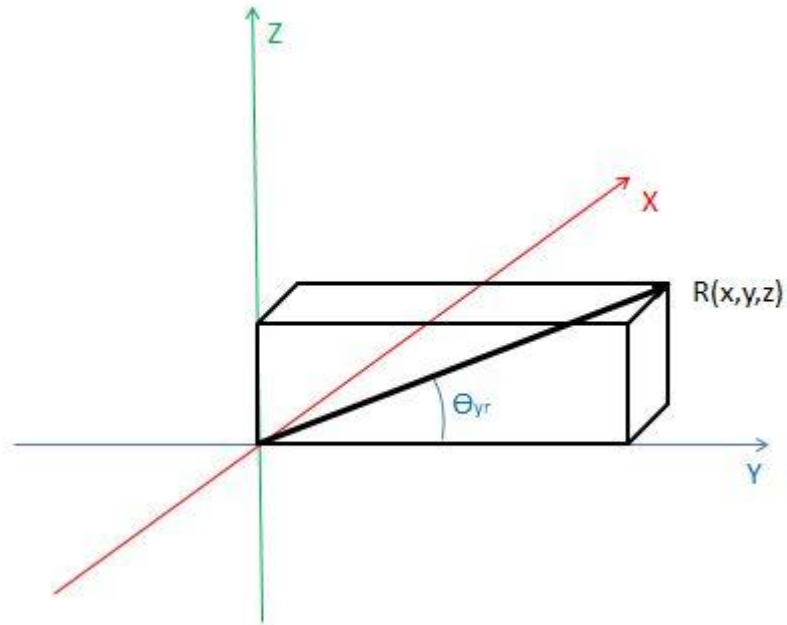
Figure 2.1: Example of orientation frame

In Figure 2.1, the orientation angle between y axis and net acceleration R can be calculated as:

$$\theta_{yr} = \arccos(\frac{y}{\sqrt{x^2 + y^2 + z^2}})$$

Where x, y, z are the acceleration measurements taken from each axis [36]. As the accelerometer is only influenced by gravity when static, the angle between each measuring axis and earth gravitation axis can be calculated as:

$$\theta_i = \arccos(\frac{Acc_i}{g}) \qquad\qquad (2.1)$$

Where θ_i , the angle between i axis and earth gravity axis, can be calculated from the i axis's acceleration reading and earth gravitation [36]. Equation 2.1 is used in yaw, pitch and roll orientation systems. [9, 10, 11] Accelerometer's measurements will only be accurate under static or very slow movement situations when there is low motion noise [37].

Gyroscope

A gyroscope is a device used to maintain or measure orientation. The device is based on

the theory of conservation of angular momentum which involves a spinning rotor in one of the axes. With a spinning rotor, the spin axis will be maintained in one direction due to inertia [38]. In digital systems, a MEMS gyroscope is used to detect rotations. A sensing arm and several parallel drive arms are attracted to the centre stator, vibrations caused from the rotation produces sensing motion between the sensing arm and drive arms [39].

As a gyroscope is measuring angular velocity on each axis, the rotation angle on each axis can be defined as:

$$\theta_i(n) = \sum_{i=1}^{n}\left(\omega_{gi}(i) \times \Delta t(n)\right) \hspace{3cm} (2.2)$$

Where θ_i is the rotation angle on the i axis and ω_{gi} is the angular velocity in °/s measured with gyroscope. Δt is the time lapse between two measurements [36]. However, a low cost MEMS gyroscope usually contains more than 5% error in readings, which causes drifting white Gaussian noise error when adding the velocity readings up [40]. Figure 2.2 shows how the rotation output based on gyroscope drifted up when the sensor was static.
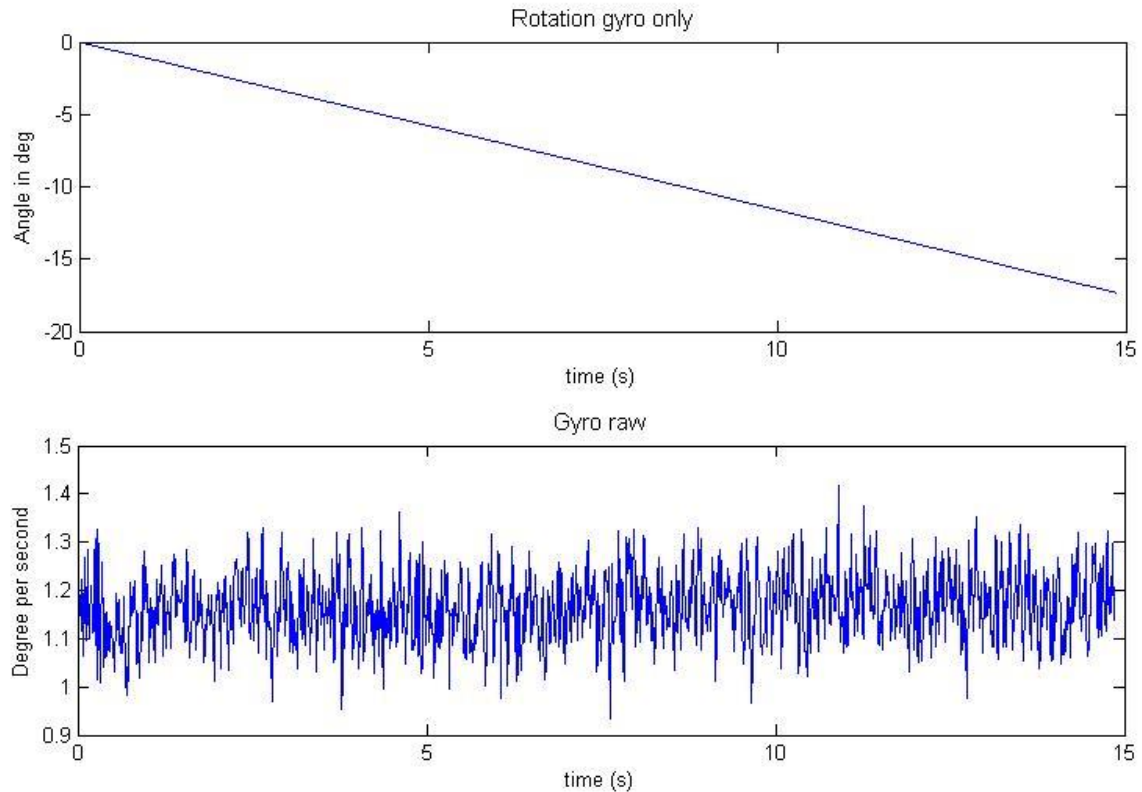
Figure 2.2: Gyroscope drifting output

As shown in Figure 2.2, the rotation angle calculated using equation 2.2 was clearly drifting up instead of remaining in zero as the sensor was static during measurements. The bottom plot shows the gyroscope's mechanic noise in raw readings when the ideal reading is expected to be zero.

Magnetometer

A magnetometer is an instrument for measuring the strength a magnetic field. In modern digital devices, a magnetometer is usually used as an electronic compass [41]. Magnetometers provide measurements of the earth's magnetic field at the current location. However, magnetometer readings are easily affected by environment changes and are not able to provide consistent, stable and accurate orientation measurements [42, 43]. Magnetometer readings captured in all the trials in this thesis were not used, but kept for future reference as it was conveniently available. As the primary focus was on human joint angle measurements, magnetometer readings were excluded in the current

sensor fusion methods.

2.3.2 Existing work in sensor fusion algorithms

As discussed in previous paragraphs, both accelerometer and gyroscope are limited in angle measurements under certain conditions. Sensor fusion algorithms were developed to compensate both gravitation and angular velocity measurements in order to improve the accuracy of angle measurement. In orientation estimation studies, the current orientation angle on one measuring axis can be presented as:

$$\theta_c = \theta_0 + \theta_r \qquad (2.3)$$

In equation 2.3, the current orientation angle θ_c can be split into the sum of the initial angle θ_0 plus total rotation θ_r. Since gyroscope can only track angular rate, the initial angle of gyroscope output is always zero [39]. The initial angle can only be measured with accelerometer using equation 2.1. Thus, the most basic sensor fusion method using accelerometer and gyroscope in orientation estimation can be represented in the following equation 2.4.

$$\theta_c = \theta_{a0} + \theta_g \qquad (2.4)$$

Where the initial angle in equation 2.3 is measured by accelerometer as θ_{a0} and the rotation angle θ_g is the gyroscope output [37].

Complementary filter is one of the most basic and widely used sensor fusion methods involving IMUs [44, 45]. It fuses the accelerometer through a 1st-order low pass filter and adding gyroscope's output through a 1st-order high pass filter.

$$\theta_k = h(\theta_{k-1} + \omega_k \Delta t) + l(a_k) \qquad (2.5)$$

Where θ_k is the estimated angle, $\omega_k \Delta t$ is the gyroscope's angular velocity measurement times the sampling time, a_k is the angle output based on accelerometer. The sum of the high pass filter factor h and low pass filter factor l is always 1 [46]. The idea of complementary filter is to use the gyroscope's output to track details of angular change, and use the accelerometer's measurements to cut down the gyroscope's drifting problem. Complementary filter is the basic concept of other advance sensor fusion algorithms. It is a fast and simple method to be implemented in orientation estimation systems.

A constant high pass and low pass filter factors are not flexible enough to identify environmental influences on accelerometers and gyroscopes. Kalman filters introduce a dynamic filtering factor which is selected based on a number of matrix computations [45, 46]. Several studies have been successful in producing accurate orientation measurements using Kalman filters [47, 48]. However, Kalman filters normally require heavy computational data loads, which would not be efficient enough for clinical trials with fast sampling rates [32, 45].

Robert Mahoney et al. [49] presented the use of nonlinear complementary filters on special orthogonal groups. The methods applied a 2nd order, single-axis filter to each coordinate separately. These methods require a PI controller to correct angular drifting error. Premerlani and Bizard [50] followed Mahoney's algorithm and developed a direct cosine matrix in a model plane's altitude adjustment. Sebastian Madgwick presented a Gradient Descent based Orientation Filter (GDOF) using a quaternion representation and added magnetometer sensor readings into the algorithm [51]. The use of a magnetometer in the Madgwick's algorithm requires geo-coordination calibration, and its magnetic field measurements are susceptible to interference by any nearby metallic or magnetic object [52]. Both Mahoney's and Madgwick's algorithms were feasible choices for altitude and heading reference system where the gravitation vector is sufficient. However, the computation and implementation would be significantly complex in human joint angle measurements.

2.4 Human joint measurement systems

2.4.1 Simple poses upper limb modelling system

Zhang et al. [22] have developed an upper limb motion capture model using wearable micro-sensors. The project developed an extended Dynamic Bayesian Network (DBN) [53] using accelerometer and gyroscope to model the constraints among human body segments. The method used each sensor to represent a single human body segment. A drift modelling algorithm was developed to define and cancel the drifting bias throughout time. As a result, the system could accurately capture human pose. However, the system has limitations in capturing complex movement because the drifting cancelling process works better in static situations. As a body segment modelling system, it was also not focused on measuring precise joint angle.

2.4.2 Single Thigh mounted IMU based gait modelling system

Abayasinghe et al. [9] have done research on human gait modelling for infrastructure-free, inertial navigation tools to help visually impaired people. They used a single thigh mounted IMU to estimate thigh flexion and extension. Gait models were developed to estimate level walking, step length and gait phases. A zero crossing detection method was introduced in the gyroscope based algorithm for step counting which delivered a 97% step counting accuracy for level walking at different speeds. A single axis orientation estimation algorithm was developed and validated against an optical system. The root mean square error reported was less than 2.5 °. The algorithm was based on gyroscope's readings and only used accelerometer's data when static. Although the algorithm works well in thigh angle measurement and gait analysis, it has limitation in measuring other human joint parts where there is not a zero crossing event that could be used for drift calibration.

2.4.3 IMU-based joint angle measurement using the kinematic constraints

Seel et al. [11] developed methods for joint axis estimation and joint position estimation that exploit the kinematic constraints. Their method used one IMU on each human

segment across a joint, and the difference in angular velocity was the main source in spherical joint angle estimation. The method was tested for gait analysis using a 40 Hz sampling rate. The result only proved the concept that the methods can define the initial joint angle on the kinematic constraints models. The details of the results on the output accuracy were not provided. A large amount of data was required in their four-dimensional estimation algorithm, as predicted. The application of this method is limited in high sampling rate systems, and in the study of more complex human joint movements.

2.4.4 Calibrated 2D angular kinematics by single-axis accelerometers

Bagala et al. [37] developed a method to estimate multi-link angular kinematics in the sagittal plan using single axis accelerometer and a reference system (encoder or stereo-photogrammetry). The method calibrated dynamic accelerometer readings by estimating the sway angle. The sway angle was the angle caused by angular acceleration. An algorithm was developed to correct the sensor reading with estimated gravitational acceleration. The method was resulting in less than 1 °RSME for both shank and thigh angle measurements. The limitation of the method was it had a restricted requirement of sensor positioning. As the measurements were heavily depended on gravitational acceleration, the method was not applicable under rapid movements.

2.4.5 Human joint angle estimation and validation

El-Gohary et al [24] have developed a novel human joint tracking method using an unscented Kalman filter (UKF) with two sensors representing two segments of the human body. The method was validated with a robotic arm which produced repeated peak to peak flexion and extension angle movements. Results showed a 3 °average RSM angle error and less than 10 °peak error. Although a 3 °average RSM angle error for 15 minutes dynamic movement trials was good for motion tracking, the system would not be a reliable choice for peak human joint angle measurements.

2.4.6 Upper limb joint angle measurement in occupational health

Alvarez et al. [25] have developed a prototype system for upper limb ambulatory measurements. Four IMU sensors were attached to the participant's chest, arm, upper limb and hand. A global axis frame was defined with the initial position of the four sensors. A robot validation test was used to validate the feasibility of the system. A pan and tilt unit with two degrees of freedom (DOF) was used to simulate hand movements. With a sensor placed on the table simulating a static forearm, the sensor measurement accuracy was validated with the robot angles. Results showed a $2\,°$ to $10\,°$ errors range depending on the rotation axis. The result was reported as feasible to use in occupational health research. However, the validation tests did not show how the system performed without having a sensor as static reference. The method's global axis frame required the sensors to be at a defined initial position, which would be a limiting factor in many human tests.

2.4.7 Commercial wireless IMU measurement systems

Commercial sensor systems are usually expensive. A single wireless sensor with supported data processing software can cost hundreds, if not thousands, of dollars. Yost Labs' 3-space sensor [28] uses quaternion-based orientation filtering algorithms. The basic version using Bluetooth low energy for wireless communication cost 130 US$ per unit. X-IMU [29] uses gradient descent based orientation filter and cost £249 for one single device with supporting software. Xsens MVN [30] is a high end human motion analysis system with a biomechanical software model. The cost of Xsens MVN is £1200. Another high end human motion analysis sensor is the Opal sensor produced by APDM wearable technologies [31]. The Opal sensor has the ability to store data locally which prevents data loss associated to the transmission rate. The opal sensor requires a quote in advance of purchasing and the price is relatively expensive compared to other commercial products. X. Fang et al. published a normative gait database of 292 healthy adults using the APDM Movement Monitoring inertial sensor system in January 2018 [54].

2.5 Summary

Many physiotherapy and kinematical studies require a precise analysis of human joint movements. The objective of the research work reported in this thesis was to develop an economic and flexible solution to measure human joint movement. A literature review was conducted to track down the direction of motion capture methods using IMU based systems. Inertial sensors and existing sensor fusion algorithms were discussed in this Chapter. Based on the study of sensor fusion algorithms, a lighter and more effective human joint angle measuring method was developed as reported in Chapter 5.

The literature review on human joint measurement systems provided a panoramic view of the different approaches followed in human joint studies. The outcomes and limitations of the research reported in the literature were also discussed. Motion capture systems reported in studies [9, 11, 22, 25] require a standard set position during the measurements. The RSME output in studies [9, 24, 37] is not good enough for   human joint measurement studies as RSME did not fully interpreted the performance of the sensor when measuring peak angles. Research reported in studies [11, 25, 37] used robotic systems to validate sensor performance for clinic applications. Such validation methods did not completely describe the properties of sensors system under specific situations. In this thesis specific and objective sensor validation methods are presented in Chapter 6.

This page is intentionally kept blank.

Chapter 3

Methodology

3.1 Research method used

The main objective of the research is to develop a flexible, low cost motion measurement solution for medical research to precisely identify and capture human joint movements. As a cross field study, knowledge about both motion capture technologies and human joint movement is required. The scientific method was used to conduct a logical and objective procedure for the research [55, pp. 10].

In order to have a better understanding on motion capture and modulating technologies, the "extensive literature survey" method [55, pp. 13] was followed. A broad literature review on motion capture applications was carried out. Also, a study on electronic sensors was carried out to expand ideas and plan the future design. A systematic study of problems with human joint measurement studies found gaps where engineering solutions might apply.

This research was carried out in collaboration with a medical research team studying human wrist movement measurements in cerebral palsy patients. This collaboration had a major influence in this research. As discussed in section 2.4, the solution for identifying human wrist joint movements can be expanded to capture human joint movement in other medical applications. This research followed the problem solving and validating cycle shown in Figure 3.1.
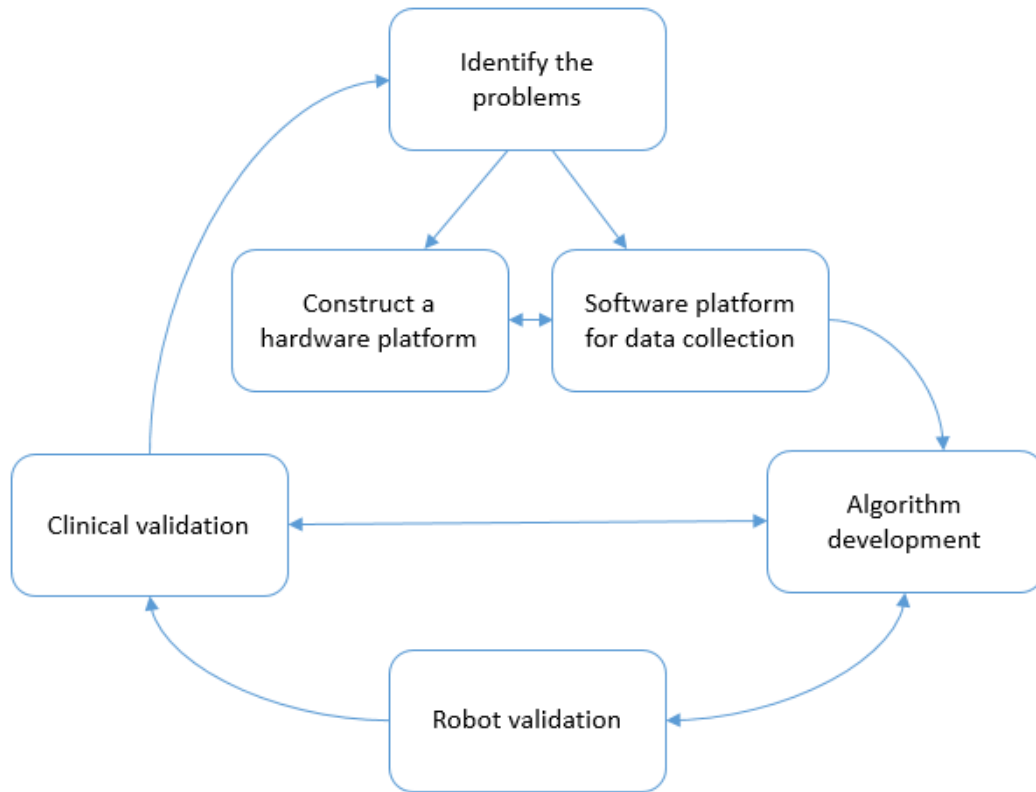
Figure 3.1: Research method flow chat

The method represented in Figure 3.1 involves the following activities: "Execution of the project", "Collecting the data", "Analysis of data" and "Hypothesis testing" [55, pp.18-19].

Principally, a human joint measurement study requires a considerable amount of data collection and taking measurements from a defined object. In Figure 3.1 identifying the problems means defining the object needed to be measured and understanding its purpose. As the cerebral palsy wrist study requires a certain level of accuracy in wrist flexion and extension measurements, ideas about how such movements can be captured were expected to come out based on these requirements.

Once the problem and the objective were clear, a model for collecting the wrist movement was produced. A sensor data collection terminal was designed and developed.

With the system converting human joint movements into sensor reading signals, an algorithm was developed to analyse the raw measurements to obtain experimental results. As figure 3.1 shows, robot-based validations as well as clinical validations with real patients were performed to verify the algorithm's outcome. Issues related to the size of the sensor and the system's stability were identified during clinical trials and used to further improve the data collection method.

3.2 Construction of a hardware platform

A prototype system including wireless measurement sensors and a matching receiver dongle to achieve basic movement monitoring and measuring was developed for a research team working in collaboration with Princess Margaret Hospital (PMH). Then, further research was carried out to design a more accurate, flexible and stable portable motion capture system. Details of the structure of the hardware platform are discussed in Chapter 4. The outcome was a stable, wireless and small size joint movement capture system. The receiver had to be able to communicate with multiple sensors in real-time.

3.3 Software platform for data collection

Once the hardware platform was built, a computer program for data collection was developed. The program offered all the basic functions like a data terminal with a channel matching the hardware design. As part of the collaboration with the medical research team, the software also addressed the needs of clinical use, like data management features. The data analysis algorithm was also built into the software after successful validation. The information of the data collection software can be found in section 5.2 and 5.3.

3.4 Algorithm development

An algorithm was developed to determine angles from the raw reading of sensors. The cerebral palsy wrist study required the measurement of flexion and extension; hence the algorithm needed to provide an efficient filtering model to produce highly accurate

results. A highly optimized algorithm was also preferred to lower the requirement of the running platform and expand the potential to do real time analysis. Algorithm developments are discussed in Chapter 5.

3.5 Validation

Validation was one of the major focuses in this research. The outcome of validation was used to determine the accuracy of motion measurements and the efficacy of the solutions proposed in this research.

As mentioned in the section 2.4, there is no clear standard of wrist angle measurement, and the current method to determine its orientation has many limitations. In contrast, a robotic system can be controlled with a certain level precision. Thus, robotic arms simulating wrist movements were used to quantify the accuracy of the sensor system.

The clinical validation was conducted in collaboration with the team working in cerebral palsy research. The purpose of these experiments was to determine the ability of the sensor system to measure actual human wrist motion. The outcome of clinical validation verified the feasibility of the proposed solution.

Details of the validation process including setup, results and discussion can be found in Chapter 6.

Chapter 4

Hardware platform

4.1 Introduction

As mentioned in previous chapters, one of the major purposes of this research was applying the proposed system in medical applications and real clinical practice. The hardware platform was designed to meet the following requirements: high accuracy in joint orientation measurements, wireless communication, reduced size with wearable ability, and high data collection capacity. Three versions of custom-made sensor models were developed in order to achieve a better performance and a smaller size to serve the need for young age children cerebral palsy studies. Details of the hardware platform are discussed in the following sections.

4.2 High-level design

4.2.1 Sensor Hardware description

Figure 4.1 shows the high level description of the developed system. The system includes several wireless sensors that are attached on the articulation of interest for motion capture. Sensors send their acquired data to a receiver dongle connected to a local computer to collect the data for further processing.
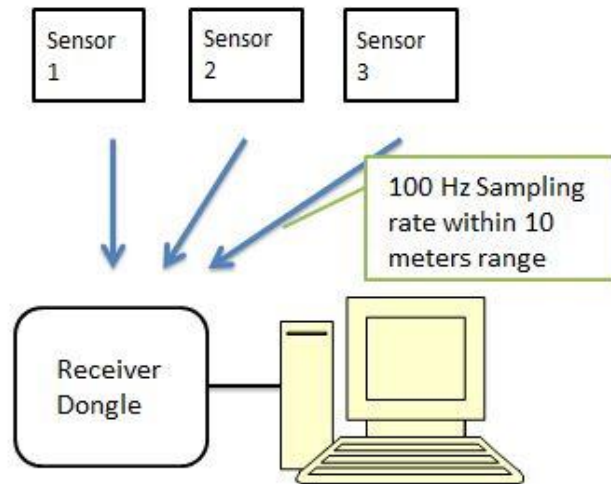
Figure. 4.1: Design block diagram. All sensors wirelessly send raw measurements to the computer at a 100 Hz sampling rate via the receiver dongle.

Figure 4.2 shows version 3 of the wireless sensors together with its 3D printed case and a 5 Australian cent coin for comparison. Each custom made sensor consists of an 8-bit AVR core microprocessor, an inertial measurement unit (IMU) and a 2.4 GHz Radio frequency (RF) radio. Each sensor is powered by a small, 90mAh, 3.7 V rechargeable lithium polymer battery that can support up to 3 hours non-stop measuring time on one charge. The green box in Figure 4.3 contains the receiver dongle.
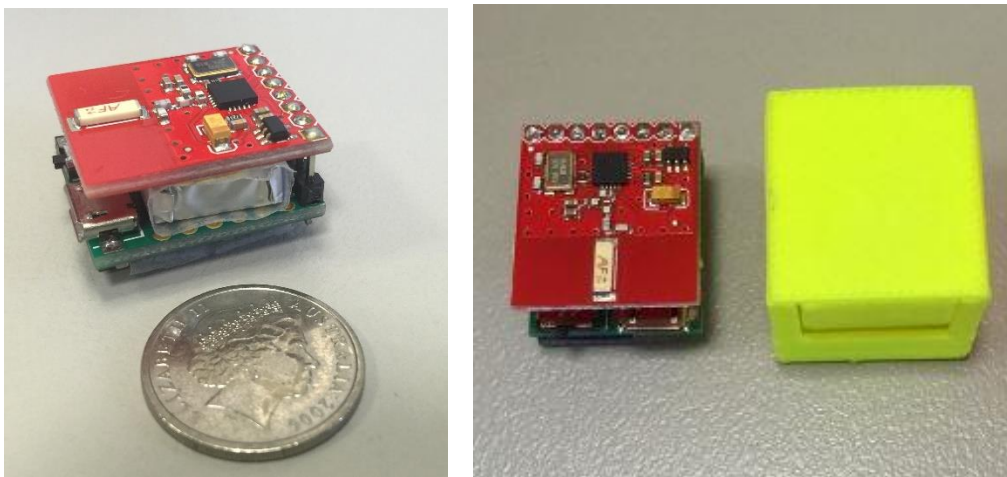
Figure. 4.2 Wireless sensor device with a 22mm × 24mm × 18mm case (right); Side view of the custom made IMU sensor next to a 5 Australian cent coin.
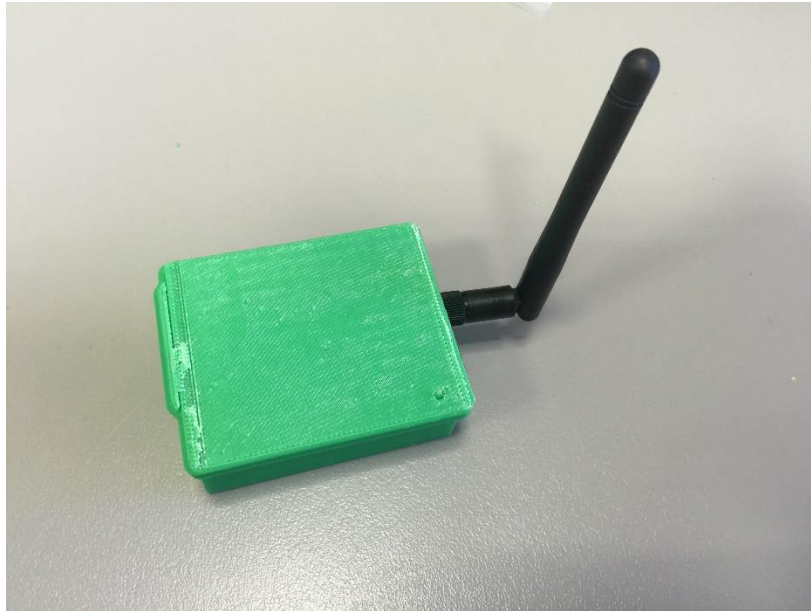
Figure. 4.3 Receiver dongle with case

The receiver dongle (see Figure.4.3) communicates with the sensors via an RF radio channel and data are sent to the computer via a serial communications link. The receiver dongle includes an Arduino Uno microcontroller board[56] with an antenna-based 2.4 GHz RF radio. The antenna boosts the signal strength to provide a better data drop rate than radios with chip antennas. Details of the communication comparisons are discussed in section 4.3.1.

The custom-made sensor was made of four major parts as shown in Figure 4.4, which includes an inertial measurement unit (IMU), a custom-made microcontroller, a radio frequency (RF) radio [57] and a lithium polymer (LIPO) battery [58].Figure 4.5 shows a 3D view of the sensor's components and their assembly.
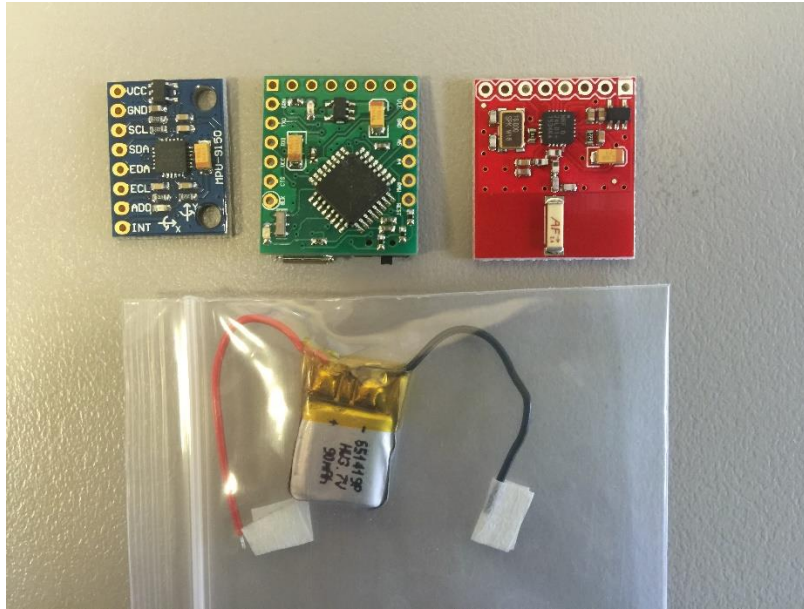
Figure 4.4: Devices and battery included in the IMU
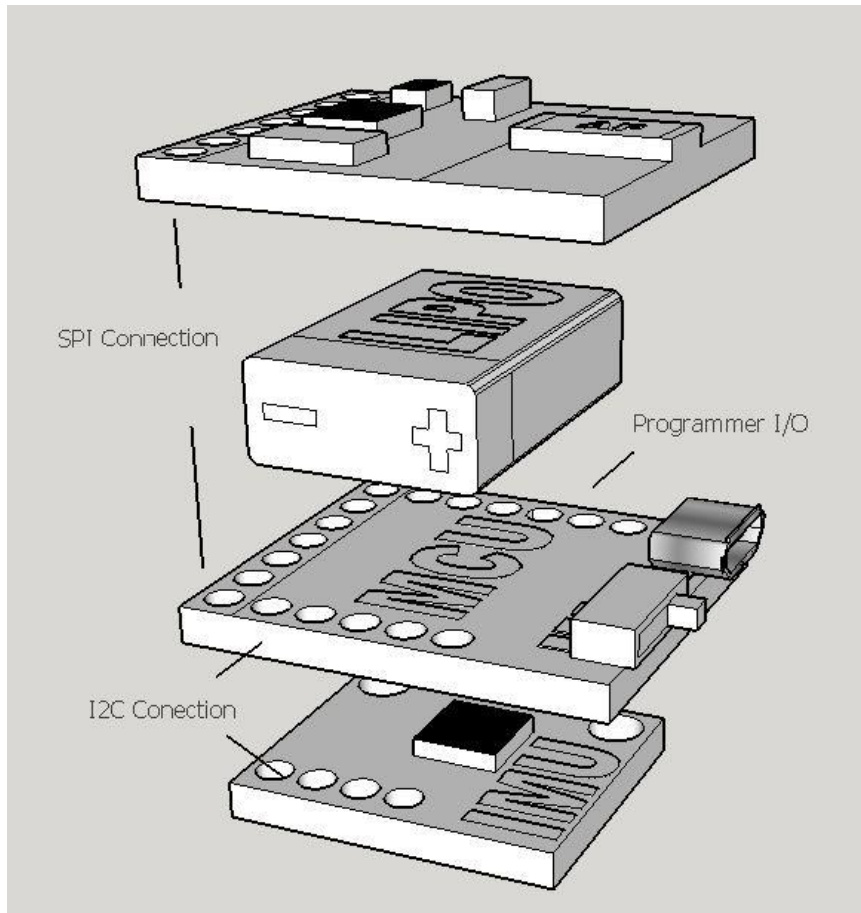
Figure 4.5: 3D model of sensor implementation with RF radio board on top

As shown in Figure 4.5, the radio device was set on the top while the IMU was set flat at the bottom of the stack. Both the radio chip and the IMU chip were directly connected into the microcontroller's connection pins. The radio connects to the microcontroller through a Serial Peripheral Interface (SPI) port [59]; while the inertial measurement unit uses an Inter-IC (I^2C) connection [60]. The receiver dongle in Figure 4.3 used an off-the-shelf Arduino connected with the same radio used in the sensor.

4.2.2 Specification

The inertial measurement sensor used in this research was the MPU–9150 by Invensense [61]. This IMU features a 9 degree of freedom motion sensor that consists of a 3–axis accelerometer, a 3–axis gyroscope and a 3–axis magnetometer. The sensor supports both I^2C and SPI interfaces. Table 4.1 shows the key specification of the MPU-9150:

Table 4.1: Key specification of MPU-9150 [61]

Specification	Accelerometer	Gyroscope	Magnetometer
Measurement Ranges	±2 g, ±4 g, ±8 g. ±16 g	±250 ^{o}/s, ±500 ^{o}/s, ±1000 ^{o}/s, ±2500 ^{o}/s	±1200 µT
Measurement Scales	16384 LSB/g, 8192 LSB/g, 4096 LSB/g, 2048 LSB/g	131 LSB/ ^{o}/s, 65.5 LSB/ ^{o}/s, 32.8 LSB/ ^{o}/s, 16.4 LSB/ ^{o}/s,	0.3 µT/LSB
Zero-point Offset	±80 mg x axis, ±80 mg y axis, ±150 mg z axis	±20 ^{o}/s	±1000 LSB
Sensitivity scale factor tolerance	±3 %	±3 % at 25 ^{o}C, ±0.04 %/^{o}C (−40 ^{o}C, +85°C)	N/A
Operating Voltage	2.375 V − 3.465 V		

The MPU-9150 was configured with the smallest measurement range settings in order to obtain the maximum precision and be able to detect small movements in human joint measurement trials in more detail.

The radio module used is the nrf24l01+ 2.4 GHz transmitter from Nordic Semiconductor [62]. It contains an on-board 3.3V LDO Regulator allowing a power supply of up to 7V. With the on-board ceramic 2.4 GHz Antenna, the radio can reach 100m range at 250kbps. The data rate of the nrf24l01+ is from 250kbps to 2Mbps. The 2Mbps data rate was used with 10m range. The sampling rate for each sensor was set to 100 samples per second. Every sample package contains eleven 16-bit values carrying the 9 degree of freedom motion measurements from the tri-axis IMU plus a sensor ID and a timestamp.

The custom-made Arduino-compatible microcomputer used an Atmel Atmega 328, 8–bit microcontroller [63] and an 8 MHz crystal. Both the schematic design and PCB footprint design is attached in Appendix A.

A 3.3 V voltage regulator was used to make the microcontroller board compatible with both the MPU-9150 IMU and the nrf24l01+ radio. The small size and high energy density of 3.7 V lithium polymer batteries make them the most suitable power source for a 3.3 V system. A 90 mAh capacity was selected due to the space limit in the sensor design.

4.3 Evolution

4.3.1 Prototypes

The first set of prototype sensors was produced in early 2015. It used an 8 MHz Arduino mini pro [64] as the main processor (Figure 4.6).

Figure 4.6: First prototype sensor set with Lego shaped cases

The prototype set was built to prove the concept to the cerebral palsy research team in Princess Margaret Hospital, Western Australia. Measurements acquired showed that the prototype sensor was able to capture human wrist joint movement. The data-capture algorithm included a basic filtering algorithm. The sampling rate was set to 30Hz. The sensor case was 3D printed as a colourful Lego block to attract young age participants' interest so that they would be more willing to wear these sensors in trials.

There were three versions of sensors developed and distributed to 6 research facilities and clinics throughout Australia to support the bigger picture of paediatric cerebral palsy research. Figure 4.7 gives a comparison to all the three versions of the custom made sensors.
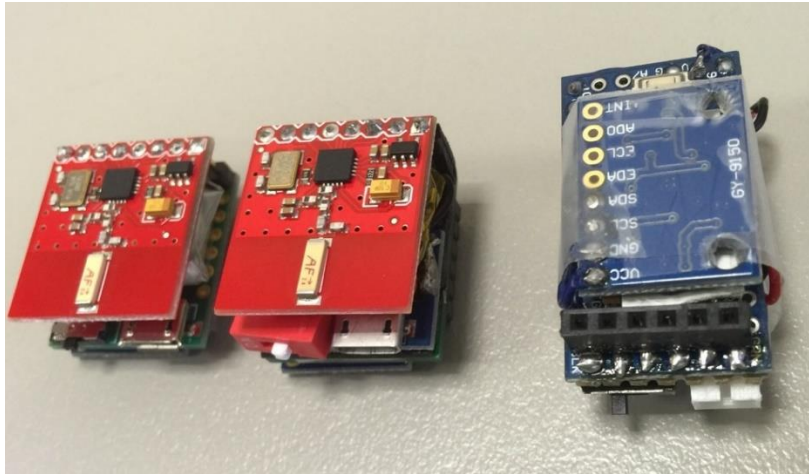
Figure 4.7: Version 1 sensor device (right); Version 2 sensor device (middle); Version 3 sensor device (left)

The version 1 sensor at the right of Figure 4.7 was designed and implemented in 2015, it was similar to the prototype sensor in Figure 4.6, with a better layout organization. However, placing the IMU on the top created an initial offset due to inconsistencies in the assembly of the stack. Another problem was that the radio antenna was partially blocked in the middle of the stack and it signals were weakened which produced a high data drop rate.

Version 2 of the sensor was designed and implemented in 2016. In this version a custom made microcontroller unit (MCU) replaced the Arduino mini pro board. The new MCU had a clearer layout organization, had less components and shorter traces. The I/O pins were positioned to match the radio and IMU's, thus avoiding the risk of loose wires and faulty soldering. The clearer layout design with short signal traces and wider ground planes also reduced the electromagnetic interference (EMI) [65] which increased the reliability of the entire system. A new off-the-shelf chip antenna RF radio was selected to improve communication performance. The IMU device was lying flat at the bottom which reduced the initial offset problem.

Version 3 of the sensor was designed in 2017. It further reduced the physical size to be used in cerebral palsy baby trials. The entire design was wire-free between modules so that the reliability was further improved.

4.3.2   Communications

Besides the improvements on the size of the sensors, the sensor evolved to be more stable during data collection. Figures 4.8 to 4.11 show the communication performance of different versions of the sensor. All the graphs show the time it took for each data package to be transmitted. Note that the vertical axis shows a different range in each graph.

Although the sampling rate for all the communication tests was set to the ideal 100 Hz, some data drop would always occur because the communication channel was set as one direction communication with no feedback for data drop protection. As many studies use 40Hz to 50Hz sampling rate in human motion measurements[24][66], a 50 Hz sampling rate means taking 50 measurements every second which would be enough for human joint movement capture. However, a data drop longer than 0.2 seconds increases the risk of missing critical measurements, such as peak angle movements and direction turning.

Figures 4.8 to 4.11 show a significant improvement on the communication stability. The latest design dramatically reduced the signal interference produced by the blocked antenna, loose wire connections, and on board EMI interference. Since one of the objectives of this research was to create a medical data collection system, the consistency and stability of data-acquisition was given high priority during the development of the sensors.

All graphs in Figures 4.8 to 4.11 show the sample reciprocal time in seconds per sample (y axis) versus the sample number (x axis). These figures show that communication was generally clean and stable (10 ms/sample) at the set sampling rate. Spikes indicate a longer time for one sample and worse communication performance. As RF communication channel was one way without any reciprocal feedback, it was common to have some data drop due to the communication throughput clashing with multiple sensors talking to the same receiver. A large seconds/sample indicates that some data were missing during the transmission period.
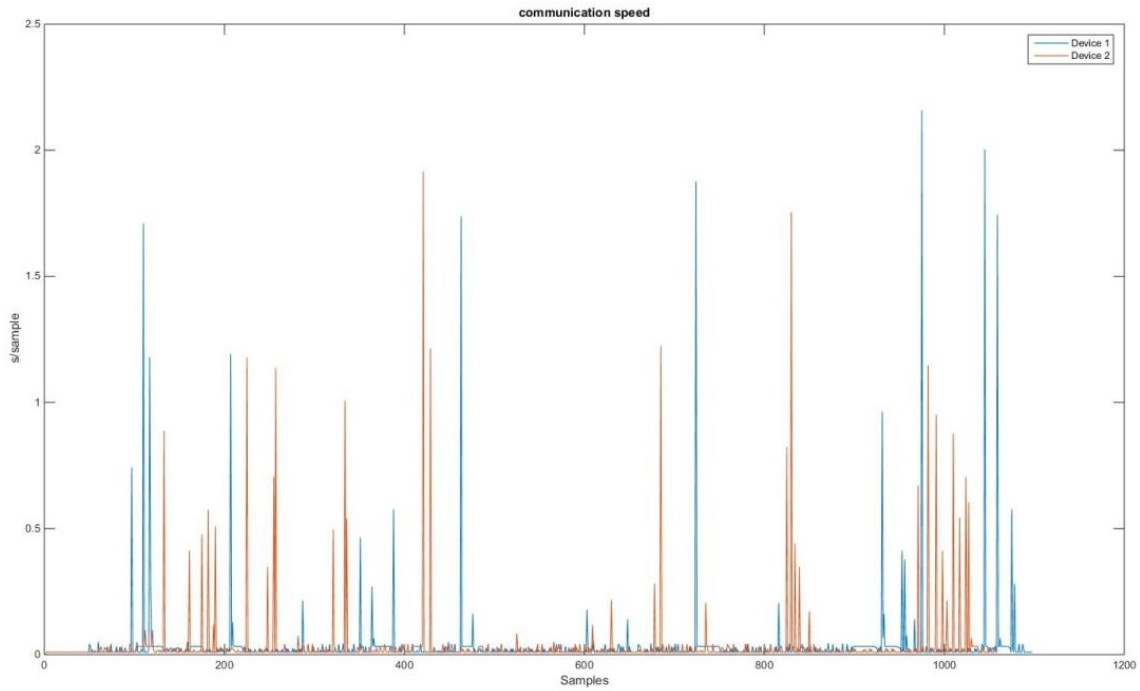
Figure 4.8: Communication performance of version 1 over short period[1]
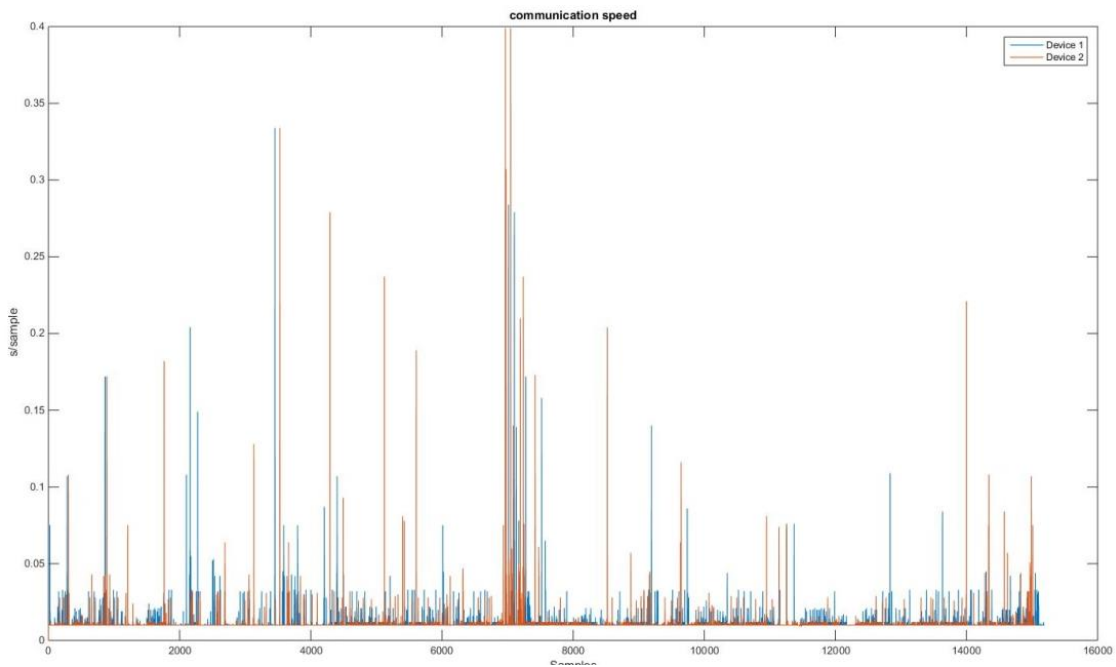
Figure 4.9: Communication performance of version 1 over long period[1]
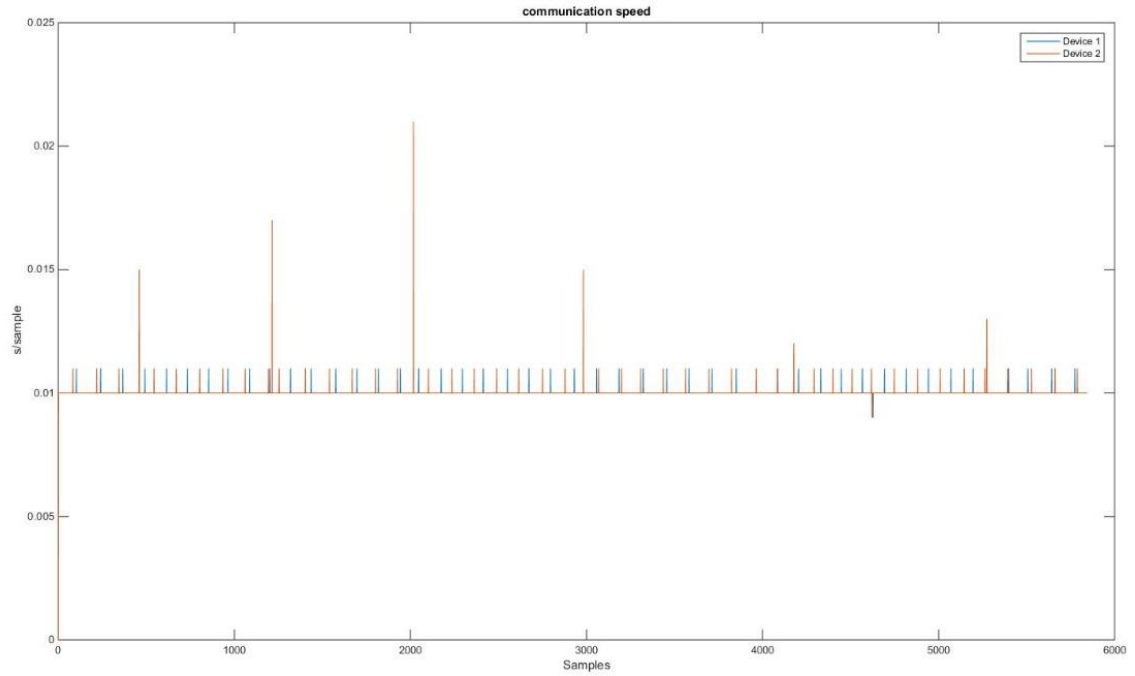
Figure 4.10: Communication performance of version 2[1]
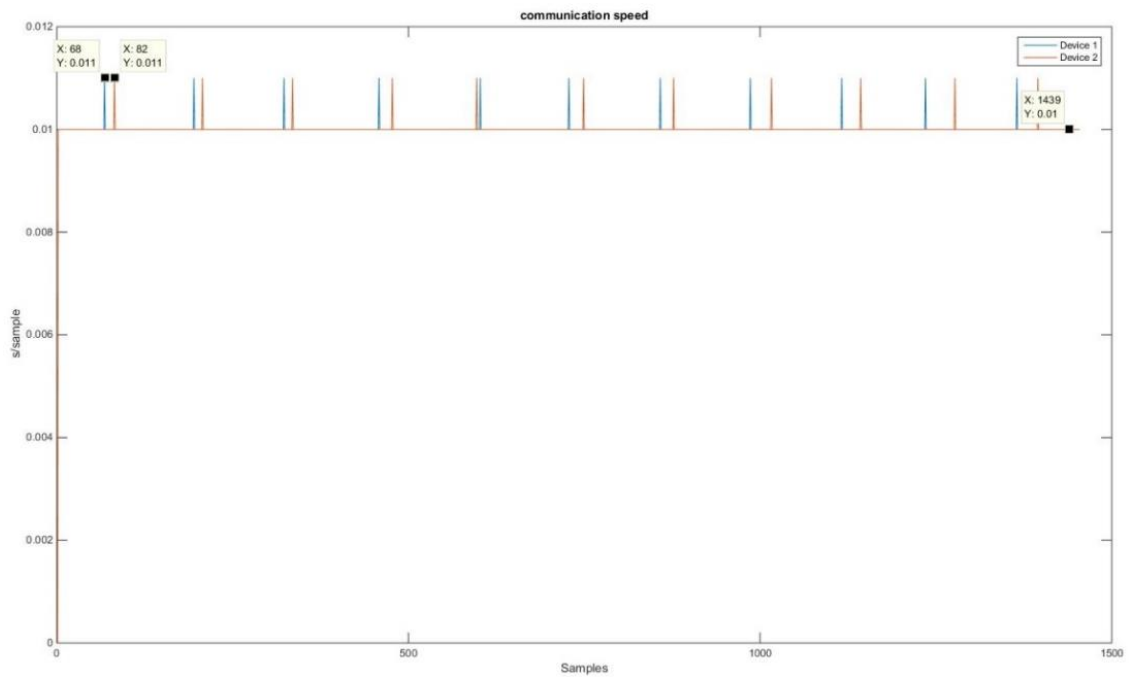
Figure 4.11: Communication performance of version 3[2]

[1] In comparison, the maximum Y-scale of Figure 4.8, Figure 4.9 and Figure 4.10 are 2.5 second/sample, 0.4 second/sample and 0.025 second/sample.

[2] The maximum sampling period captured in Figure 4.11 was 0.011 second.

Another significant communication improvement was achieved by using different types of radios in the receiver dongle. As shown in Figure 4.3, the receiver dongle used an external antenna rather than the chip antenna used in the sensors (see Figure 4.4). The loss in a transmission path can be calculated using Friis's Transmission Formula [67]:

$$L = 20 \times Log_{10}(\frac{4\pi d}{\lambda})$$

Where L is the path loss in decibels, λ is the wavelength and d is the distance between transmitter and receiver. Friis's formula shows that the higher the transmitter-receiver distance d is, the higher the path loss L will be. The path loss can be correlated to signal attenuation, hence a high L indicates a weak signal strength.

Figures 4.12 and 4.13 show the communication status of both the chip mode radio receiver and the external antenna mode radio receiver, with the transmitting sensor recording rapid movements at 5 meters.
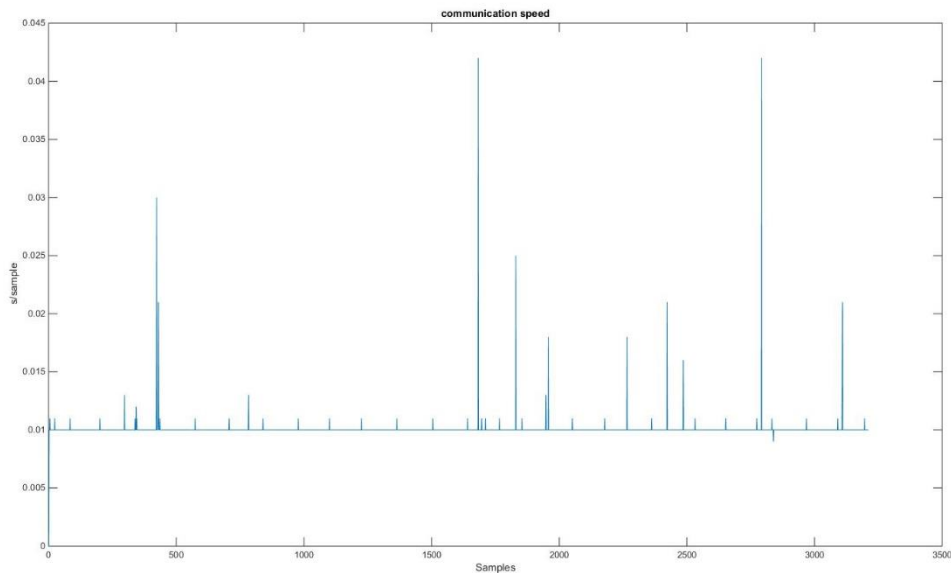
Figure 4.12: Communication performance of external antenna radio
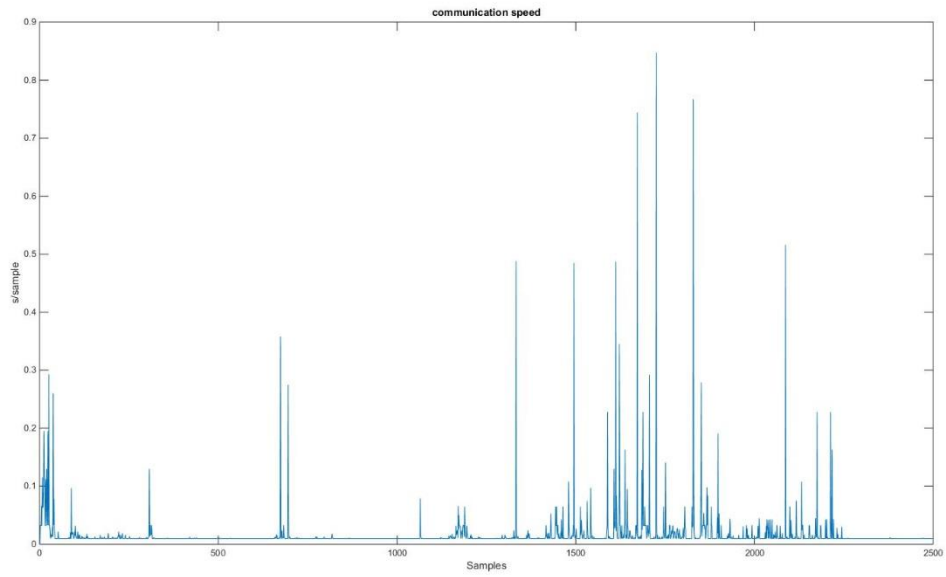
Figure 4.12: Communication performance of chip antenna radio

Both tests reported in Figures 4.11 and 4.12 were performed with the same sensor device at 5 meters range. Figure 4.11 shows minimal noise occurring when the receiver used the external antenna. The worst transition time was 0.04 seconds. Figure 4.12 shows that the communication performance for the receiver with chip antenna was unstable, with big data drops regularly occurring. These results demonstrate that using a radio with an external antenna provides a more reliable communication signal coverage and signal penetration than using a chip antenna radio.

4.4 Summary

The hardware platform designed in this thesis was a multi-sensor system. The system includes several wireless sensors that are attached on the articulation of interest for joint measurement. Sensors send their acquired data to a receiver dongle connected to a local computer via serial communication to collect the data for further processing.

The latest version out of the three versions of sensor is enclosed in a 22mm $\times$ 24mm $\times$ 18mm box. Each custom made sensor consists of an 8-bit AVR core microprocessor, an inertial measurement unit MPU-9150 and a 2.4 GHz Radio frequency (RF) radio. Each sensor is powered by a small, 90mAh, 3.7 V rechargeable lithium polymer battery that can support up to 3 hours non-stop measuring time on one charge. The latest version of receiver with external antenna can read accelerometer and gyroscope measurements transmitted from each sensor at 100 samples per second within a 10 meter range.

Chapter 5

Joint movement measurement and algorithms

5.1 Introduction

This Chapter presents the software platform and algorithms developed as part of this research. The software platform was primarily designed to record live serial data sent by the wireless sensors and collected by the receiver. As part of a medical data collection system, the supporting software application was also featured with user friendly data management functions and live sensor communication status monitoring.

The design and implementation of algorithms was one of the major contribution of the research discussed in this thesis. The algorithms were developed for two-sensor-based joint orientation measurements. Both the high level description and details of the two-sensor-based joint orientation algorithm are discussed in Section 5.3. Further observation and validation of the algorithm are discussed in Chapter 6.

5.2 Data collection

5.2.1 Raw data

As mentioned in Chapter 4, each measuring device developed for the research contained a 9 degree of freedom motion sensor that consists of a 3−axis accelerometer, a 3−axis gyroscope and a 3−axis magnetometer. With system identifier value and time stamp added in front of 9 sensor measurement values, each package of raw data contained 11 parts of independent information. The system identifier includes the batch number and an individual sensor ID at the beginning of the raw data package. The identifier is used to separate measurements from each sensor and prevent clash between different systems. The time stamp is generated when one package is captured and transmitted, and its calculation is based on the processor's internal timer.

Table 5.1 shows the format of each raw data package.

Table 5.1: raw data format

Package	Sensor ID	Time stamp	Ax	Ay	Az	Gx	Gy	Gz	Mx	My	Mz
Sensor transmutation	2-digit Decimal Integer	16-bit signed Binary (2's compliment) each 160 bits in total									
Receiver encoding	ACSII(00 to 99)	ACSII(-32768 to +32767)									

As shown in Table 5.1, each package of raw data measured and transmitted from the sensor contains one 2-digit system ID and ten 16-bit binary measurements. On the receiver side, the raw data is packed into ASCII format [68] as comma-separated values, thus the data can be easily processed by the computer after being collected via USB serial terminal.

5.2.2 Serial terminal data collection software

The user interface was developed as a Windows 7 compatible and executable application, the latest version was compatible with the most recent Windows 10 system. The original purpose of developing the software interface was to create user friendly serial terminal software for physiotherapy researchers to validate sensor data within a collaborative medical research. The collaboration project is discussed in Chapter 7. The application was named as "Serial validation terminal" which directly describes the nature of the interface. With this application, the local computer is able to pick up data through serial communication from the attached receiver dongle and save it into a local CSV file for further processing. The flow diagram in Figure 5.1 shows the design of the software.
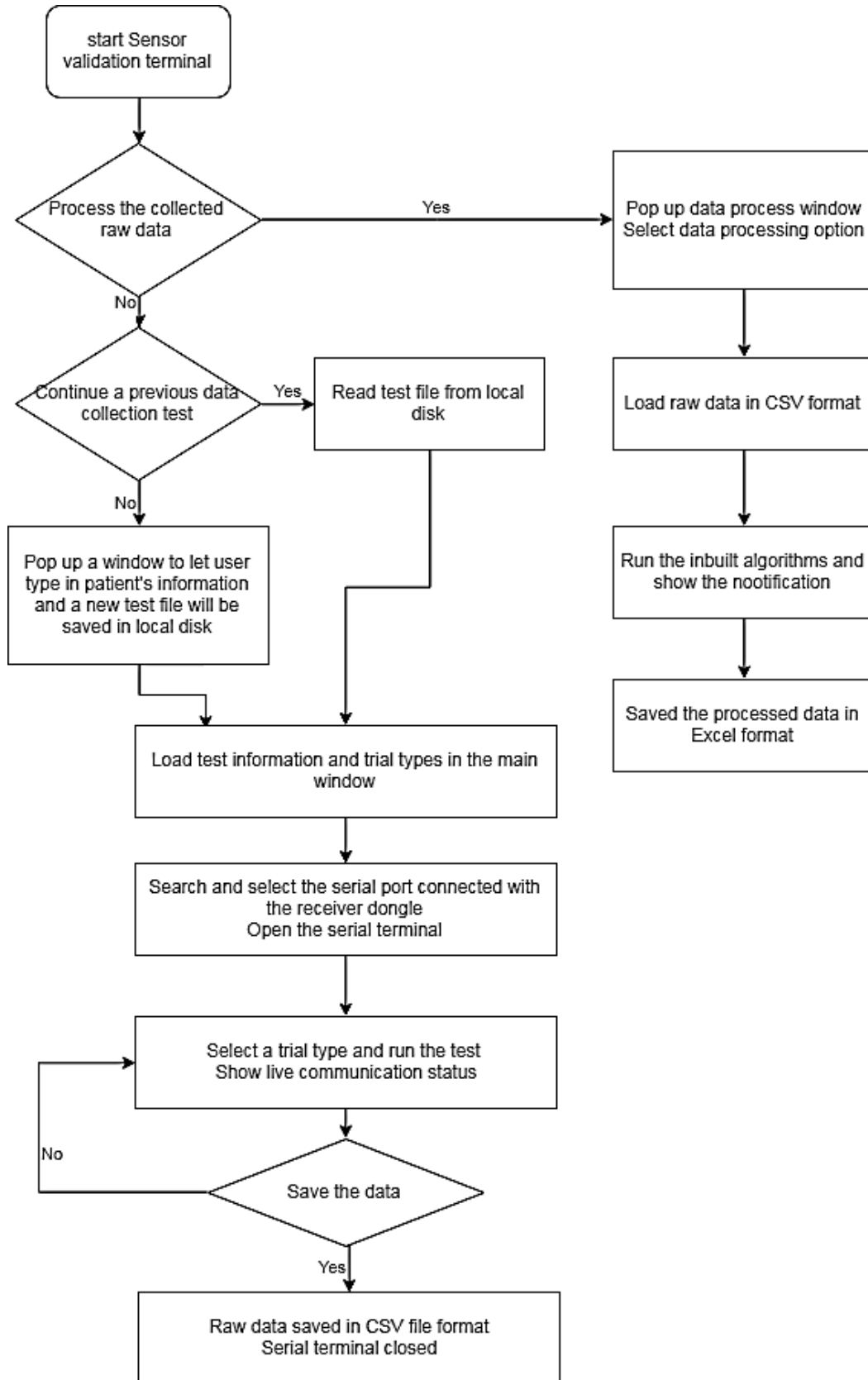
Figure 5.1: Serial validation terminal software flow diagram

One of the biggest concerns about the data collection software was to create a user friendly interface for users with no engineering background. The software also features patient file management and trials data organization. The latest version of the software also includes a data processing function that uses built-in algorithms. The software was developed using programing language C# (Csharp). The biggest advantage of using C# is that it has a user friendly IDE for windows system. It was the most efficient way to make updates base on medical researchers' request about the user interface and new experiments.

The home window of the sensor validation terminal software shown in Figure 5.2 is the main user interface during the data collection process. The patient's information is displayed at the top right area of the window. The software supports up to 10 different, user-created, trial types at the same time. The serial terminal operation panel (area 1 in Figure 5.2) and data capturing buttons (area 3) are held in the middle area together with a test timer (area 2). In the lower monitoring area, up to four sensors can be connected and monitored with synchronized flashing signals. Each online sensor flashes in a different colour while offline sensor stays in grey.
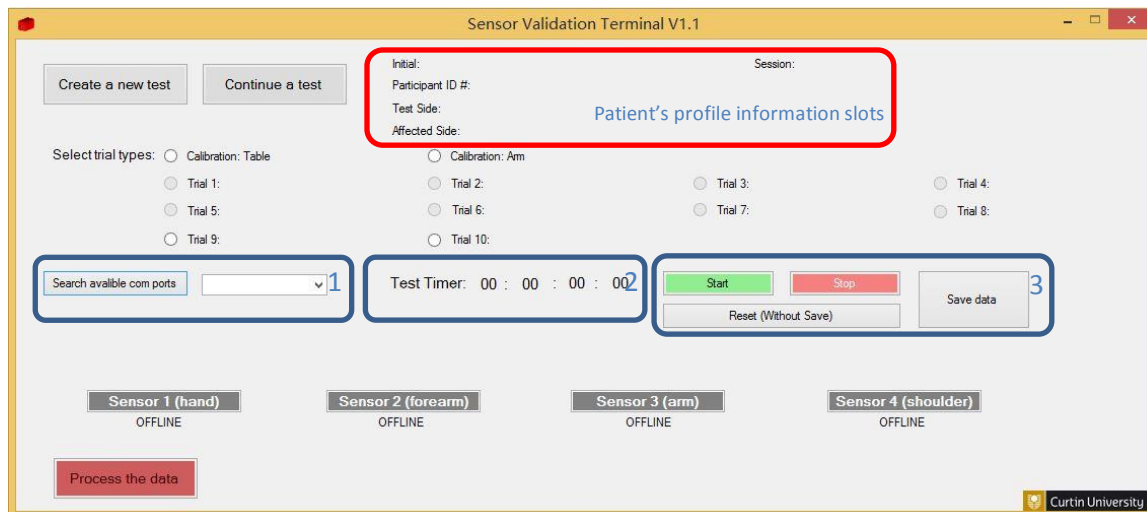
Figure 5.2: Sensor validation terminal software *home* window

The top left button from the home window of the sensor validation terminal allows users to create a new testing profile. As shown in Figure 5.3, the patient's profile information

slots were designed to meet the requirements of the cerebral palsy research project discussed in Chapter 7. The patients profile information and trial types are saved in a local folder named with the patient's initial and ID. The same folder will also contain all test files and data process results.
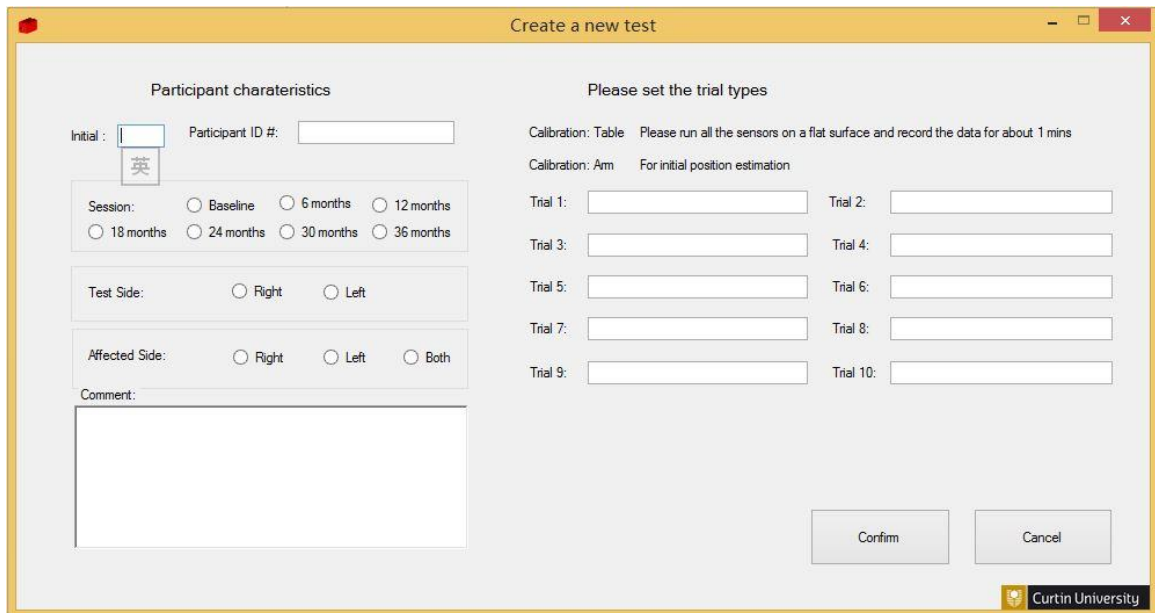
Figure 5.3: Sensor validation terminal software *test creating* window

The data processing window shown in Figure 5.4 can be opened by clicking the red "*Process the data*" button at bottom left area of the main window. Currently, the data processing function processes the raw data and saves it in a new excel file for the researcher to review. Plotting and analysing features will be incorporated in future versions of the interface.
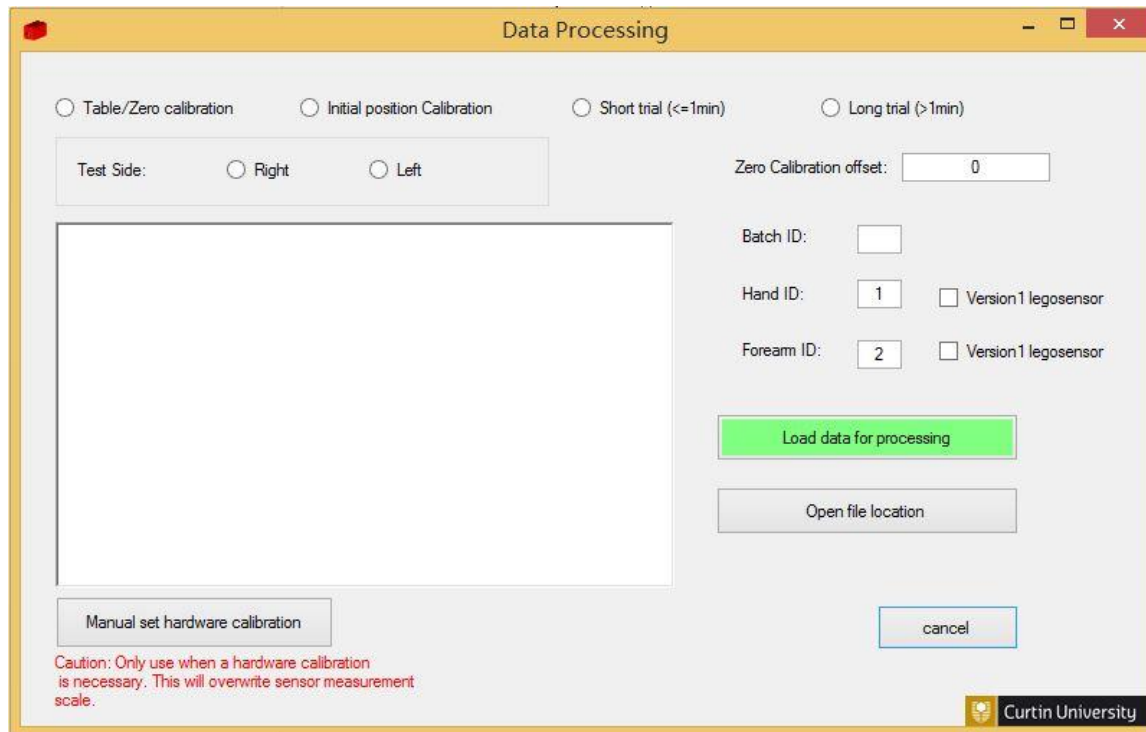
Figure 5.4: Sensor validation terminal software *data processing* window

The algorithm used to process the data was developed as a part of the thesis outcome. The algorithm was originally developed and tested in MATLAB. It will be discussed in Section 5.3.

5.3 Two-sensor based joint orientation algorithm

5.3.1 The principle of the two-sensor joint algorithm

The basic idea of the two-sensor joint algorithm is that the joint angle movement can be represented by the difference in relative movements between two sensors, when the two sensors share the same frame and the zero position. As long as all three axes from both sensors are parallel to each other in their zero position, the orientation difference between the two sensors while moving can be calculated using relative angle movements.

For example, in the wrist joint measurement study shown in Figure. 5.5, the first sensor was placed on the back of the hand and its x-axis was aligned with the line from the

middle knuckle to the wrist centre. The second sensor was located on the top of the upper limb with its x-axis aligned with the line from the wrist centre to the elbow. Both sensors' y-axis and z-axis need to be parallel to the other sensors' y-axis and z-axis. The purpose of this placement is to align both sensors' axes in such a way that the x-axis from sensor 1 and sensor 2 merge into the wrist centre, thus, the wrist joint movement can be measured as the angle difference between the two sensors. This sensor placement method can be applied to any joint measurement trials as long as both sensors are aligned with the joint's centre.
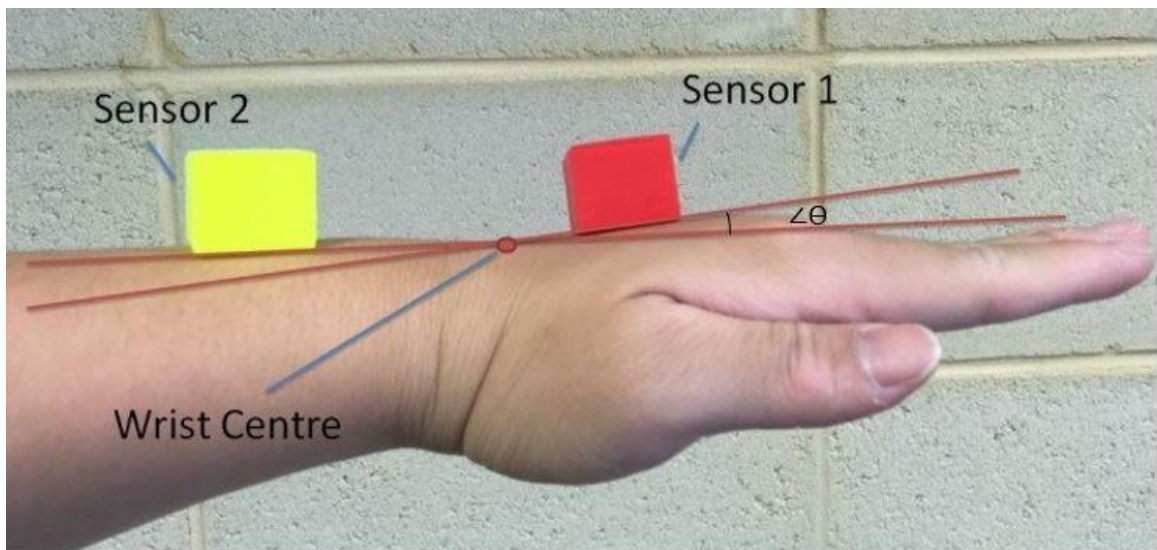
Figure 5.5: Wrist joint extension measurement

The wrist joint extension angle ∠Ө in Figure 5.5 can be calculated from sensor 1 and sensor 2 measurements.

As discussed in Chapter 2, in traditional methods complex filters are commonly applied to generate a three dimensional orientation system based on a single sensor's measurements. A yaw, pitch and roll system is frequently used to describe objects' orientation. As shown in Figure 5.6, in a single sensor system the pitch angle ∠α is regarded as the rotation from the x-y plane towards z axis. Such angle can be calculated from accelerometer readings under static conditions, where the net acceleration applied on the object is approximately equal to the earth's gravity. Sensor fusion methods were required to track angle movements with readings from different motion sensors, such methods can carry heavy computational load [25].
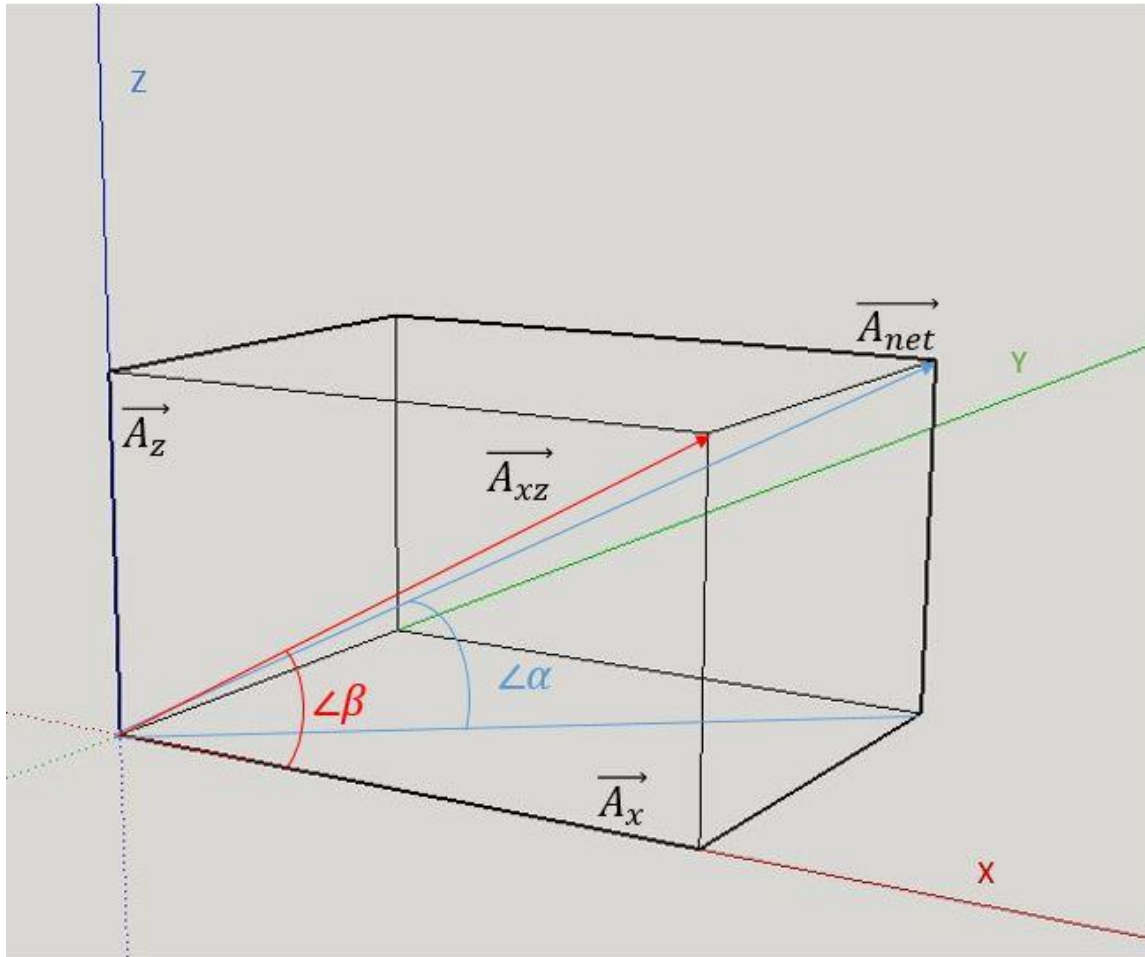
Figure 5.6: 3D system for acceleration

The proposed idea using two parallel sensors in human joint measurements contained a natural advantage which simplified all the calculations from a 3D system problem into a 2D system problem. With a pair of parallel-installed sensors, the human joint angle can be represented as the angle difference between the sensors. Since the sensors in a parallel-installed system shared same 3D coordination space, the 3D human joint angle can be represented as the three 2D projection angles on each plane (contains two axis) from both sensors. In traditional methods, if the angle $\angle\alpha$ in Figure 5.6 is the pitch angle (assuming the x-y plane is the ground plane), then the $\angle\beta$ in Figure 5.6 is the projection on the x-z plane.

Since the two-sensor system creates a relative system, the rotation on y axis or the

orientation on x-z plane can be simple regarded as:

$$\angle\beta_{diff} = \angle\beta_{sensor1} - \angle\beta_{sensor2}$$

In traditional methods, the angle measurements based purely on accelerometer readings are unreliable during movement. This is because a single accelerometer can only estimate its angular positon relative to earth's gravity. Live motion causes extra linear acceleration that tilts the net acceleration away from the gravity direction.

The angle β in Figure 5.6 can be calculated from the acceleration reading from both x and z axis:

$$\tan(\beta) = \frac{A_z}{A_x} = \frac{A_{xz}\sin(\beta)}{A_{xz}\cos(\beta)} = \frac{A_{net}\cos(x)\sin(\beta)}{A_{net}\cos(x)\cos(\beta)} \quad (5.1)$$

Where x is the angle between net acceleration and the acceleration on x-z plane. The angle β in (5.1) is not related to the magnitude of $\overrightarrow{A_{net}}$. This is possible because in a pair of relative coordinate system, there is always at least one sensor that can be treated as static. Even if there is a net acceleration different to the earth's gravity applied on the system, the relative angle movement can still be regarded as $\angle\beta_{diff}$.

5.3.2 Algorithm to calculate joint angles

The flow chart in Figure 5.7 shows an example of how the algorithm computes joint wrist flexion and extension angles from the raw readings of two sensors, after they have been stored in a file. The purpose of the algorithm is to capture the rotation angle difference between two testing sensors. Further details about the testing set up and sensor placement will be discussed in Chapter 6.
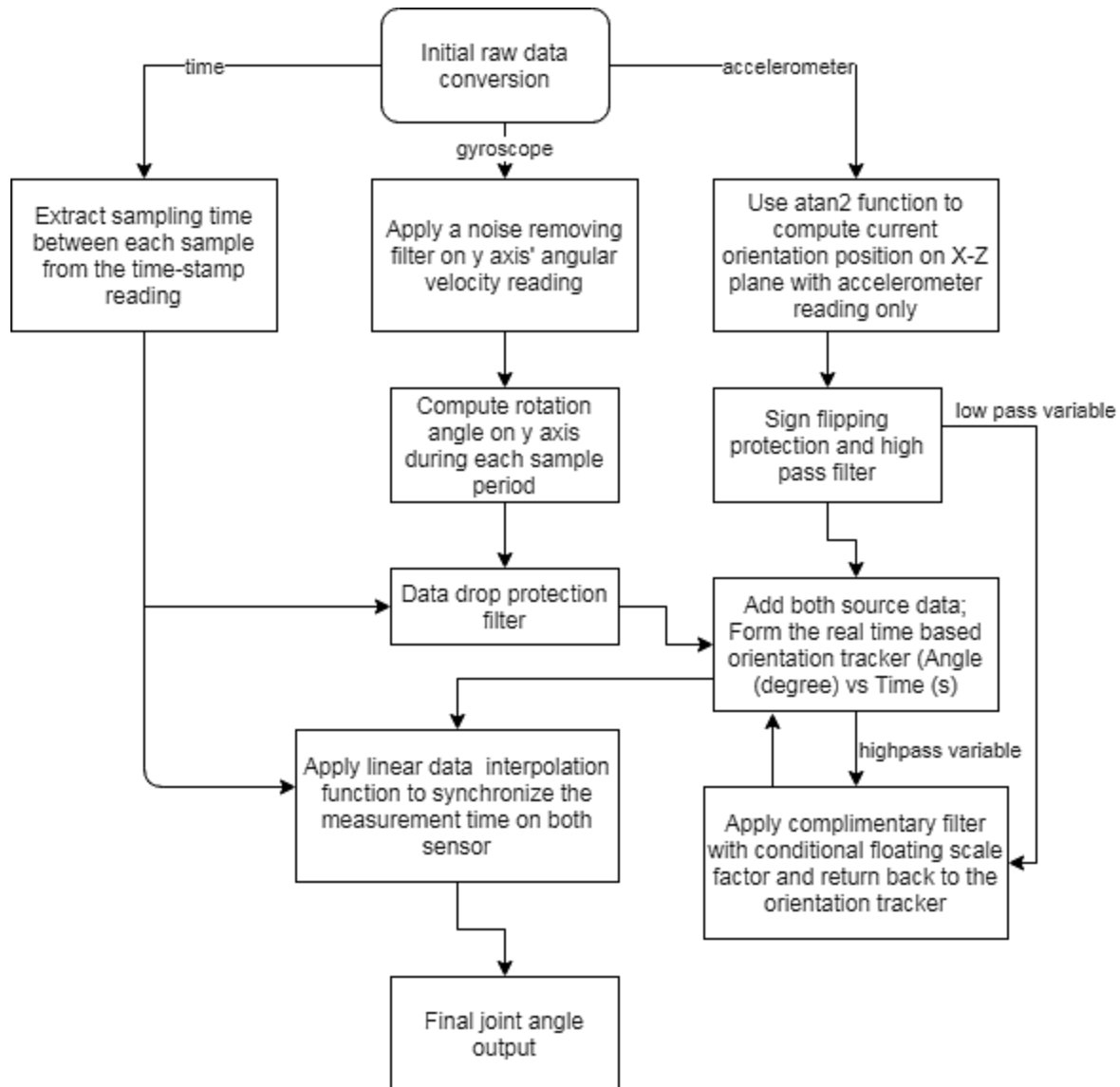
Figure 5.7： Joint angle calculation. High-level flow diagram

As mentioned, the data packages from each sensor consist of a time-stamp record, tri-axial acceleration readings and tri-axial angular velocity measurements. The sampling rate of the prototype sensor was set to 100 data packages per second.

The initial raw data conversion step in Figure 5.7 converts all the raw data captured by both sensors from a 16 bits binary value into meaningful time in milliseconds (ms), acceleration in gravities (*G*) and angular velocity in degrees per second readings.

At a data rate of 100 sps the difference of angular velocity measurements between

samples is small. A noise removing filter had to be applied to minimize the measurement error and reduce the white Gaussian noise. The Savitzky–Golay smoothing filter is recommended for post-data analysis when future samples can be used to improve the present measurement [69]. In a real-time project, a moving average offset noise can be calculated when the sensor is static, or when the offset noise is approximately equal to the average difference between each data sample. This can normally be estimated at the beginning of a trial.

The magnitude of the angle movement in each sampling period is calculated by multiplying the filtered angular velocity reading by the sampling period. The rotations on the y-axis from both sensors were used to measure wrist flexion and extension.

One of the methods in sensor fusion filtering technology is to combine the measurements of the same object from different sources. Instead of computing the rotation on each axis, an accelerometer provides real life orientation measurements by using the arctangent with two arguments function (atan2) with selected axis and plane [70] or generating a Spherical coordinate system [71]. In the present example, the acceleration data from the x and the z axis were used in the atan2 function. Unlike traditional yaw, pitch and roll orientation systems, a reference plane was unnecessary in the present algorithm because both sensors' axis were aligned in such way that the joint's movement was equivalent to the orientation difference between the sensors. Thus, only the relative motion was taken into consideration and the impact from the environment could be ignored.

 The orientation of each individual sensor could then be calculated by adding together the orientation readings and the angle movement during each sampling period. The complementary filter in Fig 5.7 [72] introduced a high pass filter to the main orientation tracker, and adjusted with a low pass value from the accelerometer's orientation measurement.

Before applying the complementary filter, a protection filter was introduced to prevent data drop error by ignoring the angular velocity reading when the sampling time

difference was too big. In addition, a sign flipping error occurs when the arctangent function miscalculates its minimum and maximum values at the points where -180° was equal to 180° (see Figure 5.8). The orientation tracker would then lose its consistency because any hardware tolerances from accelerometer could cause the orientation measurement to flip rapidly from -180° to 180°.
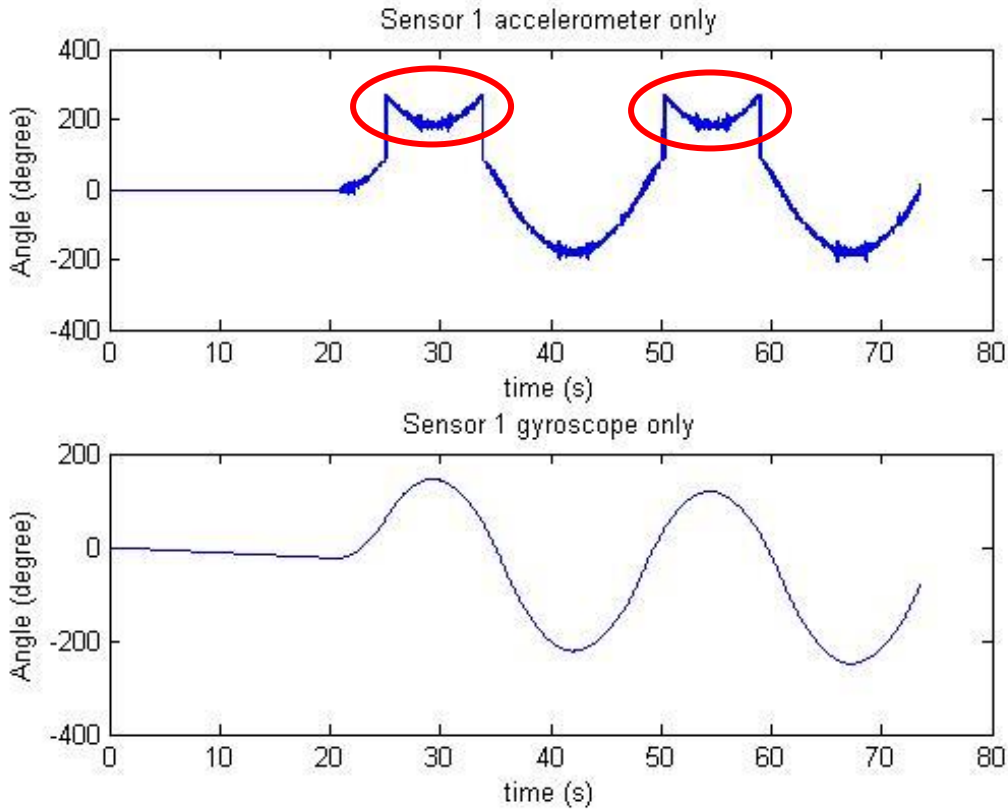
Figure 5.8: Example of a sign flipping error base on accelerometer's measurements

Both plots in Figure 5.8 are single source angle outputs without using any sensor fusion algorithm. The top plot is generated with accelerometer reading only while the bottom plot uses only gyroscope measurements. The red circles highlight the area where sign flipping problem occurred. In comparison, the gyroscope measurement does not have any sign flipping problem but the results are clearly drifting down. The outcome of sign flipping protection filter is showed in Figure 6.1.

Finally, a data samples linear interpolation function (linear interpolation) [73] was used to synchronize the time-related orientation measurements from both sensors so that the final orientation difference could be determined.

5.3.3 2D atan2 function

Based on the idea and assumption presented in section 5.3.1, the human joint angle measurement problem was simplified into finding the projected orientation angle in each 2D plane.

With the functionality of the multi-valued inverse tangent:

$$\begin{Bmatrix} \theta_{zx}(i) \\ \theta_{yx}(i) \\ \theta_{zy}(i) \end{Bmatrix} = \begin{Bmatrix} \text{atan2}(z,x) \\ \text{atan2}(y,x) \\ \text{atan2}(z,y) \end{Bmatrix} \quad (5.2)$$

Where $\theta_{zx}, \theta_{yz}, \theta_{zy}$ are the projected orientation angle on x-z, x-y, z-y planes.

Atan2(z, x) function is defined as the angle in Euclidean plane [87]. The standard atan2 function in the range $(-\pi, \pi]$ can be expressed as follows:

$$\text{atan2}(z,x) = \begin{cases} \arctan\left(\dfrac{z}{x}\right) & if\ x > 0, \\ \arctan\left(\dfrac{z}{x}\right) + \pi & if\ x < 0\ and\ y \geq 0, \\ \arctan\left(\dfrac{z}{x}\right) - \pi & if\ x \geq 0\ and\ y < 0, \\ +\dfrac{\pi}{2} & if\ x = 0\ and\ y > 0, \\ -\dfrac{\pi}{2} & if\ x = 0\ and\ y < 0, \\ undefined, & if\ x = 0\ and\ y < 0. \end{cases}$$

As shown in Figure 5.8, a sign adjustment filter is required to fix sign flipping problem where -180° is at the exact same position as 180° in an atan2 system.

When:

$$|\theta(n+1) - \theta(n)| > 270^\circ$$
$$\theta(n+1) = -\theta(n+1)$$

Where *n+1* is the current order of the sample. The last equation is a simple sign flipping operation. Since the thesis was designed for human joint movement measurement, it was assumed that it would be impossible to move more than $270°$ in 10 milliseconds.

5.3.4 Gyroscope White Gaussian noise filtering

As mentioned in Chapter 2, the white Gaussian noise present in the gyroscope's angle measurements is caused by the device's mechanical measurement tolerance [40].

The original orientation angle calculated from gyroscope's reading can be represented as:

$$\begin{Bmatrix} \theta_{gx}(i) \\ \theta_{gy}(i) \\ \theta_{gz}(i) \end{Bmatrix} = \sum_{i=1}^{n} \left(\begin{bmatrix} \omega_{gx}(i) \\ \omega_{gy}(i) \\ \omega_{gz}(i) \end{bmatrix} \times \Delta t(i) \right)$$

Where $\theta_{gx}, \theta_{gy}, \theta_{gz}$ are the rotation angle on each axis and $\omega_{gx}, \omega_{gx}, \omega_{gx}$ are the angular velocity in °/s measured with gyroscope. Δt are the time taken between two measurement.

With mechanical error:

$$\omega_g(t) = \omega'_g(t) + E_m$$

Where the output angular velocity measurement from each axis ω_g is equal to the actual angular velocity ω'_g plus the average mechanical error E_m.

Thus:

$$\begin{Bmatrix} \theta_{gx}(i) \\ \theta_{gy}(i) \\ \theta_{gz}(i) \end{Bmatrix} = \sum_{i=1}^{n} \left(\begin{bmatrix} \omega'_{gx}(i) + E_{mx}(i) \\ \omega'_{gy}(i) + E_{my}(i) \\ \omega'_{gz}(i) + E_{mz}(i) \end{bmatrix} \times \Delta t(i) \right)$$

$$= \sum_{i=1}^{n} \left(\begin{bmatrix} \omega_{gx}'(i) \\ \omega_{gy}'(i) \\ \omega_{gz}'(i) \end{bmatrix} \times \Delta t(i) \right) + WN(i)$$

Where the white noise drift: $WN(i) = \sum_{i=1}^{n} \left(\begin{bmatrix} E_{mx}(i) \\ E_{my}(i) \\ E_{mz}(i) \end{bmatrix} \times \Delta t(i) \right)$

The average filter was introduced to estimate the white noise at the beginning of each trial when the sensor was static:

$$\overline{D_s} = \frac{1}{m} \left[\left(\sum_{i=n}^{n+100} \omega_g(i) \right)\% + \left(\sum_{i=n+r+100}^{n+r+200} \omega_g(i) \right)\% + \cdots \right.$$
$$\left. + \left(\sum_{i=n+(m-1)r+100(m-1)}^{n+(m-1)r+100m} \omega_g(i) \right)\% \right]$$

Where $\overline{D_s}$ is the average static drift, n, m and r are random integers and m is larger than 3. The total number of samples is required to be larger than $n + (m-1)r + 100m$.

The average static drift was subtracted during the rotation measurements. A Savitzky-Golay filter was applied to calibrate the moving average drift [69]. The angular velocity measurement after filtering can be represented as:

$\omega_{gf}(t) = 0.5[\omega_g(t)] + 0.3[\omega_g(t+1) + \omega_g(t-1)] - 0.05[\omega_g(t+2) + \omega_g(t-2)] - \overline{D_s}$
(5.3)

In the last equation (5.3), ω_{gf} is the filtered gyroscope, angular velocity measurement. Since the sampling period of each sensor was set to 10 milliseconds per sample, the Savitzky-Golay filter was designed as a moving average applied to data every 50 milliseconds.

5.3.5 Sensor fusion

The purpose of sensor fusion is to increase the measurement accuracy by combining the sensory data measured from difference sources [74]. In this thesis, a complementary filter with conditional floating factor was used to combine the angle measurements from both accelerometer and gyroscope.

The expected outcome of the system in human angle measurement was to capture the angle movement on x-z, x-y, z-y planes. Since the accelerometer's outputs were independent by each sample throughout the measurements period, the accelerometer's output $\theta_{zx}, \theta_{yz}, \theta_{zy}$ in equation (5.2) was used as the rough measurement. The gyroscope's angular velocity measurement ω_{gf} in (5.3) was added to describe the actual change between each sample.

The following sensor fusion function used in this thesis is based on the complementary filter discussed in section 2.3.2:

$$\sigma_c(n+1) = h\left(\sigma_c(n) + \omega_{gfc}(n+1) \times \Delta t(n)\right) + l(\theta_{ab}(n+1)) \qquad (5.4)$$

In the last function (5.4), a, b, c are the name of measurement axis and n+1 is the current order of the sample. $\sigma_c(n+1)$ is the current filtered angle on c axis. The angular velocity ω_{gfc} represents the rotation on the c axis and θ_{ab} is the current angle on a-b plane based on accelerometer measurements. The combination of the high pass factor h and the low pass factor l is 1.

Both of the h and l factors in the sensor fusion filter were set based on the reliability from both accelerometer and gyroscope.

Thus,
When

$$\left|\omega_{gfc}(n+1) \times \Delta t(n)\right| \leq |\theta_{ab}(n+1) - \sigma_c(n)|$$

$$h = \left[95 + \frac{5\left|\omega_{gfc}(n+1) \times \Delta t(n)\right|}{|\theta_{ab}(n+1) - \sigma_c(n)|}\right]\% \qquad (5.5)$$

$$l = 1 - h$$

When

$$\left|\omega_{gfc}(n+1) \times \Delta t(n)\right| > |\theta_{ab}(n+1) - \sigma_c(n)|$$

$$\sigma_c(n+1) = \theta_{ab}(n+1) \qquad (5.6)$$

Equation (5.5) (5.6) show that the sensor fusion filter is only applicable when the gyroscope's reading is more reliable. With the floating conditional factor in (5.4), the sensor fusion filter will work more effectively.

5.3.6 Interpolation and final outcome

A linear data interpolation function was used to match the results from both sensors. As shown in the following Figure 5.9:
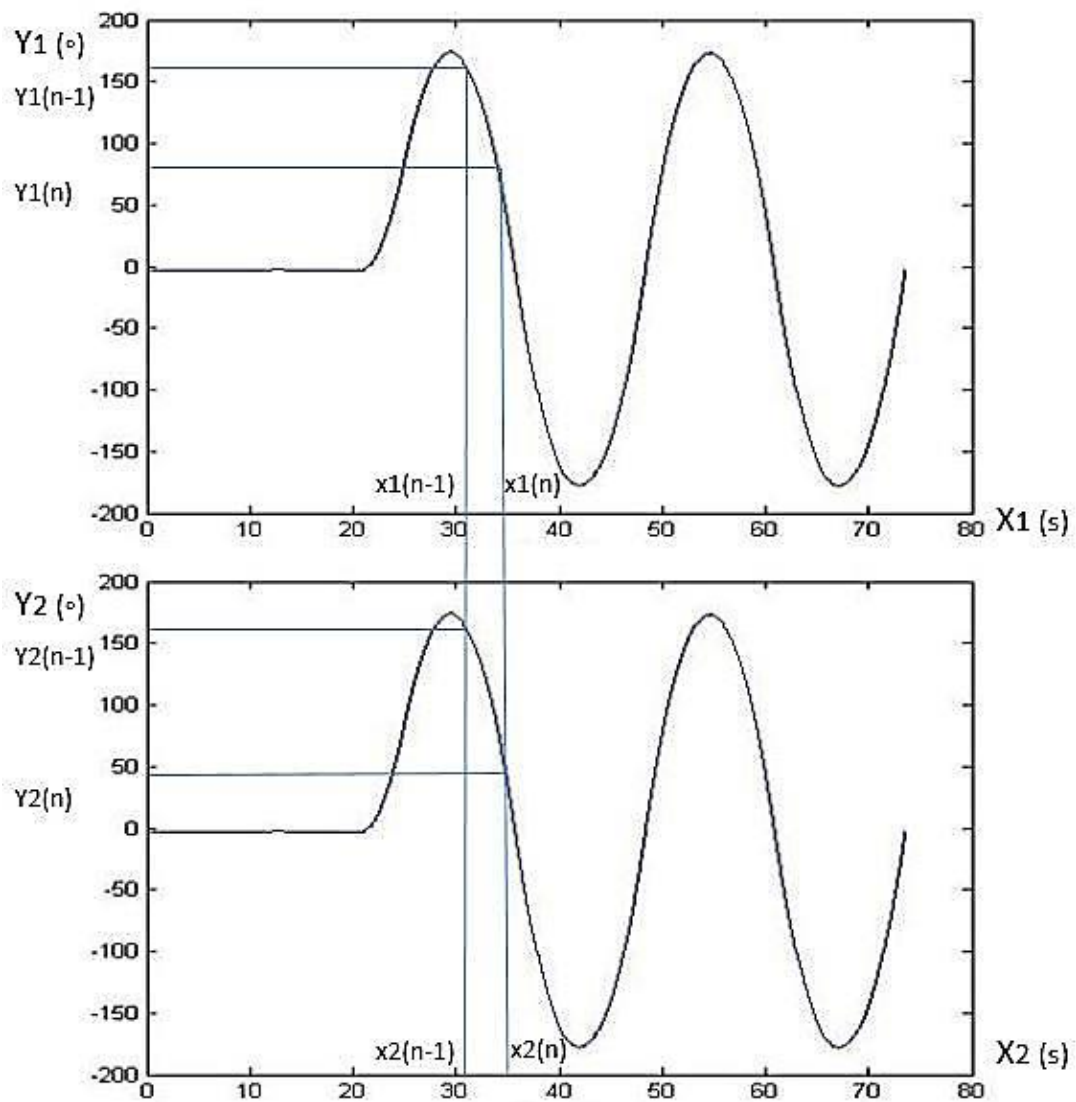
Figure 5.9: Example of linear data interpolation

The two plots in Figure 5.9 are the output of two sensors doing synchronized movement. Although the difference is not visible between the two plots, there is a few microseconds delay that exists between the two plots. As discussed in Figure 5.5, the central idea of the two-sensor algorithm is to use two parallel placed sensors measuring the related human joint angle. The final measurement coming out of the system has to be a series of results of the difference between the two sensors' measurements. Thus, a tiny delay between each sample transmitted from both sensors will cause a deduction of the final joint angle measuring resolution. The interpolation function is used to adjust the tiny delay that exists between the two plots.

From Figure 5.9:

$$Y_2'(n) = \frac{Y_2(n)-Y_2(n-1)}{X_2(n)-X_2(n-1)} \times [X_1(n) - X_2(n-1)] + Y_2(n-1) \quad (5.7)$$

Where

$$X_1(n) \leq X_2(n-1)$$

Figure 5.9 shows two related angle versus time data plots. The last equation (5.7) interpolates all the data in the lower data trace to synchronize it with the first trace. However, such linear data interpolation function only works under ideal conditions when there is zero data lost from both sensors' measurements. In practice, data drop and communication delays make the time recorded with the first sensor $X_1(n)$ in Figure 5.9 larger than the original time recorded with the second sensor $X_2(n)$. The concept of linear data interpolation is to relocate a point from the original plot. A relocated point is a new point in the angle vs. time plot predicted base on the nearest two sample point. Relocated time value is the new x value on time axis. Having the relocated time $X_1(n)$ greater than the original time $X_2(n)$ while interpolate new angle value $Y_2'(n)$ implies the relocating location of the new point is not within range of the exist plot. Such point relocation operation may cause a big error because the new point after interpolation will be calculated as a predicted point.

A better way to ensure the interpolation process is always taken place within the

range of the plot is to always use the closest next point as the reference point.

Thus, the complete interpolation function can be re-written as:

$$Y_2'(n) = \frac{Y_2(n+m) - Y_2(n-1)}{X_2(n+m) - X_2(n-1)} \times [X_1(n) - X_2(n-1)] + Y_2(n-1)$$

Where

$$X_2(n+m-1) \leq X_1(n) \leq X_2(n+m)$$

Thus, the final joint angle output is:

$$Y_{final}(n) = Y_1(n) - Y_2'(n) - E_{Table} - E_{placement} \quad (5.8)$$

Where E_{Table} is the table offset which can be measured while placing both two sensors on a flat surface. The $E_{placement}$ offset is only applicable when a zero position is specially defined before any trials.

5.3.7 Limitation of initial placement adjustment

In practice, it can never be expected that a pair of sensors will be placed with a perfect match in every measuring axis. Especially in medical applications, testing sensors will not even be able to start from the ideal zero position. Thus, some methods about sensor placement were developed to provide more accurate initial position for testing and self-calibration. These are explained in Chapter 7

5.4 Summary

The data-acquisition program was developed to provide functionality and user friendly features for sensor data recording, medical data management and data processing. The software was developed in C sharp. It was designed to open a serial communication port on a PC and store the raw data received from the receiver dongle. Each package of data includes one 2 digit decimal sensor ID plus eleven 16-bit binary measurements and the full data set is saved in a CSV text file.

The algorithm developed in this thesis was the two-sensor based joint orientation algorithm. With the combination of readings from two sensors placed across the target joint, a clear and accurate measurement of wrist angle has been obtained. The idea of using paired IMU sensors to measure human joint angles also reduces the data load during filtering of environmental noises as only relative changes between two sensors are accessed. Also, the proposed algorithm simplifies the problem of wrist angle measurement from a 3D orientation problem into a 2D projection angle measurement.

Unlike single sensor based applications, the proposed algorithm can work particularly well for movements where there is no pre-determined reference position (rest position). Self-calibration methodologies require a reference position that is continuously reached on repetitive movements, under these conditions sensors can recognize the rest position and use it as reference for their measurements. However, the number of human joint studies where a calibration pose can be identified and systematically used is very limited. With the two-sensor system, the relative position between the sensors can be regarded as static. The joint movement will be the only outcome from the measurements. Further validation tests and results are discussed in the next chapter.

Chapter 6

Results

6.1 Introduction

This Chapter presents the robot validation and human experiment results with the sensor system. First, section 6.2 presents an example with step by step output plots for each of the blocks in the high level diagram in Figure 5.7.

Validation tests using a robotic arm were used to validate reliability and accuracy of the sensor system. Three types of validation tests are discussed in the following sections:

- Section 6.3: Pan and tilt robot simulation
- Section 6.4: Two-sensor stepper test
- Section 6.5: Precise sensor accuracy validation

The Pan and tilt robot followed a sequence of predefined movements to validate the reliability and accuracy of the sensor. The two-sensor stepper test used two independent stepper motors with one sensor on each. Both motors were programmed to rotate in opposite directions following a designed sequence. Such tests were expected to validate the performance of the algorithm while having two sensors moving at the same time. Precise sensor accuracy validation used a custom made angle measurement mechanism to measure the exact motor movement angle. The test provided a pseudo-gold standard to verify the maximum sensor measurement accuracy.

Fixed angle wrist movement tests are introduced in Section 6.6. An adjustable angle mechanism was built to set the angle between the two sensors, and keep it fixed throughout the experiment. The fixed angle mechanism was carried on the wrist when the wrist was doing rapid movements. This experiment followed on from the relative angle movement idea discussed in Chapter 5. It validated the sensors' performance when both sensors were relatively static during the movements.

6.2 Algorithm breakdown results

In this section, a pre-acquired dataset is used to demonstrate the algorithm discussed in Chapter 5. Results in this section were presented at the 2017 IEEE Student Conference on Research and Development [75]. Data was collected using the same setup discussed in section 6.4. As shown in Figure 6.10, the test used two stepper motors with attached 3D printed arms. Both motors were programmed to make synchronized movements and the difference in the angle between both sensors was expected to remain at zero. Plots in this section show the outputs of each step of the algorithm according to the high level diagram in Figure 5.7. The results provide an intuitive demonstration of the process from raw data to joint angle measurement.

Figure 6.1 and Figure 6.2 show the orientation plots (Angle (degrees) versus Time (seconds)) for each sensor without applying any filtering. The top plots in Figure 6.1 and Figure 6.2 show the sensors' orientation measurements computed from the accelerometers' readings and the atan2 function. Graphs show that the results are noisy throughout the entire moving period.

The bottom plots in Figure 6.1 and Figure 6.2 show the angle plots calculated from angular velocity measurements. By comparing the start and end points in those plots, it can be observed that the orientation readings drifted around plus/minus 200 degrees within less than 80 seconds. This kind of drift can be treated as white Gaussian noise as discussed in section 2.3.1.
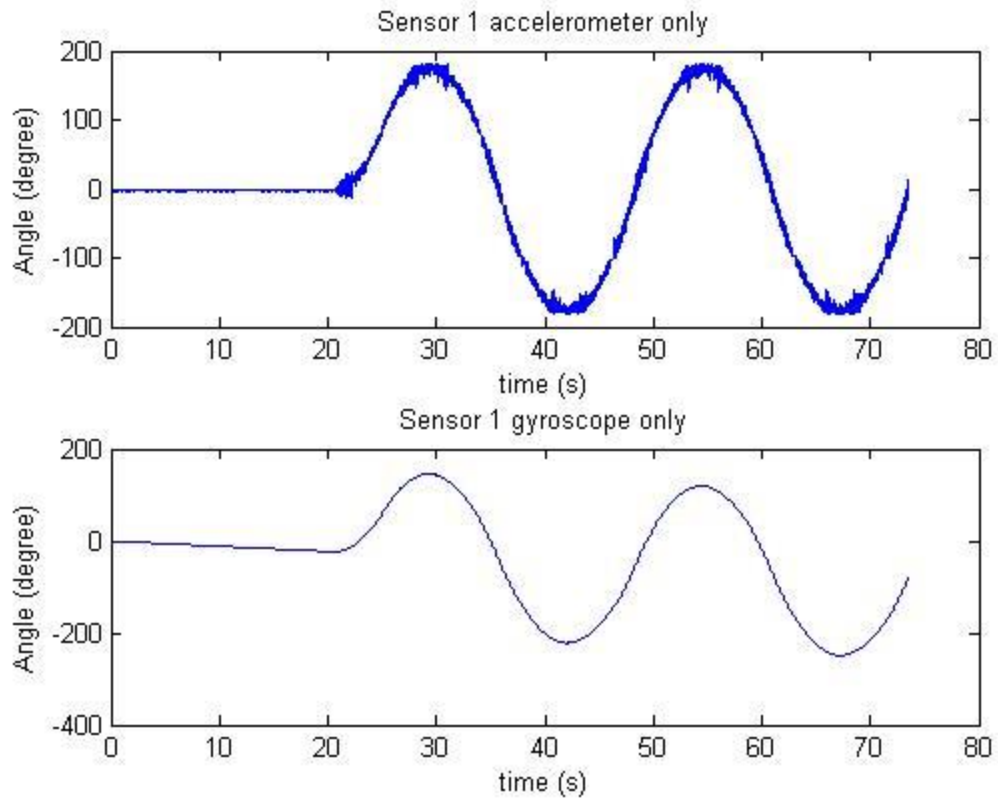
Figure 6.1: Sensor 1 orientation output without sensor fusion

By comparing Figure 6.1 with Figure 5.8 in Chapter 5, it can be observed that the sign flip problem from accelerometer's reading was perfectly fixed with the sign flip fix algorithm.
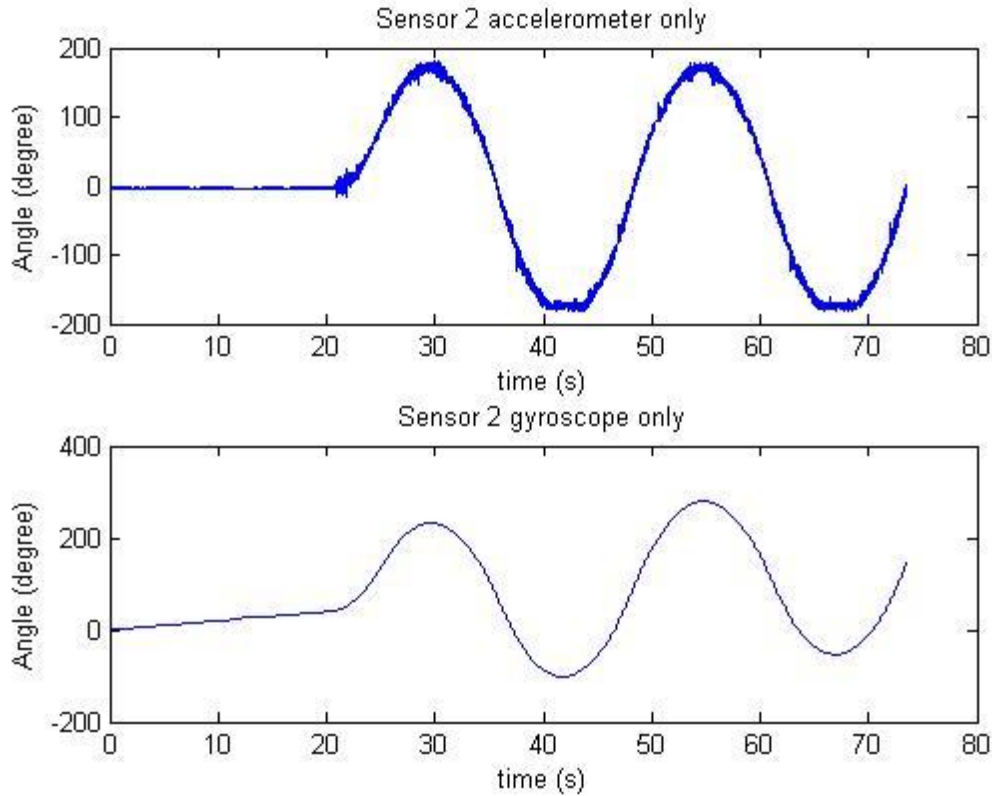
Figure 6.2: Sensor 2 orientation output without sensor fusion

Both Figure 6.1 and Figure 6.2 show of the acceleration noise and gyroscopes' white Gaussian noise as discussed in Chapter 2 where the plots based only on accelerometers' readings were noisy and unstable. The gyroscope's white Gaussian noise drifted measurements could be clearly observed.

Another example of raw measurement noise is showed in Figure 6.3: the static table calibration results. The static test was performed prior to any other trials in order to produce an initial alignment offsets. One calibration was enough for each set of sensors. The test was demonstrated with both sensors placing in line and set statically on a flat table surface.
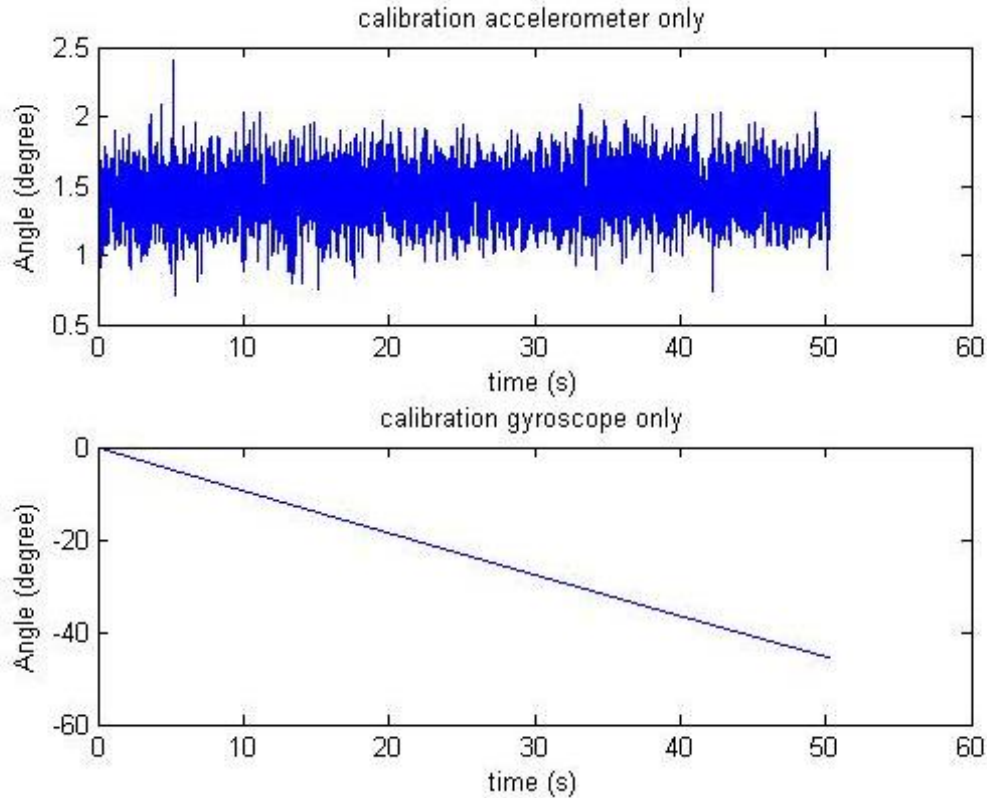
Figure 6.3: Static table calibration test

The outcome from static table calibration after applying sensor fusion filters was used as the E_{Table} offset value in the final joint angle equation 5.8 discussed in Chapter 5.

The plots shown in Figure 6.4 are the result of applying a sensor fusion filter to calculate the angular movements from sensor 1. A comparison between Figure 6.1 and Figure 6.4 shows that the floating factor high pass filter discussed in Section 5.3.2 could effectively fix the angular velocity drifts and the low pass filter created a frame to fit the shape of the plot. The sum of coefficients of the low pass filter and the high pass filter was set to 1, while each coefficient was dynamically adjusted to adapt to the present data conditions as discussed in Section 5.3.5.
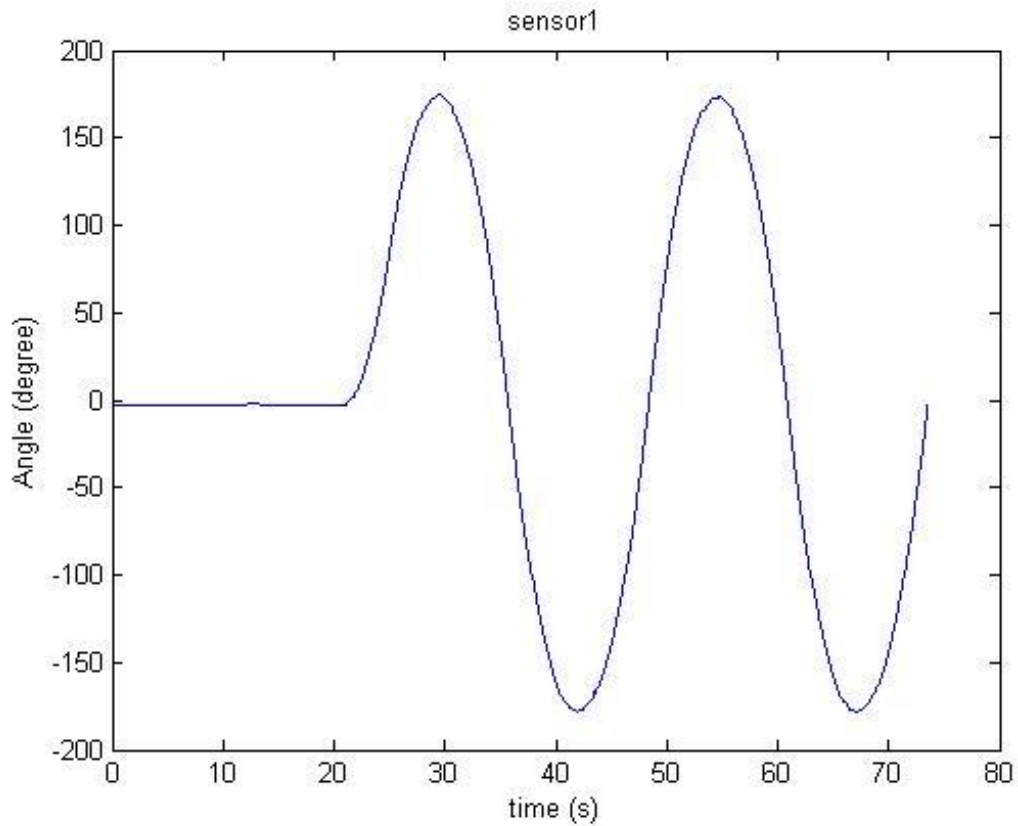
Figure 6.4: Sensor 1 filtered result

The plot in Figure 6.5 shows the difference between the measurements of the two sensors. The results were computed from the data used to produce the plots in Figures 6.1 and 6.2. As a last step a linear synchronization function was applied.
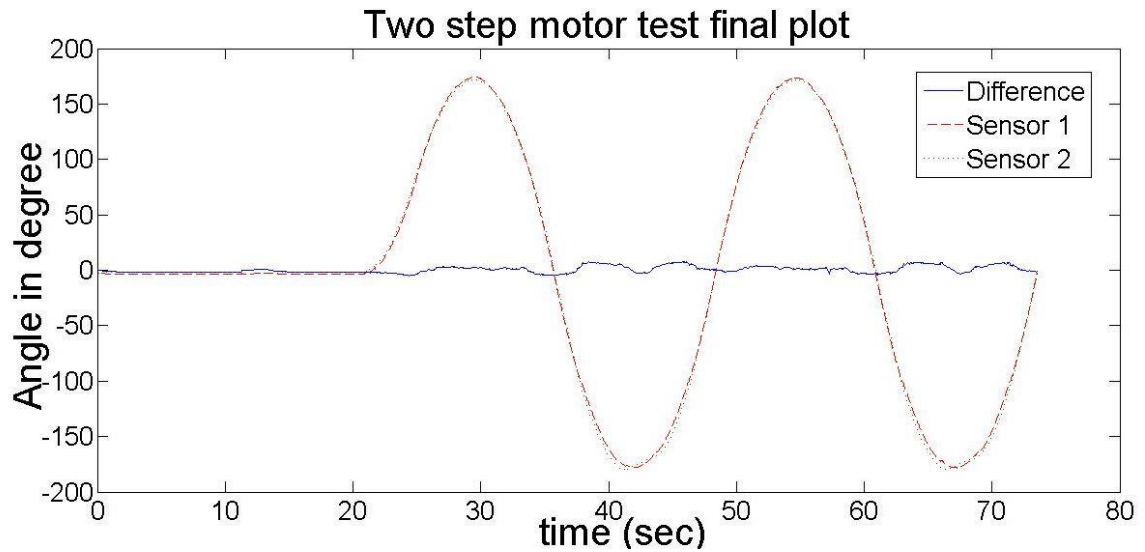
Figure 6.5: Final difference of two step motor example trial

In figure 6.5, the maximum error after comparing the actual motor movements is plus/minus 2.5°, the results were presented in the paper [75]. Since the accelerometer's measurements contain less noise during a static position, moving the two sensors at the same time created an extreme test condition. In a clinical trial the relative movement between sensors is expected to be less pronounced. The continuous sequence implementation also verified that the algorithm can generate precise measurements without the need of any common reset position for calibration.

The result of this test demonstrated that the two-sensor, joint orientation algorithm can precisely capture the angle difference between two coordinated sensors. More details about the experiment set-up will be discussed in section 6.4. The output of the algorithm is a clean measurement of the relative motion between two sensors, with most of the environmental noise and drift produced by the large range of movements filtered out.

6.3 Pan and tilt robot simulation

6.3.1 Design of experiments

A pan and tilt unit is a mechanism with a servo motor [76] to provide rotation in the horizontal plane and a servo motor attached to the first that provides rotation in the vertical plane. The pan and tilt unit used in this research is shown in Figure. 6.6. A servo motor is a closed-loop servomechanism whose position is controlled by a pulse-width modulation (PWM) signal [77]. In this experiment, the pan and tilt mechanism was used to provide repeatable and precise positions to an attached sensor. The reliability of the sensor system was validated by comparing the sensor's measurements against the predefined moving sequence of the servo motor.

As shown in Figure 6.6, one sensor was attached to the pan and tilt mechanism while the second sensor was placed statically on the table in line with the first sensor. Sensors were enclosed in the black boxes shown.
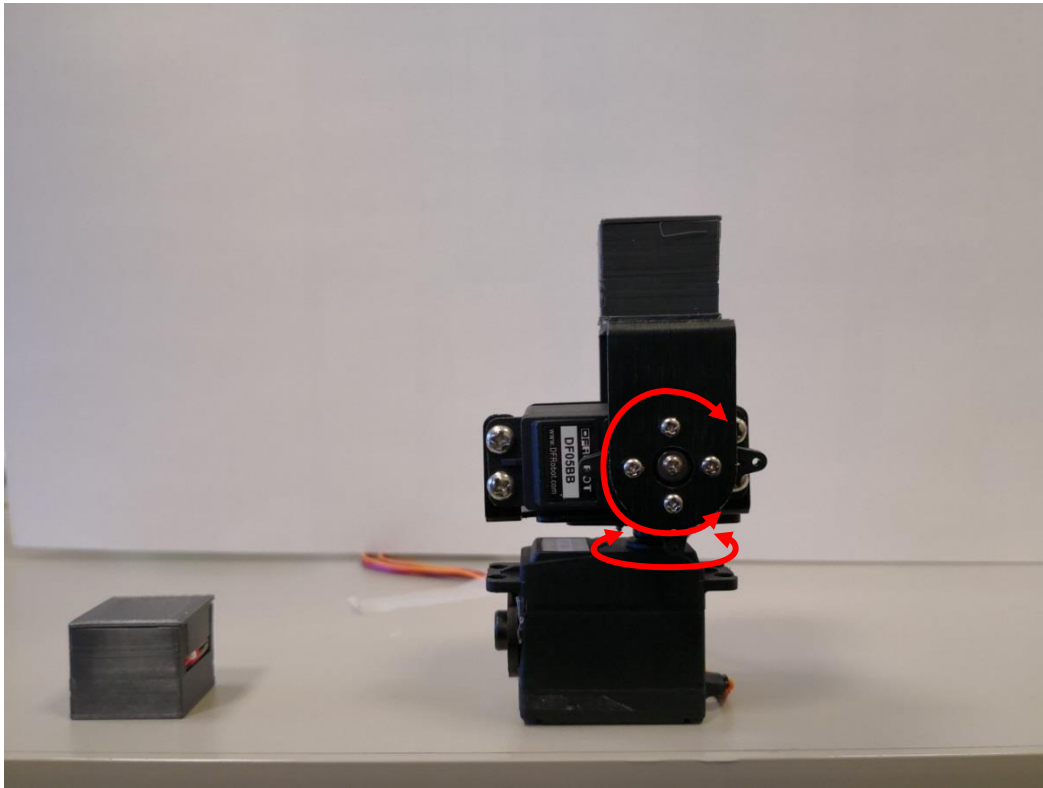
Figure 6.6: Pan and tilt mechanism

Both flexion and deviation movement are anatomical terms of motion in kinematic studies. In this test, the simulated flexion movements were set in a vertical direction and deviation movements were taken on the horizontal plane. Figure 6.7 shows an example of an approximately 80 degrees wrist flexion position.

Figure 6.7: Wrist flexion at approximately 80 degrees

Figure 6.8 shows the sequence that was sent to the top motor in Figure 6.6, which mimics simulated flexion movement for the experimental output comparison. The bottom motor was controlled with random deviation movements to test if the two-sensor algorithm can filter the deviation noise movement while focusing on flexion motion only.

Flexion movement sequence setup
With random deviational sequence as noise
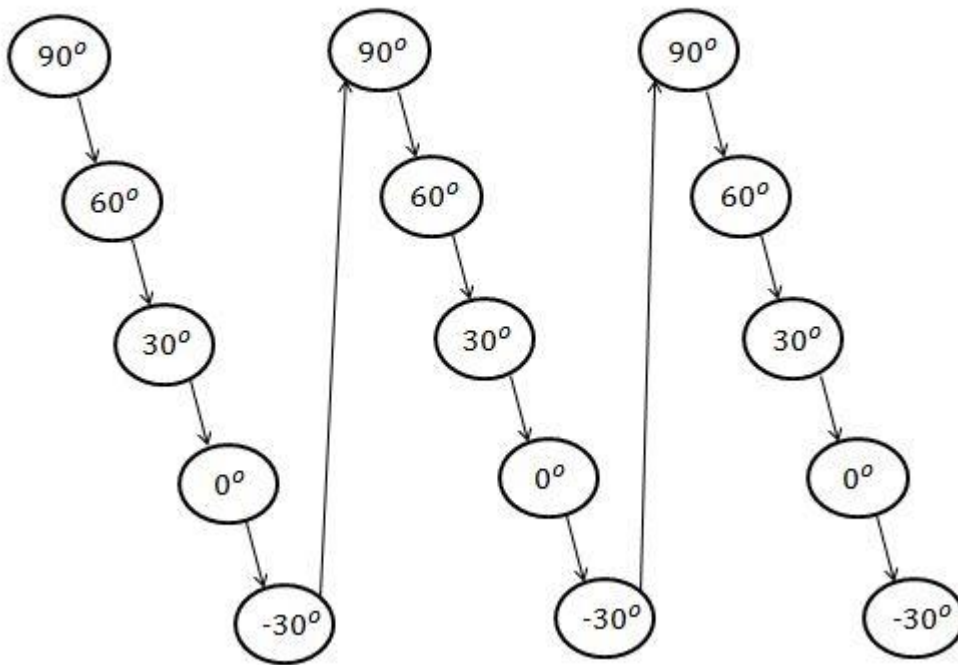
Figure 6.8: Servo motor flexion motion sequences

As shown in Figure 6.8, the pan and tilt mechanism emulated flexion motion by changing the relative angle of the sensor in 30° steps, from 90° to -30° at a velocity of 90° per second. There was a 250ms pause between each step and the sequence was repeated three times. For comparison, a 125ms pause time setting between each steps was also used to test the sensor performance when there was less static period during the movement.

6.3.2 Results

The plots in Figure 6.9 and Figure 6.10 illustrate all three sequence movements as designed without any data drifting or obvious distortion.
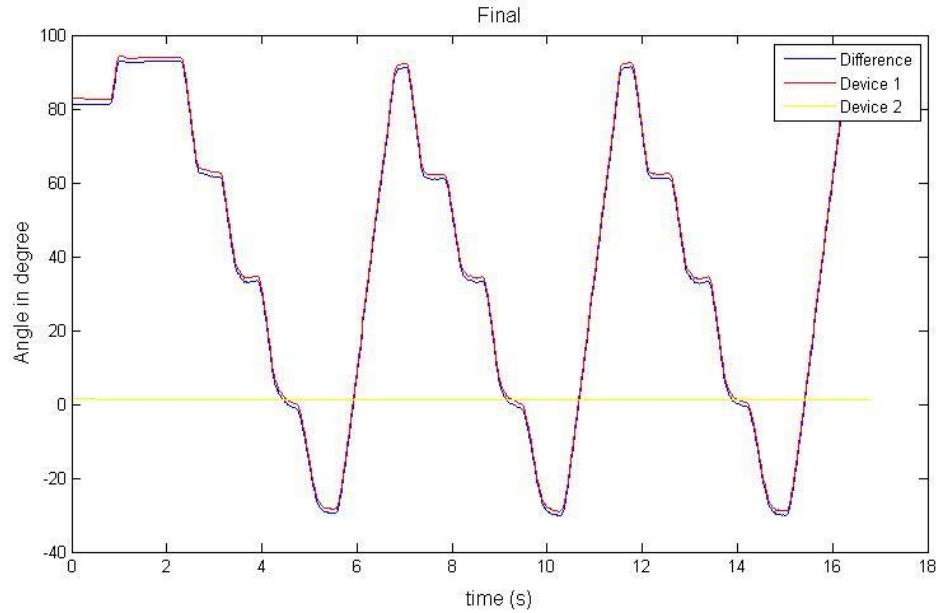
Figure 6.9: Pan and tilt flexion orientation output plot with 250ms pause between each steps
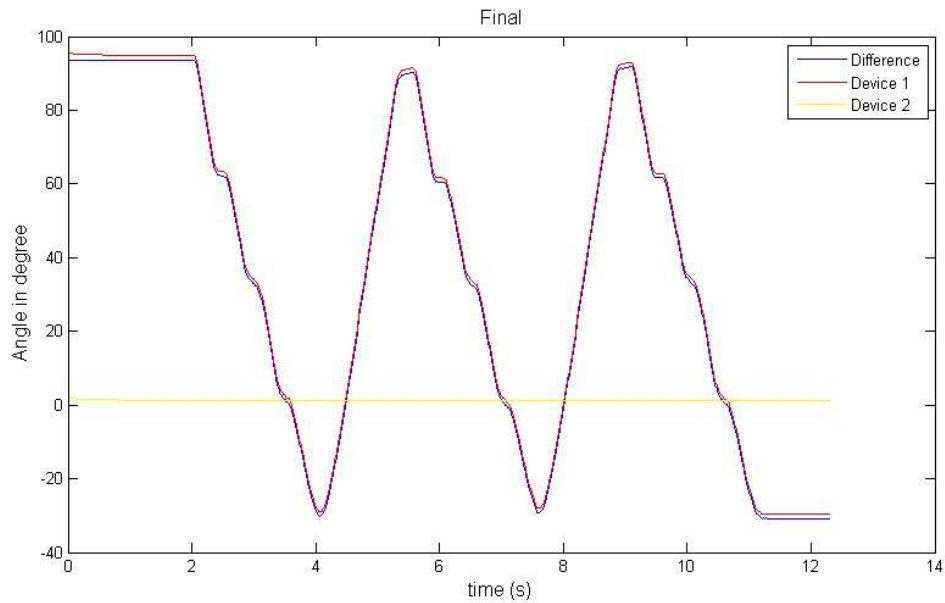
Figure 6.10: Pan and tilt flexion orientation output plot with 125ms pause between each steps

Table 6.1 shows measurement results from Figure 6.9. The largest differences from the sensor's measurements compared to the set angle are -0.99^o and 2.17^o. The maximum differences between each reading are mostly less than 1°, which prove the consistency of the system.

Table 6.1: Pan and tilt flexion test result (250ms step pause)

Set angle	1st Sequence	2nd Sequence	3rd Sequence	Largest difference	Maximum difference between each readings
90°	91.55^o	90.51^o	90.53^o	1.55^o	1.04^o
60°	60.84^o	$60.11^{o.}$	60.38^o	0.84^o	0.73^o
30°	32.16^o	32.17^o	31.88^o	2.17^o	0.29^o
0°	-0.99^o	-0.58^o	-0.51^o	-0.99^o	0.48^o
-30°	-30.29^o	-30.85^o	-30.76^o	-0.85^o	0.56^o

Table 6.2: Pan and tilt flexion test result (125ms step pause)

Set angle	1st Sequence	2nd Sequence	3rd Sequence	Largest difference	Maximum difference between each readings
90°	93.02^o	90.38^o	91.45^o	3.02^o	2.64^o
60°	62.20^o	$60.42^{o.}$	61.55^o	2.20^o	1.78^o
30°	31.53^o	31.44^o	31.96^o	1.96^o	0.52^o
0°	-0.73^o	-0.73^o	-0.75^o	-0.75^o	0.02^o
-30°	-30.10^o	-29.18^o	-30.17^o	0.82^o	0.35^o

The results in table 6.2 were captured from the test with 125ms step time. As shown in Figure 6.10, the servo motor was not able to generate any static position under 125ms step time since the motor required a small amount of time to stop and restart. As a result, the maximum difference readings were slightly bigger than the 250ms step test, this was due to the bigger acceleration noise during none-static positions. However, the sensors still were able to show excellent consistencies as the average difference are all less than

2°. Given that the motors' performance has some mechanical tolerances, an experiment designed to test the precise measurement accuracy of the sensors is discussed in Section 6.5.

6.4 Two sensors stepper test

6.4.1 Design of experiments

The two sensors stepper test includes two stepper motors [78] with a 3D-printed robot arm attached, as shown in Figure 6.11. The two stepper motors were programmed to perform synchronized movement at the same speed with opposite starting positions. Both motors were set vertically with a distance in between to allow both robot arms to pass through without interception. The setup was for the purpose of validating the sensor performance when both hand and arm sensors are moving.
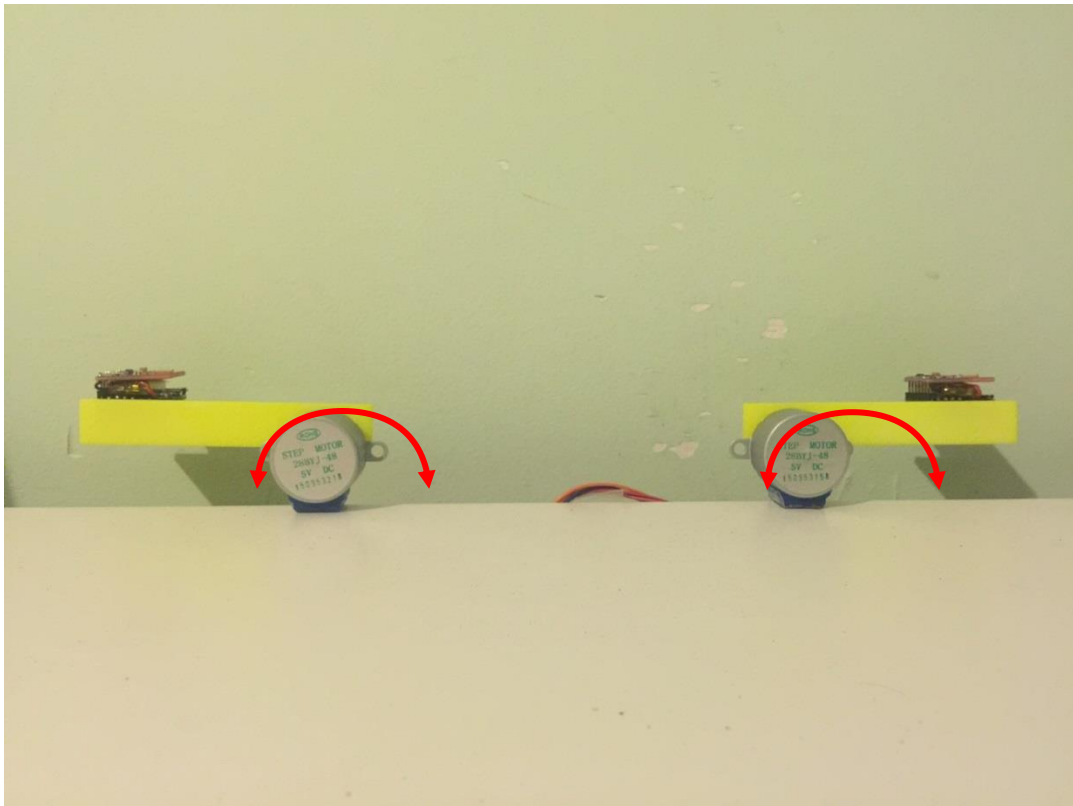
Figure 6.11: Two sensors stepper system

Although the starting positions of both robot arms were opposite to each other as shown in Figure 6.11, the sensors would only pick up the angular motion relative to its axial origin. The distance from the sensor to the joint centre is irrelevant. Both sensors started at a defined angle. The sensors measure positive angles while performing clockwise rotation and negative angles on anticlockwise rotation. Figure 6.12 shows that the measurement range of each sensor was from -180° to 180°.
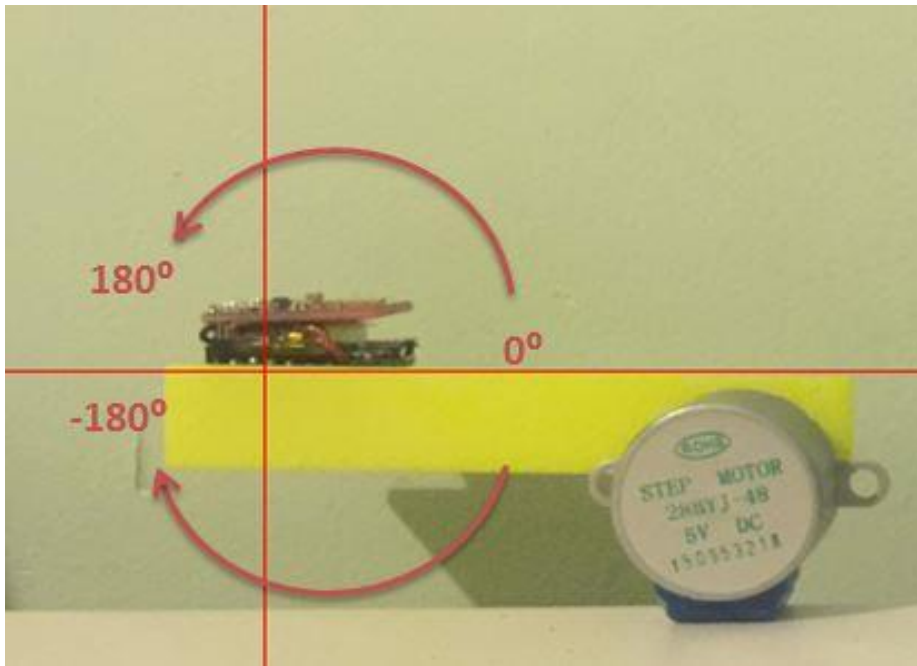
Figure 6.12: Sensor measuring range in the two stepper motor setting.

During the tests, both motors were programmed to rotate in opposite directions. Figure 6.13 shows the sequence of the butterfly test.
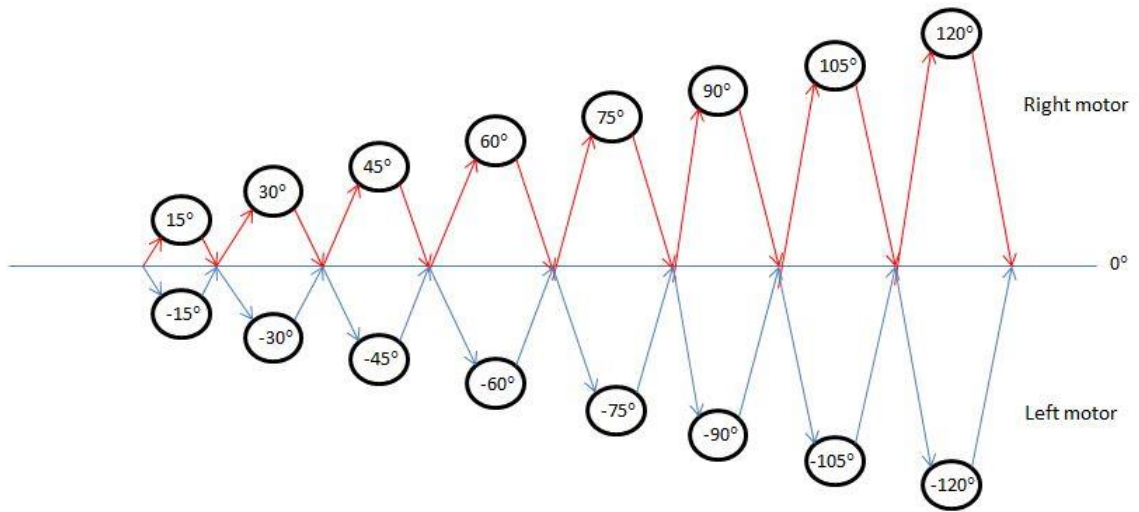
Figure 6.13: Butterfly test sequence

As the red line shows in Figure 6.13, the right-side motor in Figure 6.11 was programmed to make some steps in clockwise direction; each step would come back to zero in anticlockwise direction after reaching the designed angle. The left-side motor in Figure 6.11 was programmed with the completely opposite movements compared to the right-side motor.

Table 6.3 gives the peak value of each step and the expected outcome of the test is the angle difference between two motors' arms.

Table 6.3: Theoretical outcome

	Right Motor (Sensor 1)	Left Motor (Sensor 2)	Expected outcome
Step 1	15°	-15°	30°
Step 2	30°	-30°	60°
Step 3	45°	-45°	90°
Step 4	60°	-60°	120°
Step 5	75°	-75°	150°
Step 6	90°	-90°	180°
Step 7	105°	-105°	210°
Step 8	120°	-120°	240°

The trial was repeated three times at two different motor speeds. The slow rotation speed was set at 30 degrees per second while the fast speed was set to the 180 degrees per second of angular velocity. The experimental results were plotted and compared with the expected outcome from Table 6.3 in the following section.

6.4.2 Results

All the results from slow speed trials in Figure 6.14, 6.15, 6.16 and fast speed trials in Figure 6.17, 6.18, 6.19 exhibits both sensors captured sequence movements as designed without any data drifting or obvious distortion.
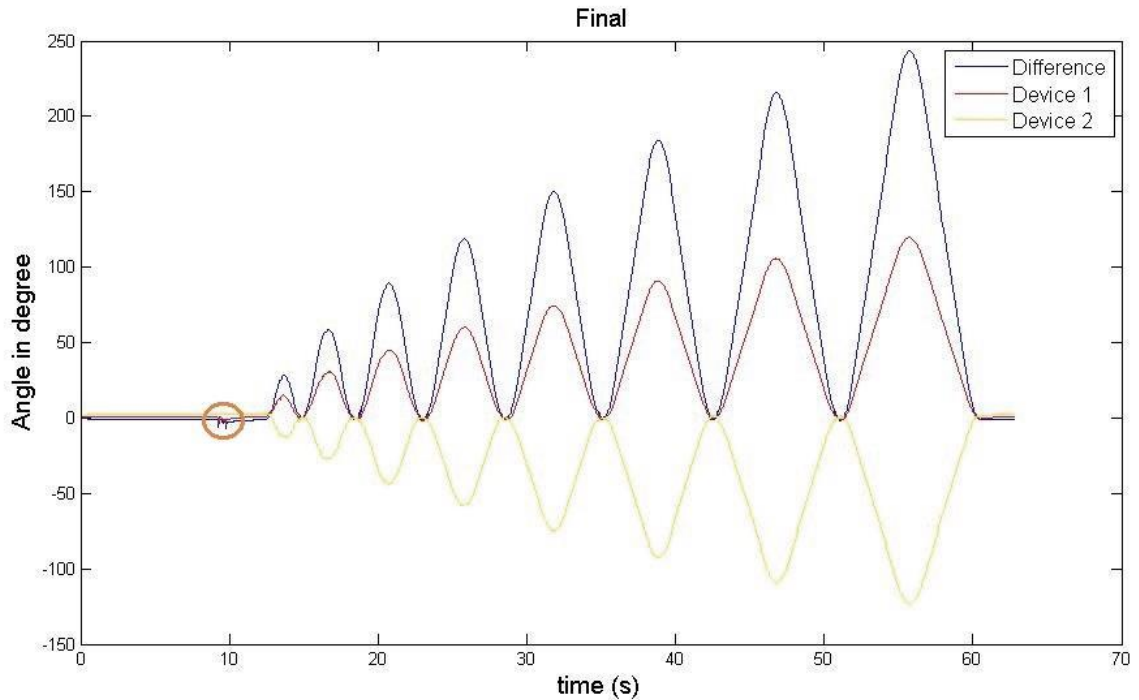
Figure 6.14: Trial 1 slow speed (30 degrees per second)

The small signal spikes highlighted in a red circle in Figure 6.14 recorded a tapping action from the test performer. A tapping action was used to show the actual starting time of the test. A test demonstrator was asked to gently tap on the back of one of the sensors. Although the starting time of a robot test is obvious, it will be necessary for medical measurements in real life practice. The tapping signal can also be used to synchronize the starting time of other measuring methods for validation purpose.
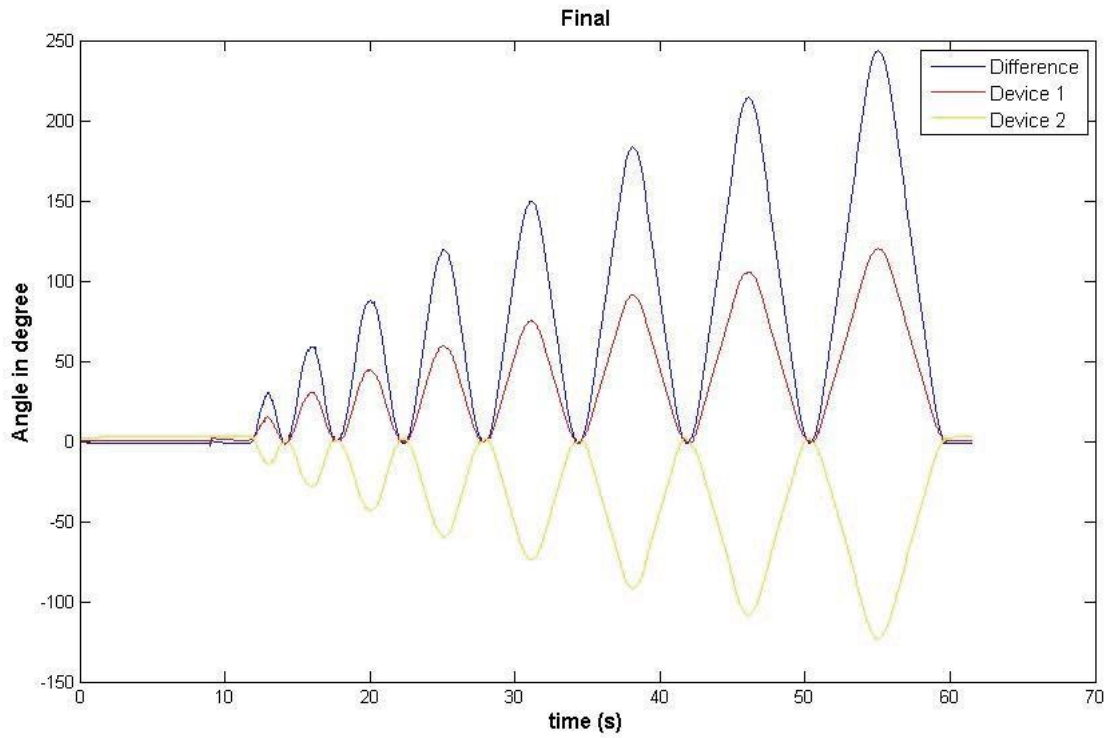
Figure 6.15: Trial 2 slow speed (30 degrees per second)
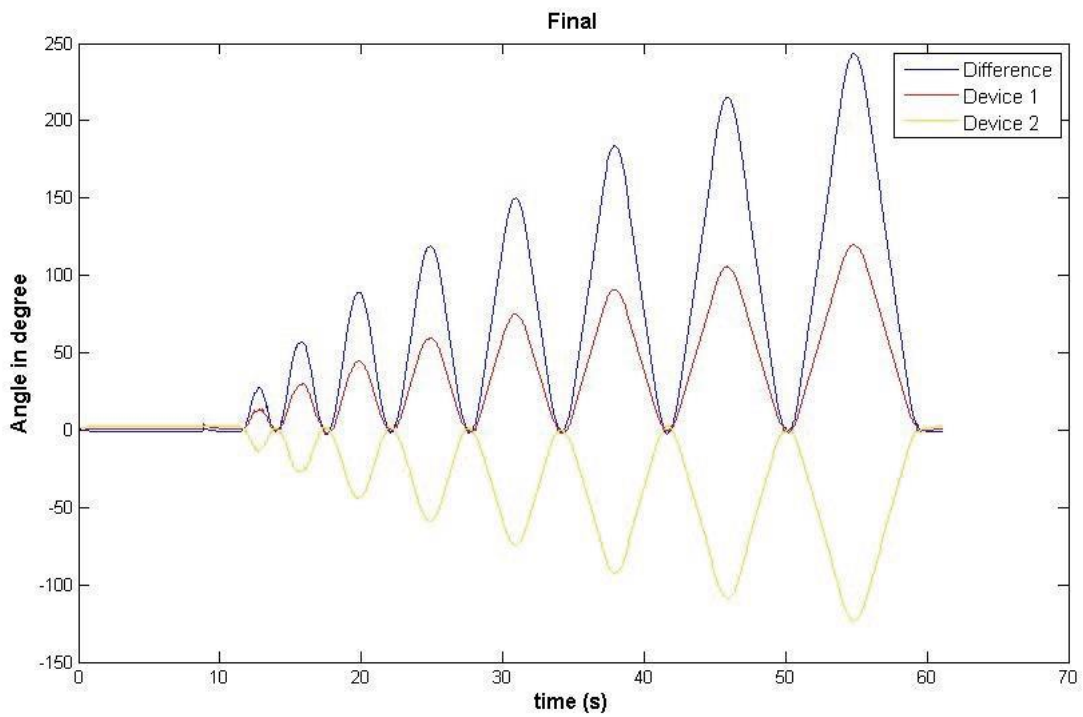
Figure 6.16: Trial 3 slow speed (30 degrees per second)
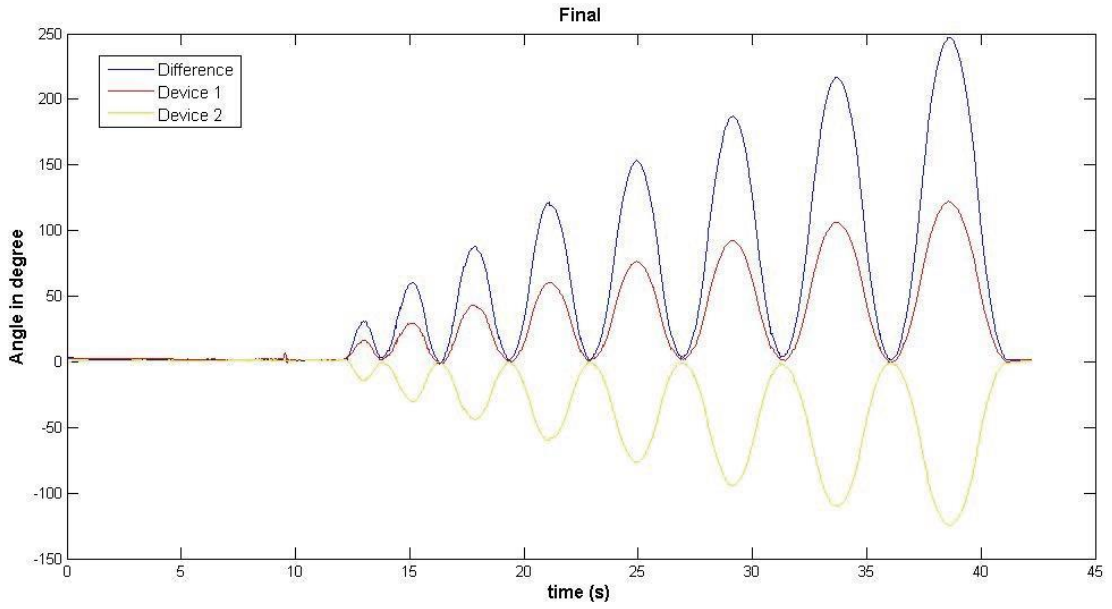
Figure 6.17: Trial 1 fast speed (180 degrees per second)
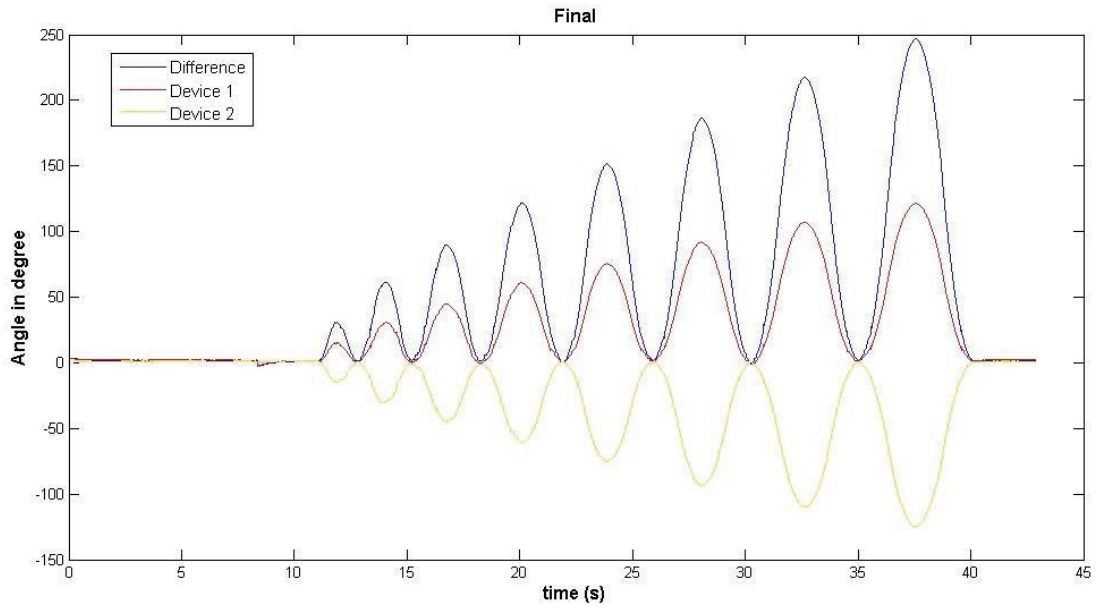
Figure 6.18: Trial 2 fast speed (180 degrees per second)
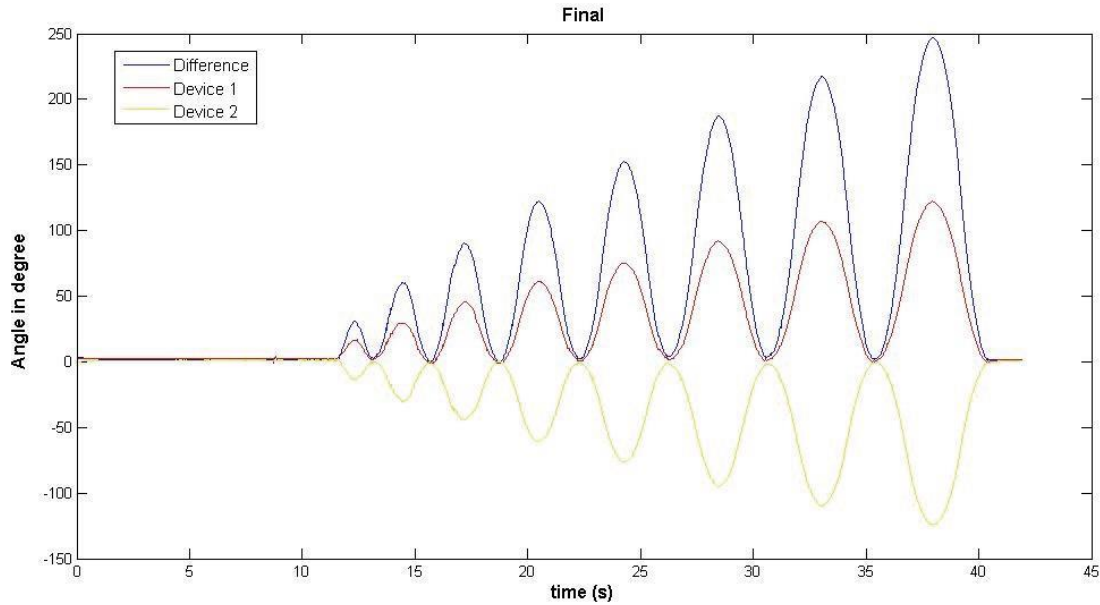
Figure 6.19: Trial 3 fast speed (180 degrees per second)

All the plots from Figures 6.14 to Figure 6.19 clearly illustrate the 8 steps movements as designed. The fast speed trail took longer testing time than expected as the motor spent more time on accelerating and decelerating when changing the direction. As both accelerating and decelerating will significantly reflect on accelerometers' reading, the purpose of fast speed trials for demonstrating the worst sensor testing condition is still valid.

Table 6.4 shows all peak readings from each step of each trial, the results are compared with the expected outcome.

Table 6.4: Two sensors stepper test result

	Expected outcome	Slow Trial 1	Slow Trial 2	Slow Trial 3	Fast Trial 1	Fast Trial 2	Fast Trial 3
Step 1	30°	28.7°	30.1°	27.7°	31.3°	30.9°	30.9°
Step 2	60°	58.7°	59.2°	57.3°	60.6°	61.5°	60.4°
Step 3	90°	89.5°	87.8°	89.3°	88.2°	90°	90.3°
Step 4	120°	118.9°	119.7°	119.1°	121.3°	121.9°	122.4°
Step 5	150°	150.2°	149.7°	150°	153.4°	151.8°	152.6°
Step 6	180°	184.2°	183.6°	183.9°	187.3°	186.2°	187.6°
Step 7	210°	214.4°	214.6°	215.3°	217.1°	217.5°	217.5°
Step 8	240°	243.7°	243.8°	243.6°	247.3°	247°	247.1°
Average difference		2.1°	2.0°	2.4°	3.8°	3.4°	3.6°
Largest difference		4.4°	4.6°	5.6°	7.3°	7.5°	7.6°
Average difference (excluding step 7, 8)		1.4°	1.2°	1.8°	2.6°	2.1°	2.4°

As results in Table 6.4 show, the average difference for slow speed trials is slightly above 2°, a quite precise accuracy for future human joint measurement under such large range of movements. As expected, the fast speed trials produced bigger errors because of rapid accelerating and decelerating changes due to high rotation speeds. However, the literature indicates that less than 4° average error standard still meets the need of many kinematic studies [6, 9, 10]. All the largest differences occurred in step 7 and step 8 where each motor moved more than 90° and the relative movement between the two sensors was more than 200°. Since the algorithm was focused on the moving range from -180° to 180° as discussed in chapter 5, an over-ranged movement might cause a loss in accuracy.   Considering that there are very few human joints that move more than 200°   [79], the results excluding readings from step 7 and step 8 show excellent accuracy of the system in measuring relative angular movements.

6.5 Precise sensor accuracy validation

6.5.1 Design of the experiment

The precise sensor accuracy validation test was demonstrated to verify the true measurement accuracy of the sensors. In Sections 6.3 and 6.4, the performance of the sensor under a variety of situation was tested. However, as the motors have mechanical tolerances, the sensor measurement accuracy had to be validated against a 'gold standard' of angle positions.

Both the cheap motor system and the visual method introduce a certain degree of error. A very accurate way to determine the value of an angle is by using inverse trigonometric functions. In a right-angled triangle, the value of all angles can be calculated if the length of the triangle's sides is known [80]. Figure 6.20 shows the setup of the custom made 'gold standard' for angle position verification.
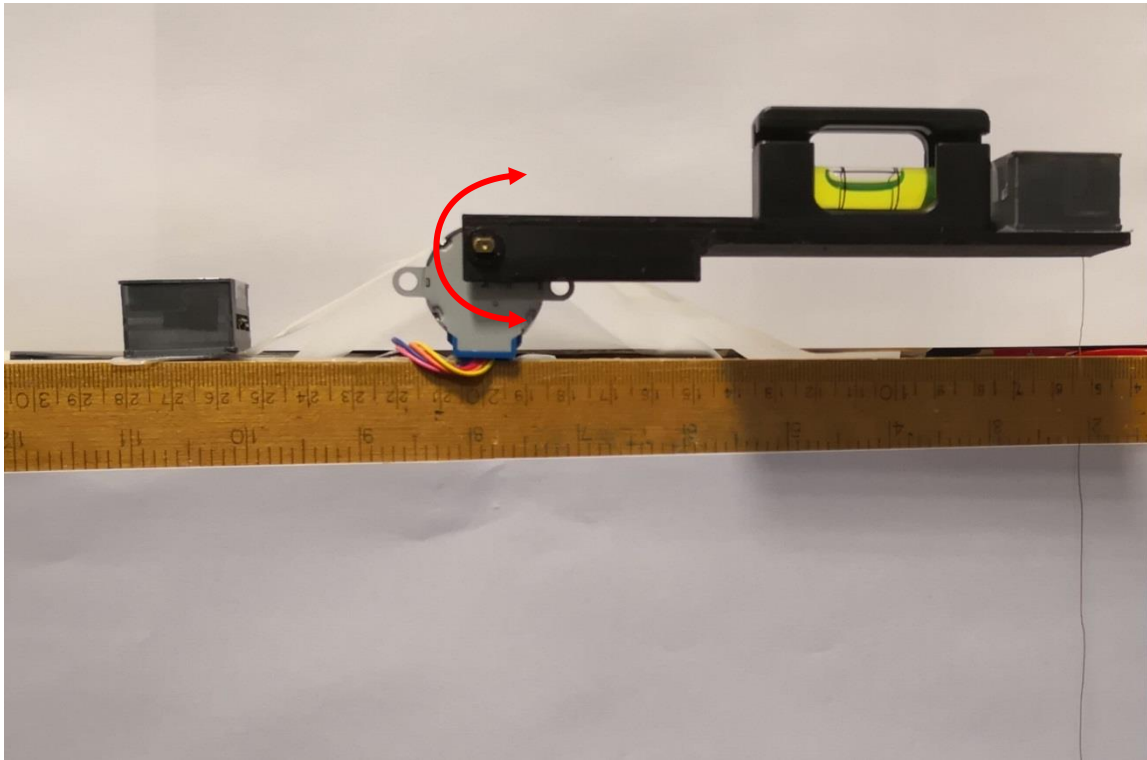
Figure 6.20: Precise sensor accuracy validation test setup

In Figure 6.20, a long ruler was installed at the edge of the desk; a stepper motor with a

3D printed arm was placed at 20 cm scale. A string with some hanging weight was attached at the end of the arm. One sensor was attached on the robot arm in Figure 6.20 and the other sensor was placed statically on the surface of the desk. The spirit level was used to calibrate the starting position of the motor. After the motor rotated the arm into a certain position, the rotation angle was calculated with equation 6.1:

$$\theta = arccos\left(\frac{B}{A}\right) \qquad (6.1)$$

In the equation 6.1, A (the hypotenuse) is the length of the motor arm which was measured as 14.2 cm from the string end to the centre of the rotor. B is the length of the bottom edge (adjacent cathetus) measured at the point where the string intersected the ruler. Figure 6.21 shows how the length of B was measured.
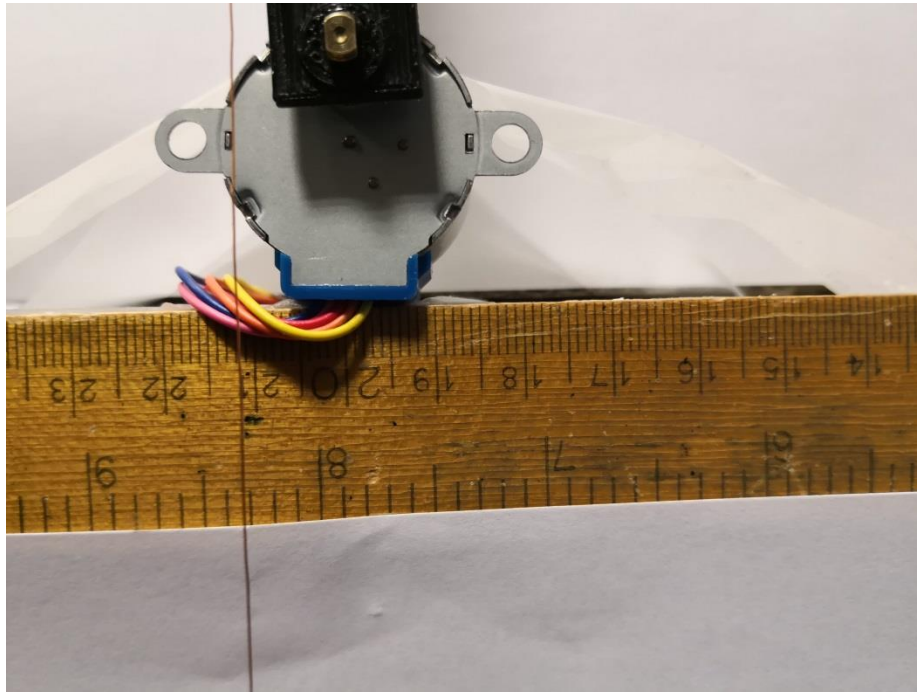
Figure 6.21: Measure the length of the bottom edge

In Figure 6.21, the centre of the motor is at 20 cm and the string is at 21.2cm. Thus, the length of the bottom edge B is -1.2cm.

As the string with the hanging mass would swing during the arm rotation, the

measurement of specific angles was taken before and after each trials. Only one desired angle position was set during each trial. In each trial, the motor was programmed to move to the desired position and return back to zero after 5 seconds delay. Five step movements were performed during each trial. Three tests with the target angle set at 30⁰, 60⁰ and 90⁰ were conducted, and each test was repeated twice.

6.5.2 Results

Figures 6.22, 6.23 and 6.24 show the comparison of both trials in each test. The output of the two repeated trials for each test were plotted in same figures, the starting time of each trials were aligned. Most plots in each figure are aligned perfectly which further validates the consistency of the sensor measurements.
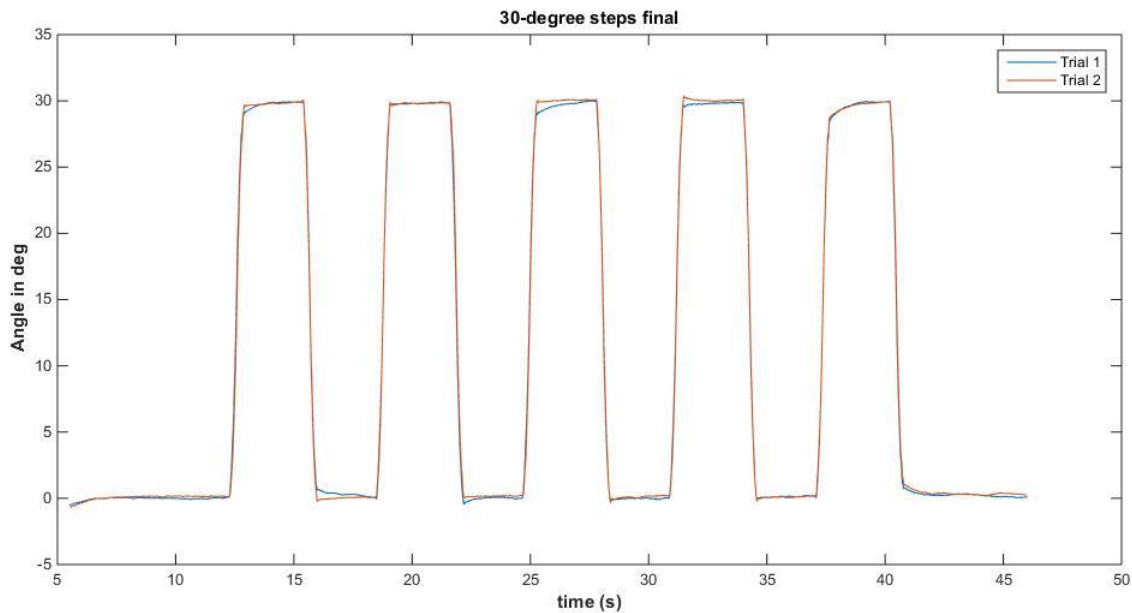
Figure 6.22: 30⁰ steps final outputs

From observation, both plots aligned to each other throughout most of each testing period while some distortions occurred at the peak reading in low angle position because the hanging weight from the string was pulling down the motor.
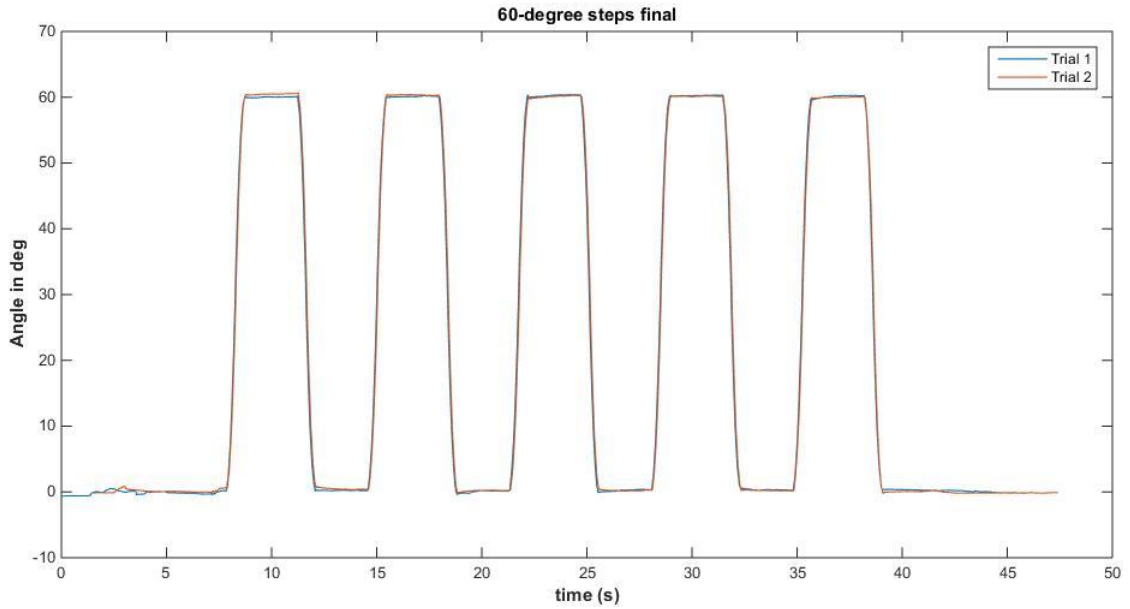
Figure 6.23: 60⁰ steps final outputs
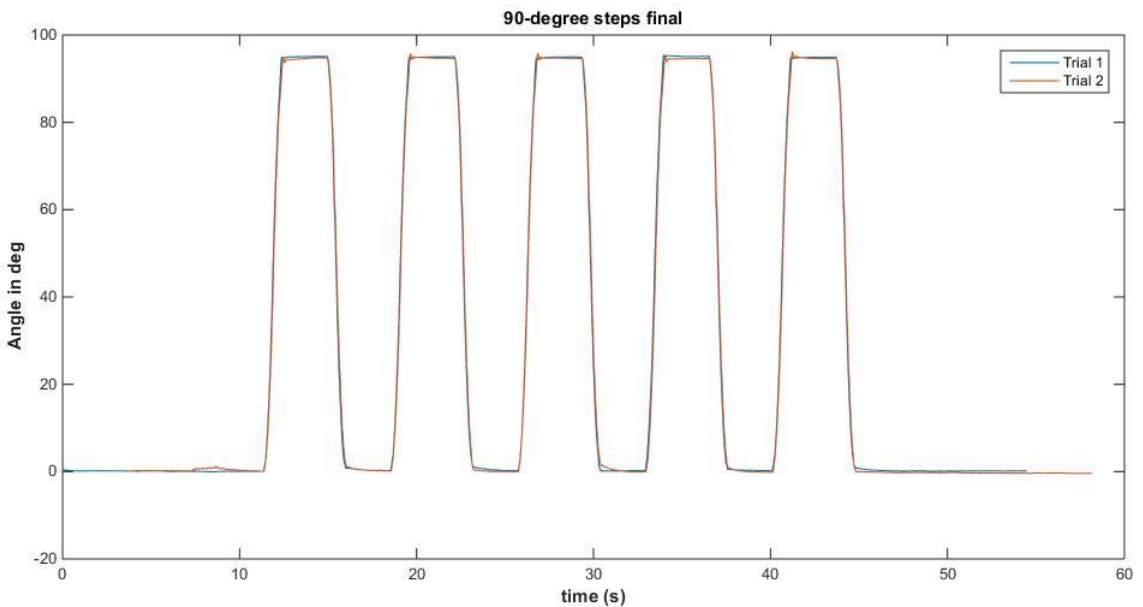
Figure 6.24: 90⁰ steps final outputs

Table 6.5 shows the measurements of bottom edge length from each trial. The expected angles were the calculated 'gold standard' angle as discussed in the last section. Table 6.6 shows all the peak reading of each step of each trial.

Table 6.5: The expected angles

Trials	Length of the bottom edge	Length of the robot arm	Actual robot angle
30º Trial1	12.3 cm		29.98º
30º Trial2	12.3 cm		29.98º
60º Trial1	7.1 cm	14.2 cm	60.00º
60º Trial2	7.1 cm		60.00º
90º Trial1	-1.2 cm		94.84º
90º Trial2	-1.2 cm		94.84º

As discussed in the last section, a spirit level was used to calibrate the starting position of the robot arm. Thus, the stepper motor moved into the exact position in both trials of each test. As shown in table 6.5, there was a 4º overshoot when the motor ran to 90º since the weight of the robot arm fell into the opposite direction. However, the motors were only used to deliver and hold a certain position. The motor's programmed rotation angle was not relevant in this test. The actual robot angle in Table 6.5 was calculated from the length of the bottom edge and the length of the robot arm using equation 6.1.

Table 6.6: Precise sensor accuracy validation result

Trials	Expected outcome	Step 1	Step 2	Step 3	Step 4	Step 5	Maximum difference
30º Trial1	29.98º	29.94º	29.86º	29.86º	29.74º	29.83º	0.24º
30º Trial2	29.98º	30.06º	29.90º	30.08º	30.15º	29.95º	0.17º
60º Trial1	60.00º	60.16º	60.07º	60.32º	60.21º	60.13º	0.32º
60º Trial2	60.00º	60.67º	60.30º	60.24º	60.18º	60.08º	0.67º
90º Trial1	94.84º	95.08º	94.97º	94.96º	95.13º	94.95º	0.29º
90º Trial2	94.84º	94.80º	94.57º	94.71º	94.60º	94.53º	0.31º

The result in Table 6.6 verified the true measurement accuracy of the sensor system. The difference throughout the entire test is 0.67 °. The outcome of the precise sensor accuracy validation test represents the maximum accuracy of the sensor which reveals the full potential of the sensor system.

6.6 Fix angle wrist movement test

6.6.1 Design of the experiment

The fixed angle wrist movement test was demonstrated to validate the ability of the sensors capturing relative movements. A 3D printed mechanism as shown in Figure 6.25 was designed to set a fixed angle between the two attached sensors.
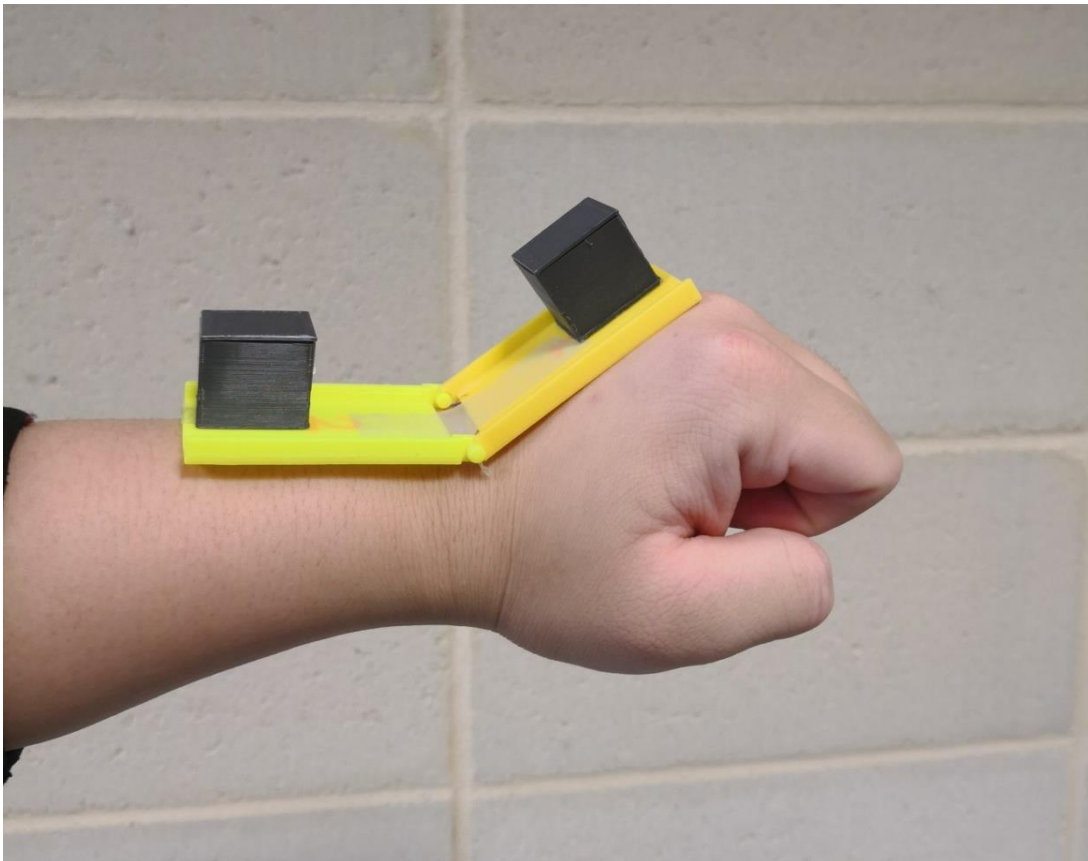
Figure 6.25: Fixed angle wrist movement test

As shown in Figure 6.25, both sensors were placed in a black case and attached to the edge of each platform. The initial angle between the two platforms could be adjusted.

Once an initial angle was measured and set with a protractor, the joint of the mechanism was locked. The fixed angle mechanism was then attached on the back of the hand and upper limb where the joint of the mechanism was aligned with the wrist centre. Instead of using the robotic mechanism to deliver certain single plane movements, the fixed angle mechanism was attached on the author's wrist to demonstrate actual human movements.

As to the accelerometer contains less noise during a static position, the hand was moved up and down five times in a wide range to create more acceleration noise. Test under such movements revealed the performance of the hardware and the algorithms under extreme conditions. The sensors were tested at three different angles (30°, 60° and 90°). Since the angle between the sensors was kept fixed by the mechanical device, the expected result was to keep reading a fixed angle, equal to the initial angle, in spite of movements of the hand. These experiments validated the performance of the two-sensor algorithm and confirmed that it can filter the relative noise from each single sensor and produce a clean reading.

6.6.2 Results

Figures 6.26, 6.27 and 6.28 show the five up and down waves performed by the participant. As expected, the final joint angle difference (blue line in the graph) is approximately a straight line since the joint angle was fixed during the experiment. Red and yellow lines in each figures show both sensors were capturing big movements throughout each trial.
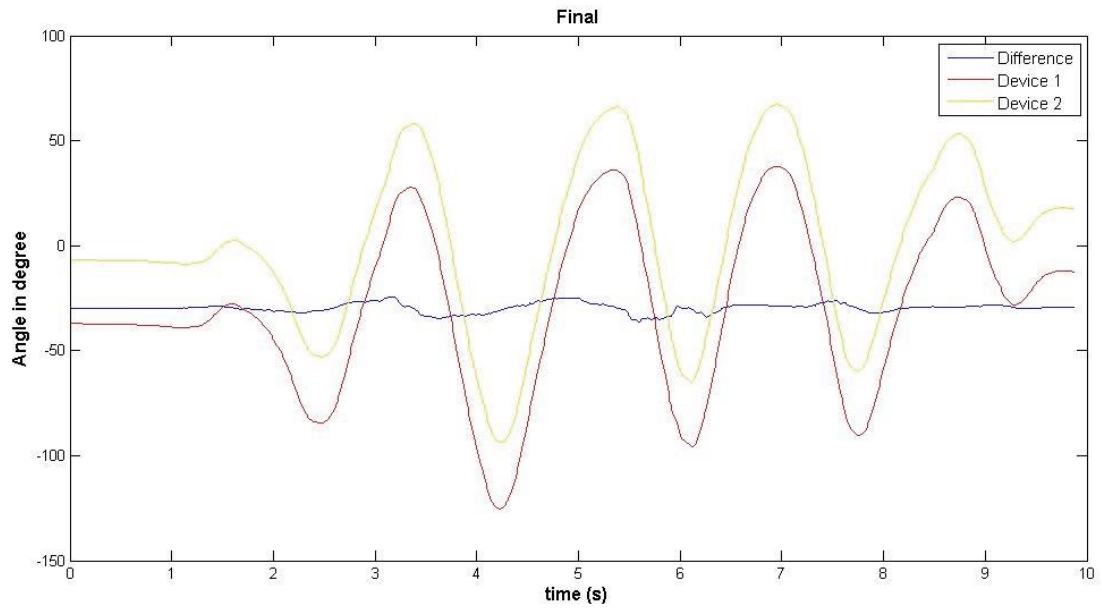
Figure 6.26: Fix angle readings at 30°
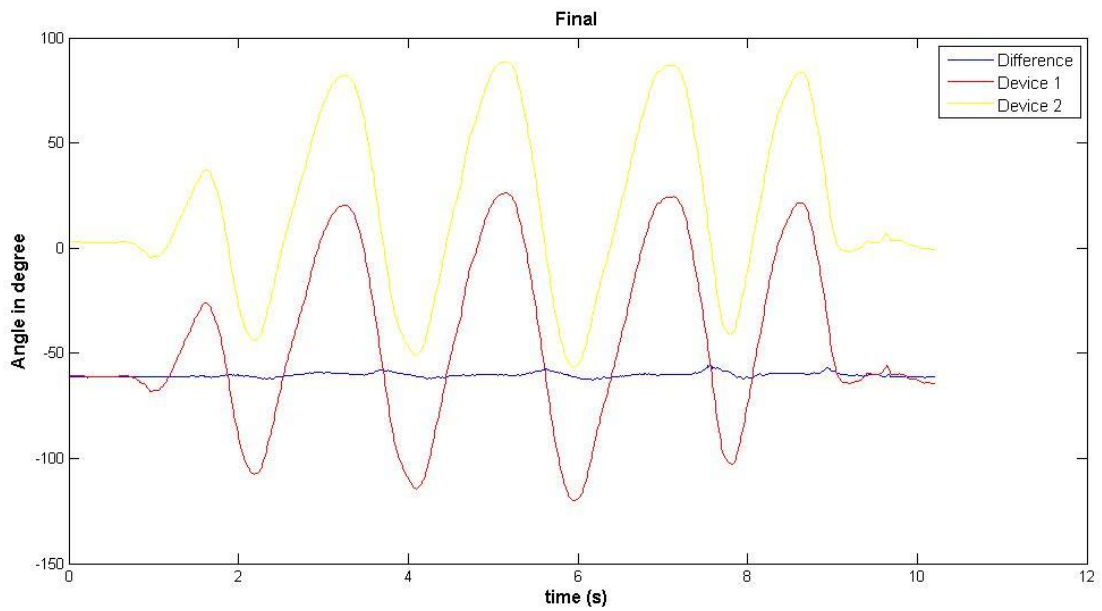
Figure 6.27: Fix angle readings at 60°
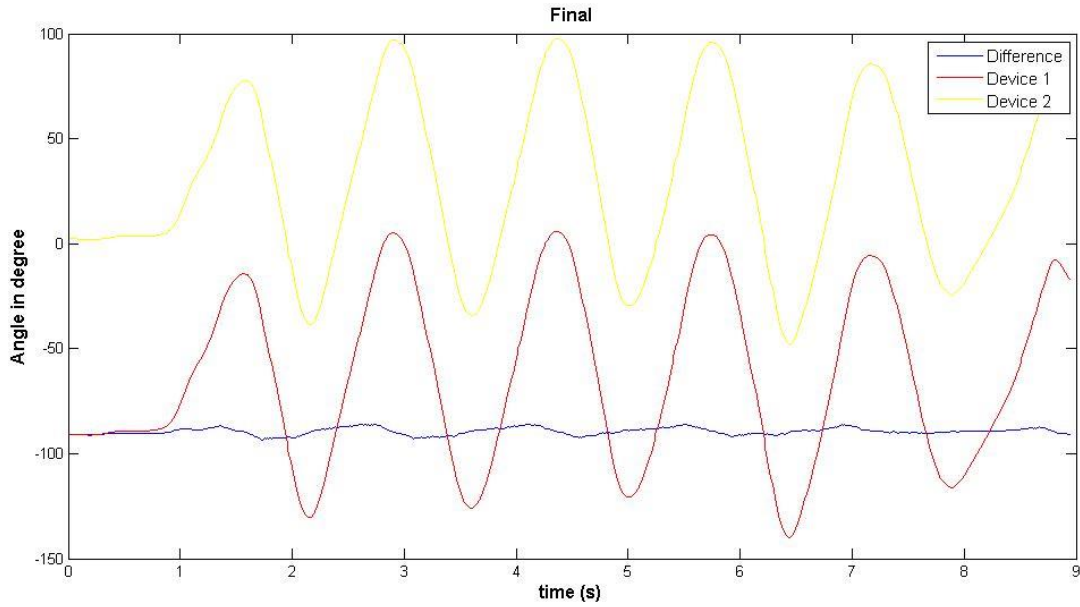
Figure 6.28: Fix angle readings at 90°

Readings in figures 6.27 and 6.28 are quite stable, almost a straight horizontal line. A small turbulence was recorded in the readings of figure 6.26. The turbulence was caused by wrist movements pulling the fix angle platform during wide movements. In table 6.7, the experimental initial angles are compared with the average readings throughout each trial. The maximum and minimum readings give the worst scenario of the experiment.

Table 6.7: Fix angle wrist movement test results

Trials	30°	60°	90°
Initial Angle	-29.8°	-61.3°	-90.5°
Average reading	-29.65°	-60.39°	-89.39°
Maximum reading	-26.14°	-56.03°	-86.77°
Minimum reading	-34.85°	-62.88°	-93.73°

Table 6.7 shows that the average readings are less than 1° in each trial, and the worst error is less than 5°. Results show the system can precisely capture the relative movement between two sensors, which validates the concept of the two-sensor algorithm and explore the potential of the sensors in wrist movement studies.

6.7 Summary

In this chapter, results from 5 different experiments were presented and discussed. Robotic tests were designed to examine the accuracy and consistency of the sensor system. The pan and tilt system used servo motors to create a repeatable and identical sequence as servo motors have the feature of receiving a position feedback signal. Only one sensor was attached to the pan and tilt system while the other sensor was placed statically on the table as a zero reference. The output of the test closely matched with the designed sequence. The result shows an excellent accuracy of less than $1°$ average error and a $3°$ maximum error.

As the thesis presented a human joint measurement system with two sensors, the two sensors stepper test was designed to validate the performance of the hardware and the algorithm while having two sensors moving at the same time. The two sensors stepper test used two stepper motors with one sensor on each. Both motors were programmed to rotate in opposite directions following a pre-determined sequence. Thus, the motors were creating the biggest possible relative movement. Results showed an acceptable accuracy. The average error was less than $2°$ for slow speed test and around $2.5°$ for fast speed test. A limitation of the sensor system was found during the two sensors stepper test: the measurement accuracy decreased when the relative movement was larger than $200°$. Such problem is not expected to cause major issues in human joint studies because very few human joints have more than $200°$ of range of motion [79].

Precise sensor accuracy validation used a custom made angle measurement mechanism to measure the exact motor movement angle. The same stepper motor from the two stepper motor test was used in this test. A string with a hanging weight was attached at the far end of the motor arm, and a ruler was placed on the horizontal plane to measure the string's displacement (adjacent edge of the right-angled triangle). With the length of the adjacent edge and the fixed length of the motor arm (hypotenuse), the actual angle position was calculated. Results showed a maximum error of $0.67°$. The accuracy of the sensors is very suitable for human joint measurements.

The fixed angle wrist movement tests validated the sensors' performance when both sensors were relatively static during the movements. A 3D printed mechanism was designed to set a fixed angle between the two sensors. Results from this test showed average errors of less than 1° in each trial. This proved that the sensor system is able to filter large movement noise in both sensors and precisely measure the relative angle between them. As the sensor was able to pick up different initial angles, the results indicate that the sensor system can deliver accurate and usable joint angle measurements without the need for an identical initial position. Such a feature provides more flexibility in many clinical applications when an identical initial position is hard to set.

Chapter 7

Collaboration project with rehabilitation researchers

7.1 Introduction

This Chapter discusses a collaboration project based on the presented system. As a medical data collection system, the prototype sensor was designed to support the real life needs of professional clinic doctors and researchers' studies. The experience gathered from such cooperation brought out both inspiration and challenges to the development of a medical prototype.

For the collaboration project the sensors were used in research trials to evaluate cerebral palsy patients. The primary focus was on wrist movement data collection. The trials ran by researchers from Princess Margaret Hospital (PMH), Perth Children's Hospital and Australia Catholic University (ACU) had the objective to evaluate baby and teenager cerebral palsy patients' wrist movement status. The system setup and some example results are discussed in Section 7.2. The major challenges on sensor downsizing and some issues with the initial position calibration are discussed in Section 7.3.

7.2 The Collaboration Project

7.2.1 A brief description of wrist measurements in cerebral palsy patients

A prototype system involving the outcome of this thesis was developed for supporting the data collection in paediatric cerebral palsy studies. Five sets, including wireless measurement sensors and its matching receiver dongle to achieve basic movement monitoring and precise wrist flexion and extension angle measuring, were delivered to four research teams in Perth, Sydney and Melbourne.

Cerebral palsy is one of the most common physical disabilities in childhood [81]. The

sensor system was used to examine upper limbs' range of movement from a group of children with cerebral palsy. The data helps doctors and researchers in the paediatric cerebral palsy study to monitor rehabilitation and understanding secondary upper limb musculoskeletal impairments [82] caused by cerebral palsy, and to track the improvements of activity performance.

The traditional method of wrist angle measurement relies on naked eye observations using very simple measurement tools such as goniometer, as shown in Figure 7.1. Such methods lack accuracy and consistency especially in time–based, symptom recognition studies.

Figure 7.1: Goniometer

In Figure 7.1, the goniometer works as the combination of a protractor and two straight rulers. It has been commonly used in passive measurements of joint flexion and extension range of movement in clinical tests.

For more advanced measurements, the modern optical 3D motion analysis method can provide more accurate and detailed movement capture. However, the optical 3D system requires multiple expensive high speed cameras and a special structured lab facility. Figure 7.2 show the motion analysis lab installed at Curtin University, Western Australia.

Figure 7.2: Curtin motion analysis lab using VICON system

7.2.2 Performance of the sensor system in wrist cerebral palsy studies

The sensor system in this thesis provided a flexible and low cost option. It could become a more feasible option for data collection with a large number of participants. The clinic teams that participated in the collaboration reported that there currently are two major on-going data collection tests groups. The two tests groups are targeting children of different age with cerebral palsy. Figures 7.3 and Figure 7.4 show examples of a child wearing sensors.

Figure 7.3: The sensors set up on a teenager participant [1]

Figure 7.4: The sensors tested on a teenager participant[3]

[3] Photograph published with consent of parent.

As shown in Figures 7.3 and 7.4 there were two sensors attached on the participants' upper limb for measuring wrist movement. All sensors were placed on the testing position; i.e. aligned with the wrist's joint centre. A series of trials were specifically designed to encourage the participant to achieve maximum joint movement. The sensors data provided the result by showing the active range of motion each participant achieved throughout the entire trial.

The current focus of the team was on single plan wrist flexion and extension measurements. Figure 7.5 shows wrist flexion and extension positions.
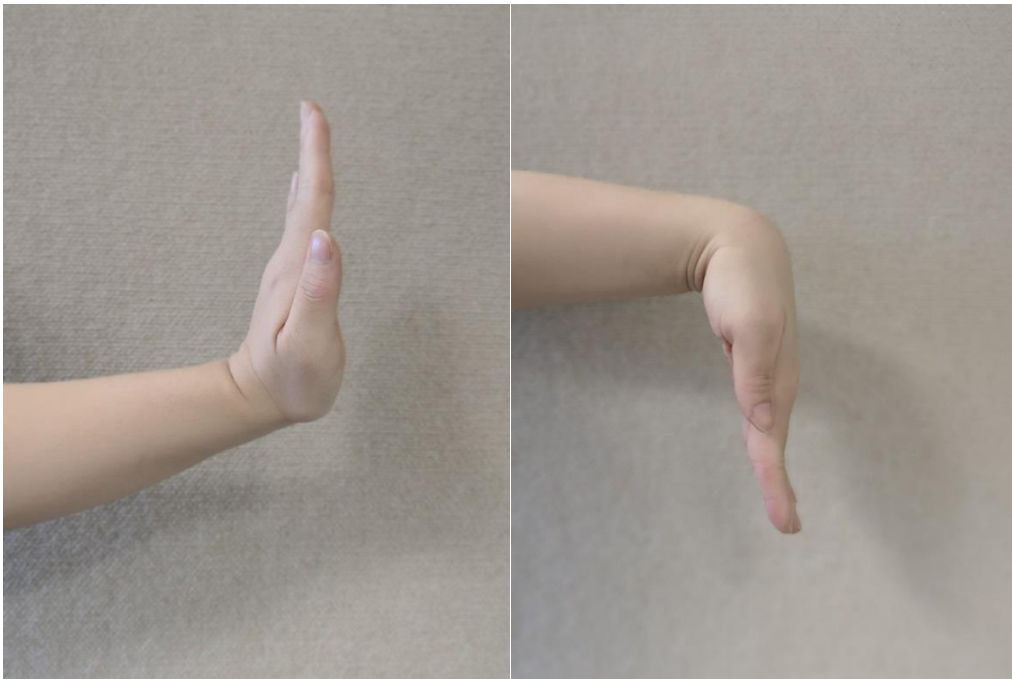
Figure 7.5: Wrist flexion (right) and extension (left) position

Figure 7.6 show an example of active human wrist flexion and extension movements captured by the sensors.
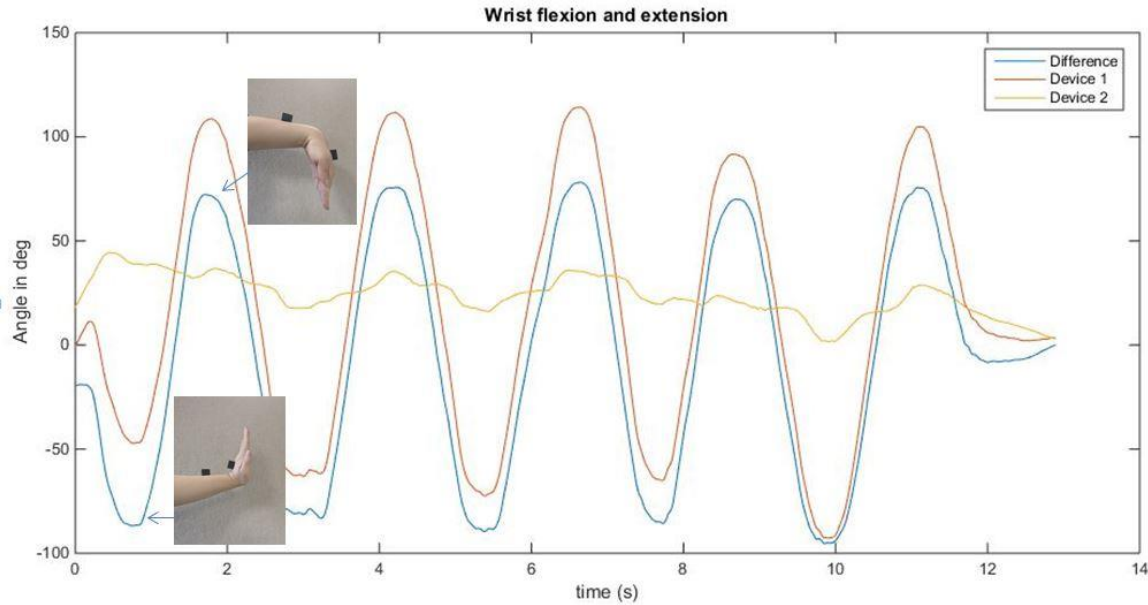
Figure 7.6: Wrist flexion and extension diagram

The sensor system has been proposed as new standard testing method for cerebral palsy studies. It could either be used as a platform for long term data collection or it could be developed as a convenient tool set for daily measurements. A technical note, currently under review for publication, compared the sensor performance in robotic experiments to evaluate the feasibility of using the sensor system in clinical assessments.

Figure 7.6 show some of the graphs that resulted from some random wrist activities captured with sensors. Although professional clinic researchers and doctors would be able to access the results with their specific protocols and standards, some interesting facts could already be observed from an engineering aspect which revealed more details and potential about the capability of the sensor system to work as a medical application.
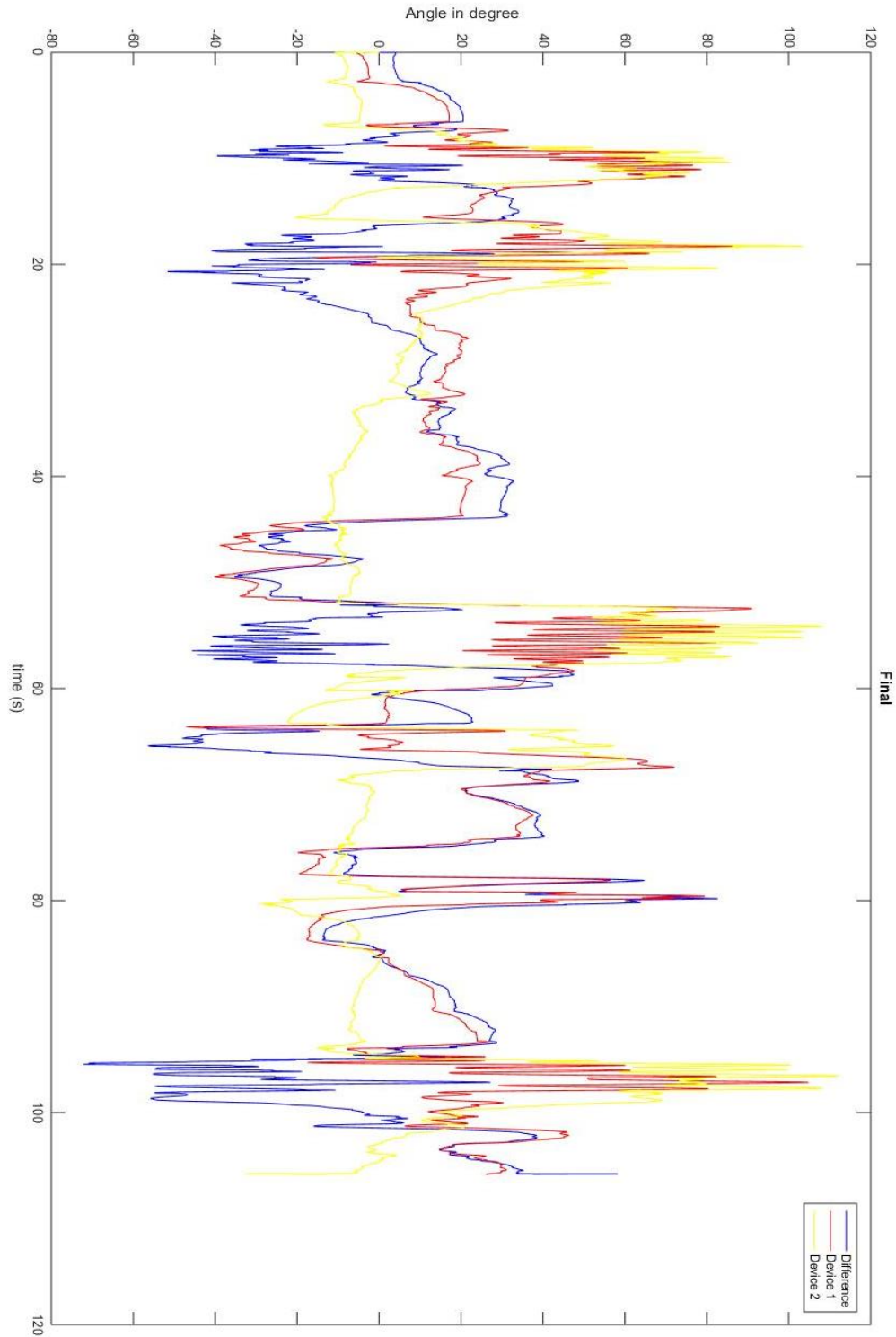
Figure 7.5: Result example for random human wrist activities[4].

[4]Detailed information of the human trials covered by ethics approval from Perth Children's Hospital, including raw and processed data, were not consented to be published in this thesis.

The blue line in Figure 7.5 shows the final wrist joint movements while the red and yellow lines show the relative movements on sensors in the hand and upper limb. Based on the observation of Figure 7.5, several sets of shaking movements can be spotted as rapid and identical movements occurring in short periods. The graphs reveal that the shaking activities were mostly varying in wrist extension angles and the range was only around 50 degrees. From an engineering perspective, the sensors captured repeating activities under rapid movements, proving the reliability of system in medical applications. The big difference of the final relative joint angle measurements compared against the movements of each sensor revealed the effectiveness of the two sensor-based joint orientation algorithm.

7.3 Challenges

7.3.1 Challenges in medical research

As one of the primary focuses of the sensor system was to be applied into medical studies, the transformation process from an engineering idea into a reliable medical prototype was without doubt quite a challenging task.

Any collaboration project involving teams from two completely different fields often requires knowledge contributions from each side. Transforming an engineering system into a data collection prototype for a medical study, incorporating the requirements from the medical area, was not as easy as expected.

Table 7.1 presents the lists of features of the sensor system prioritised by the engineering and clinic researchers.

Table 7.1: List of sensors' features in order of importance

Priority	List by engineers	List by doctors
1st	Low cost	Size of the sensors
2nd	Multiple sensors system	Wireless feature
3rd	Wireless feature	Wearable feature
4th	Rechargeable	High sampling rate
5th	Stable communication	Software support
6th	Software support	Rechargeable
7th	Wearable feature	Low cost
8th	Size of the sensors	Multiple sensors system

The engineers' list shown in Table 7.1 was based on the problem statement and priority foci defined during the designing stage. The doctors' list was gathered from opinions of the medical team. Table 7.1 shows that the priority concerns of the sensor's features for engineers and doctors were different. Although the sensor was originally validated as an engineering project, the medical team had concerns for application in their trials.

The first version of the sensors was too big to be attached on children's arms, especially for infants. As a rectangular shape box shown in Figure 4.6, the sensor placed on participant's hand had to be tilted 90° to avoid clashing with the upper limb sensor. Although the colours of the sensor boxes were bright and cheerful, some baby participants would still refuse to wear them due to the uncomfortable size. This feedback was incorporated in the latest version of the sensors, as discussed in Section 4.3. The final dimensions of the sensor distributed to the medical team were 22.8 x 25.2 x 21.5mm as shown in Figure 7.6.

Figure 7.6: Sensors distributed to the medical team

The cost of the materials and the procedure for the system set up were normally the first concerns in an engineering project. In contrast, the medical team does not require a detailed understanding of the structure of the system. As users of the application, they were looking for a user friendly system that was adaptable and reliable. As part of the protocol in any medical research project, validation tests are required when a new system is introduced into the study. In order to validate the sensor system with a pseudo-gold standard optical system, a sampling rate as fast as a 3D optical system with high speed cameras was expected from medical researchers. However, faster communication speed would have caused higher noise and data drop rate during data transmission, while the sensors would not require an extreme high sampling rate in human joint measurements. A clear explanation with supporting test on sensor communication performance was given to the medical team when the final communication speed was set.

7.3.2 Initial position calibration

As discussed in Chapter 5, the sensors were required to be placed in parallel positions so that all 3D axes were aligned to each other. However, it is a difficult task to perfectly align all sensors on the participants hand before each trial. The result would be invalid if the sensors' alignment was off by a significant angle.

Essentially, the sensors are always measuring their own positions and movements. Thus, placing sensor correctly on human's body where the sensors' reading will be

equivalent to certain human body movement is also quite a challenge. Traditional methods in other sensor based human motion measurement applications, like the ones discussed in Chapter 2, always require an initial 'zero' position where the sensors' reading can be calibrated as the starting point. However, in patients with cerebral palsy, it is usually difficult to set a perfect starting position with zero angle movement from the wrist joint.

The current method of sensor placement uses a standard protocol where the first sensor is placed in the middle of the line between the middle knuckle and the wrist centre; and the second sensor is placed mid-way between the wrist joint centre and the elbow joint centre. A further step of the solution could use camera footage to determine the actual initial offset.

7.4 Summary

The collaboration project on wrist cerebral palsy measurement revealed the potential and value of the sensor system in real life medical applications. In cerebral palsy studies, the sensor was used to collect patients' upper limb joint movement to identify both the passive and active range of motion resulting from secondary upper limb musculoskeletal impairments.

To apply the sensor system in medical studies, knowledge and understanding of the medical and engineering fields were exchanged. According to the list of important sensor features, clinic doctors were concerned about the feasibility and flexibility of the sensors, rather than the technical specifications. As a result, smaller size sensors with a friendly user interface were developed specifically for tests with babies.

The difficulty of aligning the sensors was higher when working with patients with cerebral palsy because these patients would not normally be able to give a standard zero position for initializing the sensors' position. A rigorous procedure was developed with the medical team to follow when placing the sensors onto participant's hand and upper limb. A more advanced solution involving the use of a camera to calibrate the initial position offset will be developed in the future.

This page is intentionally kept blank.

Chapter 8

Conclusions and Future Works

8.1 Conclusions

Many physiotherapy and medical kinematic studies require precise analysis of human joint movements. Naked-eye human observation with mechanical measurement apparatus (Goniometer) is regarded as common practice in most medical studies [3]. However, such method usually introduces high measurement error and is hard to apply in active motion studies [21][83]. Computer-assisted optical 3D analysis systems are the more precise methods in human movement studies and became one of the traditional standards in medical research [6]. These systems normally require expensive high-speed cameras and a specially constructed lab facility [7]. For clinical experiments, a motion analysis lab could cost millions of dollars. Wearable Micro Electro-Mechanical Systems (MEMS) inertial measurement unit (IMU) sensors have been introduced into clinical studies to serve specific purposes [9][10][11]. Rather than focusing in capturing specific human body movements, this thesis studied a flexible solution for most human joint measurement studies.

The hardware platform was designed to include the following features: high accuracy in joint orientation measurements, wireless communication, reduced size with wearable ability high data collection capacity and stability. Three versions of custom-made sensor models were developed in order to achieve satisfactory performance and a small enough size to serve in young age children cerebral palsy studies. The latest sensor is enclosed in a $22 \times 24 \times 18$ mm box. Each custom made sensor consists of an 8-bit AVR core microprocessor, an inertial measurement unit (IMU) and, and a 2.4 GHz Radio frequency (RF) radio. Each sensor is powered by a small, 90mAh, a 3.7 V rechargeable lithium polymer battery that can support up to 3 hours of non-stop measuring with one charge. The sensor can provide accelerometer and gyroscope measurements at 100 samples per second within a 10 meter range. With its portability and wireless connection, the sensors could be a

feasible option for most IMU-based applications. In comparison with most of market available IMU devices, the portable sensor developed in this thesis is one of the smallest. Table 8.1 compares version 3 of the sensor developed in this thesis against three of the most popular commercial IMU systems.

Table 8.1: Comparison with commercial IMU systems

	Xsens MVN [30]	APDM Opal [31]	Metawear C pro [84]	Sensor Version 3
Size	$47 \times 30 \times 13$ mm	$43.7 \times 39.7 \times$ 13.7 mm	22 mm diameter, 13 mm thickness	$22 \times 24 \times 18$ mm
Wireless	Yes	Yes	Yes	2.4 GHz RF radio
Sampling rate	60 Hz	50 Hz – 200 Hz	40 Hz [5]	100 Hz
Associated Software	Yes	Yes	No	Yes
Rechargeable	Yes	Yes	No	Yes
Cost	1200 EUR	TBA	60 USD	50 AUD in small prototype batch

[5]The fastest reliable speed as tested when airing both 3D accelerometer and gyroscope data

Along with the hardware, a software platform was developed in C sharp to provide functionality and user friendly features for sensor data recording, medical data management and data processing. The software opens a serial communication port on a PC and stores the raw data received from the receiver dongle in a series of files. A two-sensor filtering algorithm was developed to specifically target human joint motion estimation. The target human joint angle was measured from two sensors placed on opposite sides of the target joint. Unlike single sensor based applications, the proposed algorithm can work particularly well for movements where

there is no pre-determined set reference position (rest position). With the two-sensor system, the relative position between the sensors is the only outcome from the measurements.

The sensor system was validated using both robotic systems and an own-wrist experiment. Robotic tests were designed to examine the accuracy and consistency of the sensor system. A pan and tilt system used servo motors to create repeatable and identical movement sequences. Servo motors have a position feedback signal that produces excellent accuracy with less than 1° average error, and 3° maximum error. A two sensors stepper test was designed to validate the performance of the hardware and the algorithm while having two sensors moving at the same time. Results showed an acceptable accuracy where the average error was less than 2° for slow speed test and around 2.5° for fast speed test. Precise sensor accuracy validation used a custom made angle measurement mechanism to measure the exact motor movement angle. Results showed an outstanding accuracy of 0.67° maximum error in static condition.

Less than 1° average error was found in fixed angle test where a fix angle mechanism was attached on a moving wrist. The results proved that the sensor system is able to filter big movement noise in both sensors and precisely measure the relative angle between them. One of the significant outcomes of validation is that the sensor system requires no standard calibration position set in an initialisation stage. A 1.56° maximum RMSE was achieved throughout each continuous trial. The sensors are very accurate and suitable for most of human joint movement estimation [24].

The system is currently being used in research trials in Perth Children's Hospital to evaluate cerebral palsy patients. In cerebral palsy wrist studies, the sensor is used to collect patients' upper limb joint movement to study both the passive and active range of motion resulting from secondary upper limb musculoskeletal impairments. At the time of writing, five sets of sensor systems have been dispatched to different research groups across Australia. Hundreds of trials involving close to a hundred patients with cerebral palsy have taken place. More trials are being planned in the close future.

8.2 Future works

8.2.1 Initial position calibration

As discussed in section 7.3.2, the result of sensors could become invalid if the sensors' initial placement is significantly misaligned. The initial position is hard to calibrate during the trials with no standard or identical positions. Some studies discussed in Chapter 2 show how calibration position can be defined [9, 25]. However, in some tests such as the cerebral palsy wrist movement studies discussed in Chapter 7, a patient with cerebral palsy is normally not able to give a standard initial position with zero angle movement in the wrist joint.

Besides having a standard protocol to identify the sensors' initial position, additional methods have to be developed to calibrate/verify the initial position. One of the simplest solutions could be using image processing techniques to analyse the initial placement angles from a video taken before tests. Alternatively, additional IMU devices could be introduced into the test to provide more reference positions.

8.2.2 All in one device

The sensor currently consists of three difference boards as described in Chapter 4. An all-in-one device is a custom designed PCB including all the processor, radio and measurement sensor functions; would be necessary for big-scale medical research trials or commercial products. The PCB Gerber view in Figure 7.6 shows the current design of the processor. The current PCB was an atmel328 based microcontroller, only I2C and SPI connection was opened in order to minimise the size of the board. The future all-in-one device will merge the radio and MPU sensor into the board. As all the connection pins can be removed with internal trace, a similar size 4 layers PCB board can be expected to deliver the job. Both latest version of the schematic design and board design of the microcontroller board is shown in Appendix A.
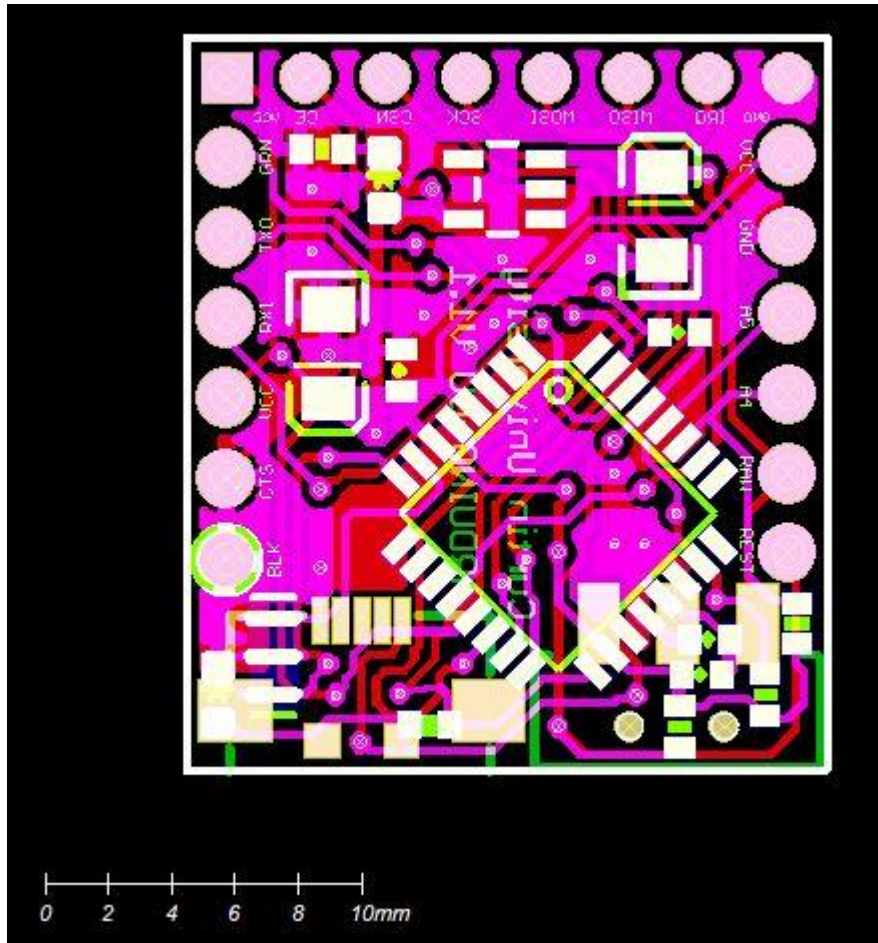
Figure 8.1: PCB Gerber view of the sensor processor

The microcontroller board design in Figure 7.6 is currently a two layer PCB with components on one side. According to Figure 4.5, the current build of the sensor also includes two commercial boards, an IMU and an RF radio. In future work, a complete custom-made sensor device with radio and measurement unit included on one board or one chip could be developed. As discussed in Chapter 7, size of the IMU system is one of the biggest concerns of the medical team involved in paediatric research. With custom-selected radio chip and measurement unit, the performance of the sensor could be further improved and the size of the sensor could potentially become even smaller.

8.2.3 More medical measurement applications

The sensor system developed in this thesis has potential application in any human joint measurement study. As long as protocols for sensor placement are developed, studies on other human joints are possible. According to the medical team of the

collaboration cerebral palsy project, the next step after wrist movement analysis would be to use the sensor system in elbow and shoulder movement studies.

The most effective way to capture and analyse human body joint movements would be having multiple sets of sensors working at the same time. The sensors could be used to capture movements from different joint orientations and they could also be used as other reference sensors to improve accuracy. The biggest challenge for multiple sets of sensors working at the same time is communication performance. Better communication methods need to be developed to avoid communication dropout with the associated loss of data.

8.2.4 Results' evaluation by machine learning algorithms

Critical tasks in motion analysis studies are identifying critical properties and movements in the data captured from random activities. Especially in children cerebral palsy studies, the activities recorded in range of motion analysis are often quite random. Currently making sense of data acquired from a long task with complete random movements is extremely hard because most of the analysis is still done by human observation of the graphs.

There is need to develop algorithms capable of analysing data and identifying faulty results that may have occurred due to hardware limitations, data drop, or hardware failure. Machine learning algorithms are considered a feasible future direction to organise data and provide more straightforward and easy to understand results. As the sensors are currently used in a big scale and long term study, the collected data and results could be perfect sources for the training of machine learning algorithms.

8.2.5 Further validation studies for medical applications

Validation of the sensor's performance is critical to determine whether the sensor can be incorporated in medical studies. Preliminary results of a study comparing data obtained with the sensor system against data acquired with a commercial optical system (a pseudo-gold standard) are very encouraging.

In medical research it is common to compare the performance of sensors against a pseudo-gold standard. Such pseudo-gold standards may have an error range larger than the sensor's precision. As presented in Section 6.5, a mechanical angle-measurement structure was created. It can work as a new pseudo golden standard for sensors' static performance validation.

In the future, the angle-measurement device can be modified into a device supporting none static angle position measurement. The current method uses a string to read the sensor position on the ground scale which will not be accessible during movement. A laser transmitter with a feedback receiver could be used to read the height of the sensor to the bottom table surface. An embedded system could be developed to calculate the angle under motion.The mechanical device could be used as the new pseudo golden standard for sensor validation.

This page is intentionally kept blank.

References

[1]   B.   Appleton,   "Joints   and   Skeletal   Movement | Boundless Biology," Courses.lumenlearning.com,   2018.   [Online].   Available: https://courses.lumenlearning.com/boundless-biology/chapter/joints-and-skelet al-movement/. [Accessed: 14 Jul 2018].

[2]   "9.5 Types of Body Movements – Anatomy and Physiology," Opentextbc.ca, 2018.   [Online].   Available: https://opentextbc.ca/anatomyandphysiology/chapter/9-5-types-of-body-move ments/. [Accessed: 06 Aug 2018].

[3]   A. Sawant, "Measurement of Joint Motion: A Guide to Goniometry, Third Edition," Physiotherapy Canada, vol. 56, no. 04, 2004, pp. 250.

[4]   J. Z. Edwards, G. A. Kenneth, . R. S. Davis, . M. W. Kovacik, . D. A. Noe and M. J. Askew, "Measuring flexion in knee arthroplasty patients," *The Journal of Arthroplasty*, vol. 19, no. 3, pp. 369-372, 2004.

[5]   M. Rehm et al., "Wave Like an Egyptian - Accelerometer Based Gesture Recognition for Culture Specific Interactions," British Computer Society, 2007.

[6]   T. Besier, D. Sturnieks, J. Alderson and D. Lloyd, "Repeatability of gait data using a functional hip joint centre and a mean helical knee axis," *Journal of Biomechanics*, vol. 36, no. 8, pp. 1159-1168, 2003.

[7]   J.C. Sabel, "Optical 3D motion measurement," in *Instrumentation and Measurement   Technology   Conference*,   1996,   DOI: 10.1109/IMTC.1996.507408.

[8]   H. Eren, "Measurments, Instrumentation, and Electronic Portable Instrument," in *Electronic Portable Instruments: Design and Applications, Boca Raton, FL: CRC Press*, 2004, pp. 1-7.

[9]   N. Abhayasinghe, I, Murray, "Human Gait Phase Recognition Based on Thigh Movement Computed using IMUs," in *2014 IEEE Ninth International*

Conference on Intelligent Sensors, Sensor Networks and Information Processing (ISSNIP), Singapore, 2014, DOI: 10.1109/ISSNIP.2014.6827604.

[10] K. Liu, T. Liu, K. Shibata, "Novel approach to ambulatory assessment of human segmental orientation on a wearable sensor system," *J. Biomechanics*, vol. 42, no. 16, 2009, pp. 2747–2752, DOI:10.1016/j.jbiomech.2009.08.008.

[11] T. Seel, T. Schauer, J. Raisch. "Joint Axis and Position Estimation from Inertial Measurement Data by Exploiting Kinematic Constraints," in *IEEE Multi-Conference on Systems and Control*, Dubrovnik, Croatia, 2012, pp. 45–49.

[12] David J. Sturman, "A Brief History of Motion Capture for Computer Character Animation," MEDIALAB, 1999.

[13] P. Nogueira, "Motion Capture Fundamentals - A Critical and Comparative Analysis on Real-World Applications," Faculdade de Engenharia da Universidade do Porto, 2011.

[14] T.W. Calvert, J. Chapman and A. Patla, "Aspects of the kinematic simulation of human movement," *IEEE Computer Graphics and Applications*, vol. 2, no. 9, pp. 41-50, 1982.

[15] J. Kleiser, "Character motion systems. Course Notes: Character Motion Systems," *ACM SIGGRAPH 93*, Anaheim, CA, pp. 33-36, 1993.

[16] M. Kitasgawa and B. Windsor, "An Overview and History of Motion Capture," in *MoCap of Artists: Workflow and Techniques for Motion Capture,* ch. 1, 2008, pp. 7-8.

[17] Vicon. [Online]. Available: http://www.vicon.com/. [Accessed 4 Jul 2018].

[18] Tracklab. [Online]. Available: http://www.tracklab.com.au. [Accessed 4 Jul 2018].

[19] K. Kong, Y. Kim, J. Kim, S. Kim and K. Baek, "Single-Package Motion Gesture Sensor for Portable Applications," *IEEE Transaction on Consumer Electronics*, vol. 59, no. 4, 2013, DOI: 10.1109/TCE.2013.6689698.

[20] Leapmotion, "How does it work?". [Online]. Available: https://leapmotion.zendesk.com/entries/39268303-Buying-a-Leap-Motion-Cont roller. [Accessed: 26 Jul 2016].

[21] Stuberg, W.A., R.H. Fuchs, and J.A. Miedaner, "Reliability of goniometric measurements of children with cerebral palsy," *Developmental Medicine & Child Neurology*, vol. 30, no. 5, pp. 657-666, 1988.

[22] Z. Zhang, Z. Wu, J. Chen and J. Wu, "Ubiquitous Human Body Motion Capture Using Micro-sensors," in *2009 IEEE International Conference on Pervasive Computing and Communications*, March, 2009, DOI: 10.1109/PERCOM.2009.4912827.

[23] S.Oniga and I. Orha, "Intelligent Human-Machine Interface Using Hand Gesture Recognition", University of Debrecen, Debrecen, Hungary, May, 2012.

[24] M. El-Gohary and J. McNames, "Human Joint Angle Estimation with Inertial Sensors and Validation with A Robot Arm," in *IEEE Transaction on Biomedical Engineering*, vol. 62, no. 7, 2015.

[25] D. Alvarez, J. Alvarez, R. González and A. Lopez, "Upper limb joint angle measurement in occupational health," *Computer Methods in Biomechanics and Biomedical Engineering*, vol. 19, no. 2, pp. 159–170, 2016.

[26] Nike, "Nike + Fuel Band SE," [Online]. Available: http://www.nike.com/us/en_us/c/nikeplus-fuelband. [Accessed: 26 Jul 2016].

[27] Kickstarter. "Control VR- The future of Virtual Reality, Animation &more," [Online]. Available: https://www.kickstarter.com/projects/controlvr/control-vr-motion-capture-for-vr -animation-and-mor. [Accessed: 2 September 2014].

[28] YET, "3-Space™ Sensors," [Online]. Available: https://yostlabs.com/3-space-sensors/. [Accessed: 14 Sep 2018].

[29] X-IMU. [Online]. Available: http://x-io.co.uk/x-imu/. [Accessed: 14 Sep 2018].

[30] XSENS. [Online]. Available: https://www.xsens.com/. [Accessed: 14 Sep 2018].

[31] APDM. [Online]. Available: https://www.apdm.com/wearable-sensors/. [Accessed: 14 Sep 2018].

[32] S.-h. P. Won, W. W. Melek and F. Golnaraghi, "A Kalman/Particle Filter-Based Position and Orientation Estimation Method Using a Position Sensor/Inertial Measurement Unit Hybrid System," *IEEE Transactions on Industrial Electronics*, vol. 57, no. 5, pp. 1787-1798, 2010.

[33] G. Pons-Moll, A. Baak, T. Helten, M. Müller, H.-P. Seidel and B. Rosenhahn, "Multisensor-fusion for 3D full-body human motion capture," in 2010 IEEE Conference on Computer Vision and Pattern Recognition (CVPR), San Francisco, CA, 2010.

[34] R. Goodrich, "Accelerometers: What They Are & How They Work," LiveScience.com, 2013. [Online]. Available: https://www.livescience.com/40102-accelerometers.html. [Accessed: 6 Sep 2017].

[35] "Accelerometer," Wikipedia.org. [Online]. Available: https://en.wikipedia.org/wiki/Accelerometer [Accessed: 13 Apr 2016].

[36] Starlino, "A Guide to using IMU (Accelerometer and Gyroscope Devices) in Embedded Applications," Starlino electronics, 2009. [Online]. Available: http://www.starlino.com/imu_guide.html. [Accessed: 3 Jul 2018].

[37] F. Bagala, V. L. Fuschillo, L. Chiari, "Calibrated 2D angular kinematics by single-axis accelerometers: From inverted pendulum to N-Link chain," *IEEE Sensors journal*, vol. 12, no. 3, pp. 479–486, 2012.

[38] "Gyroscope," Wikipedia.org. [Online]. Available: https://en.wikipedia.org/wiki/Gyroscope. [Accessed: 13 Apr 2016].

[39] EPSON, "Gyro sensors - How they work and what's ahead," epson.com, 2018. [Online]. Available: https://www5.epsondevice.com/en/information/technical_info/gyro/. [Accessed: 4 Jul 2018].

[40] I. Pasciuto, G.Ligorio, E. Bergamini, "How Angular Velocity Features and

Different Gyroscope Noise Types Interact and Determine Orientation Estimation Accuracy," in *Sensors 2015*, vol. 15, 2015, pp. 23983-24001, doi:10.3390/s150923983

[41] "Magnetometer," Wikipedia.org. [Online]. Available: https://en.wikipedia.org/wiki/ Magnetometer. [Accessed: 13 Apr 2016].

[42] InvenSense, "Compasses/Magnetometers," AN-000011 datasheet, 2014. [Revised 27 Aug 2014].

[43] T. Ozyagcilar, "Calibrating an eCompass in the Presence of Hard- and Soft-Iron Interference," Freescale Semiconductor Application Note, pp. 3-4, 2015.

[44] A. Noordin, M. Basri and Z. Mohamed, "Sensor Fusion Algorithm by Complementary Filter for Attitude Estimation of Quadrotor with Low-Cost IMU," *Telecommunication Computing Electronics and Control*, vol. 16, no. 2, p. 868, 2018.

[45] T. Islam, M.S. Islam, M. Shajid-Ul-Mahmud and M. Hossam-E-Haider, "Comparison of Complementary and Kalman Filter Based Data Fusion for Attitude Heading Reference System," *AIP Conference Proceedings*, 2017, doi: 10.1063/1.5018520.

[46] S. Colton, "Fun with the Complementary Filter / MultiWii," scolton.blogspot.com, 2012. [Online]. Available: http://scolton.blogspot.com/2012/09/fun-with-complementary-filter-multiwii.html. [Accessed: 6 Sep 2017].

[47] A.Z. Azfar and D. Hazry, "A simple approach on implementing IMU sensor fusion in PID controller for stabilizing quadrotor flight control," Signal Processing and its Applications (CSPA), in *2011 IEEE 7th International Colloquium*, 2011, DOI: 10.1109/CSPA.2011.5759837

[48] D. Simon, "Kalman filtering with state constraints: A survey of linear and nonlinear algorithms," in *Control Theory Appl.*, vol. 4, no. 8, 2010, pp. 1303–1318.

[49] R. Mahony, T. Hamel and J. Pflimlin, "Nonlinear Complementary Filters on the Special Orthogonal Group", *IEEE Transactions on Automatic Control*, vol. 53, no. 5, pp. 1203-1218, 2008.

[50] W. Premerlani and P. Bizard, "Direction Cosine Matrix IMU: Theory," 2009. [Online].   Available: https://www.researchgate.net/publication/265755808_Direction_Cosine_Matri x_IMU_Theory. [Accessed: 7 May 2018].

[51] S. Madgwick, A.Harrison and R. Vaidyanathan, "Estimation of IMU and MARG orientation using a gradient descent algorithm," in *2011 IEEE International Conference on Rehabilitation Robotics*, ETH Zurich Science City, Switzerland, 2011.

[52] V. Renaudin, M.H. Afzal and G. Lachapelle, "New Method for Magnetometers Based Orientation Estimation," in *IEEE/ION PLANS 2010*, Palm Springs, CA, 2010.

[53] K.P. Murphy, "Dynamic Bayesian Networks: Representation, Inference and Learning," PhD thesis, UC Berkeley, 2002.

[54] X. Fang, C. Liu and Z. Jiang, "Reference values of gait using APDM movement monitoring inertial sensor system," *Royal Society Open Science*, vol. 5, no. 1, pp. 170818, 2018.

[55] C. Kothari, Research methodology, 2nd ed. New Age International (P) Ltd., 2004, pp. 10-19.

[56] Arduino, "ARDUINO UNO REV3". [Online]. Available: https://store.arduino.cc/usa/arduino-uno-rev3. [Accessed: 28 Jul 2016].

[57] A. Gallo, INFN LNF, "Basics of RF electronics", *CERN Yellow Report CERN-2011-007*, pp. 223-275, 2011.

[58] T. Goonan, Lithium use in batteries. Reston, Va.: U.S. Dept. of the Interior, U.S. Geological Survey, 2012.

[59] "Serial Peripheral Interface," Wikipedia.org. [Online]. Available: https://en.wikipedia.org/wiki/Serial_Peripheral_Interface. [Accessed: 10 Oct

2017].

[60] J. Valdez and J. Becker, "Understanding the I^{2}C Bus," Texas Instruments, Tech. Report. SLVA740, Jun 2015.

[61] InvenSense, "MPU-9150 Product Specification Revision 4.3," PS-MPU-9150A-00 datasheet, 2014. [Revised 18 Sep 2013].

[62] Nordic Semiconductor, "nRF24L01+ Single Chip 2.4GHz Transceiver Preliminary Product Specification v1.0," nRF24L01+ datasheet, 2007. [Revised Mar 2008].

[63] Atmel, "8-bit AVR Microcontrollers ATmega328/P," Atmel-42735B-ATmega328/P Datasheet, 2016. [Revised Nov 2016].

[64] Arduino, "ARDUINO PRO MINI". [Online]. Available: https://store.arduino.cc/usa/arduino-pro-mini. [Accessed: 28 Jul 2016].

[65] "EMI Electromagnetic Interference Basics - a summary about EMI - electromagnetic interference - the types of EMI and how they affect electronics equipment," electronics-notes.com. [Online]. Available: https://www.electronics-notes.com/articles/analogue_circuits/emc-emi-electro magnetic-interference-compatibility/what-is-emi-basics-tutorial.php. [Accessed: 28 Jul 2016].

[66] K. T. Manal and T. S. Buchanan, "Biomechanics of Human Movement," *Standard handbook of Biomedical engineering and design*, The McGraw-Hill Companies, pp 5.1-5.26, 2004.

[67] "Path loss," Wikipedia.org. [Online]. Available: https://en.wikipedia.org/wiki/Path_loss. [Accessed: 14 Nov 2017].

[68] "ASCII Table and Description," asciitable.com, 2010. [Online]. Available: http://www.asciitable.com. [Accessed: 2 Feb 2018].

[69] A. Savitzky, M.J.E. Golay, "Smoothing and Differentiation of Data by Simplified Least Squares Procedures," *Analytical Chemistry*, vol 36, no 8, pp. 1627–39, 1964,. doi:10.1021/ac60214a047.

[70] E.I. Organick, "Some processors also offer the library function called ATAN2, a function of two arguments (opposite and adjacent)," *A FORTRAN IV Primer*, Addison-Wesley, pp. 42, 1966.

[71] P. Moon and D.E. Spencer, "Spherical Coordinates (r, θ, ψ)," in *Field Theory Handbook, Including Coordinate Systems, Differential Equations, and Their Solutions (corrected 2nd ed., 3rd print ed.)*, New York: Springer-Verlag, 1988, pp. 24–27.

[72] W.T. Higgins JR, "A Comparison of Complementary and Kalman Filtering," in *IEEE Trans. Aerospace and Electronic Systems*, vol. AES-11, no. 3, May 1975, pp. 321-325.

[73] E. Meijering, "A chronology of interpolation: from ancient astronomy to modern signal and image processing," in *Proceedings of the IEEE*, vol. 90, no. 3, 2002, pp. 319–342, doi:10.1109/5.993400.

[74] W. Elmenreich, "An Introduction to Sensor Fusion," Institut fur Technische Informatik, Vienna University of Technology, Austria, Tech. Report. 47/2001, 19 Nov. 2002.

[75] W. Xu, C. Ortega-Sanchez and I. Murray, "Measuring Human Joint Movement with IMUs: Implementation in custom-made low cost wireless sensors," in *2017 IEEE 15th Student Conference on Research and Development (SCOReD)*, Malaysia, Dec, 2017.

[76] DFRobot Electronics, "DF05BB Standard Servo (SKU:SER0020)," dfrobot.com, 19, May, 2017. [Online]. Available: https://www.dfrobot.com/wiki/index.php/DF05BB_Standard_Servo_(SKU:SER0020). [Accessed: 6 Jan 2018].

[77] H. Eglowstein, "Introduction to Servo Motors," sciencebuddies.org. [Online]. Available: https://www.sciencebuddies.org/science-fair-projects/references/introduction-to-servo-motors. [Accessed: 6 Jan 2018].

[78] Kiatronics, "28BYJ-48 – 5V Stepper Motor," 28BYJ-48 datasheet. [Revised 2017].

[79] B. Appleton, "Normal Ranges of Joint Motion," in *STRETCHING AND FLEXIBILITY Everything you never wanted to know*. [Online]. Available: https://people.bath.ac.uk/masrjb/Stretch/stretching_toc.html#SEC84. [Accessed: 15 Jul 2018].

[80] "Inverse trigonometry functions," mathopenref.com, 2011. [Online]. Available: https://www.mathopenref.com/triginverse.html. [Accessed: 14 Aug 2018].

[81] Cerebral palsy alliance research foundation, "To prevent, treat and cure cerebral palsy," research.cerebralpalsy.org.au. [Online]. Available: https://research.cerebralpalsy.org.au/what-is-cerebral-palsy. [Accessed: 11 May 2018].

[82] M. Tonkin, "The upper limb in cerebral palsy," Hand Clinics, vol. 19, no. 4, p. xi, 2003.

[83] M. A. Watkins, D. L. Riddle, R. L. Lamb and W. J. Personius, "Reliability of goniometric measurements and visual estimates of knee range of motion obtained in a clinical setting," *Physical Therapy*, vol. 71, no. 2, pp. 90-96, 1991.

[84] Mbientlab, "MetaWearC Board," mbientlab.com, 2018. [Online]. Available: https://research.cerebralpalsy.org.au/what-is-cerebral-palsy. [Accessed: 14 Sep 2018].

[85] "Kinect". Wikipedia.org. [Online]. Available: https://en.wikipedia.org/wiki/Kinect. [Accessed: 11 Jan 2019].

[86] Y. Nizam, M. N. Mohd and M. M. A. Jamil, "Biomechanical application: exploitation of kinect sensor for gait analysis," ARPN Journal of Engineering and Applied Sciences, vol. 12, no. 10, pp 3183-3188, 2017.

[87] "atan2". Wikipedia.org. [Online]. Available: https://en.wikipedia.org/wiki/Atan2. [Accessed: 11 Jan 2019].

Every reasonable effort has been made to acknowledge the owner of copyright material. I would be pleased to hear from any copyright owner who has been omitted or incorrectly acknowledged.

Appendix A

A.1: 8 bits custom made Atmel 328G based microcontroller – Arduino Curtin schematic
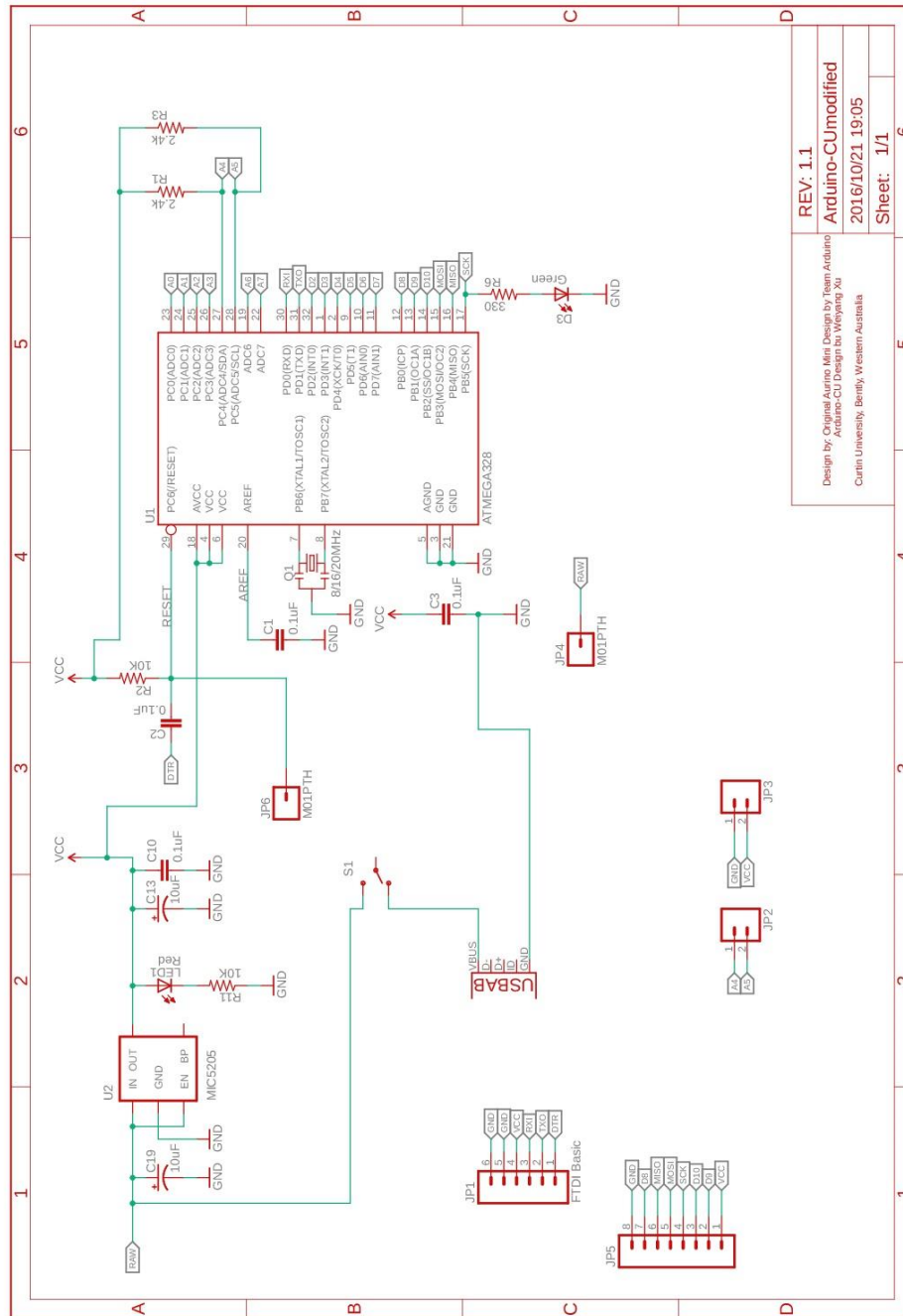
U1 is atmel328 providing the major MCU function where most analogue pins was left open as the design of the board was only used in the thesis. Limit number of outputs is one of the best ways to reduce the board size and increase the size of ground plane to avoid EMC interference. U2 is mic5205, an efficient linear voltage regulator maintain the board operating voltage at 3.3 v.

A.2: 8 bits custom made Atmel 328G based microcontroller – Arduino Curtin footprint
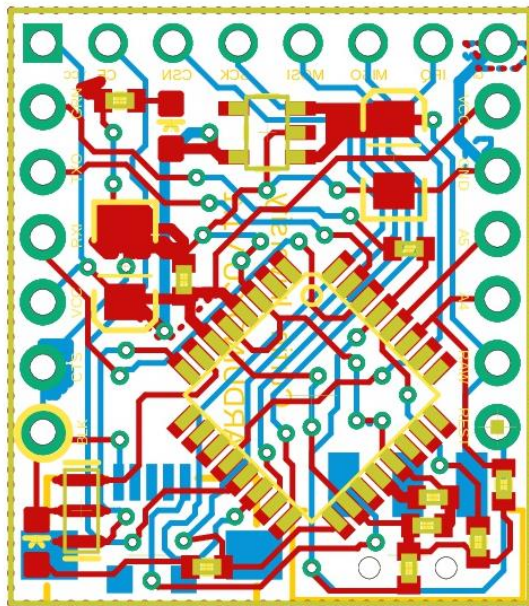
The two plane holes at bottom right corner were the place for the micro-usb header. As the micro-usb header and a switch uses a large amount of space, all the trace has been re-organized. As shown in the figure above, the 2 layers PCB board has left not places for further adjustment. In the future, pins can be removed once radio model and IMU model were merged into the board. A 4 layer PCB will be necessary.

Appendix B

This thesis includes electronic appendix. The following documents are available in a cloud drive:

- Sensor hardware: Code and part list
- MATLAB codes: data processing code
- Data collection terminal software: The terminal software that collect and process serial data
- Arduino Curtin PCB: The custom made processor PCB files
- 3D printing design: All the 3D printing cases and robot arms' sketch files
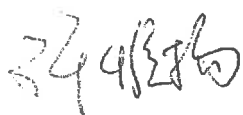
Documents are available in the following link:

https://drive.google.com/drive/folders/1tIuHRRe7puU0LJojAuFC7H9GGbi1O7V7

The file organization of the contents in the cloud drive is presented in the following figure.

This page is intentionally kept blank

To Whom It May Concern I, Weiyang Xu, contributed the conceptual design, experimental design and the results analysis to the paper/publication entitled Measuring Human Joint Movement with IMUs: Implementation in custom-made low cost wireless sensors, Cesar Ortega-Sanchez, Iain Murray, conference on 2017 IEEE 15th Student Conference on Research and Development (SCOReD), Malaysia, December 2017.

(Signature of Candidate)

I, as a Co-Author, endorse that this level of contribution by the candidate indicated above is appropriate.

1/07/2019

Cesar Ortega-Sanchez

Iain Murray